Dissertation zur Erlangung des Doktorgrades

der Fakultät für Chemie und Pharmazie

der Ludwig-Maximilians-Universität München

The potential of the natural compound Neocarzilin A as inhibitor of cell migration in breast cancer cells

Carolin Laura Pyka

aus

Düsseldorf

Deutschland

2019

Erklärung

Diese Dissertation wurde im Sinne von §7 der Promotionsordnung vom 28. November 2011 von Frau Prof. Dr. Angelika M. Vollmar betreut.

Eidesstattliche Versicherung

Diese Dissertation wurde eigenständig und ohne unerlaubte Hilfe erarbeitet.

München, den 18.07.2019

_____

Carolin Laura Pyka

Dissertation eingereicht am:	18.07.2019
1. Gutachter:	Prof. Dr. Angelika M. Vollmar
2. Gutachter:	Prof. Dr. Johanna Pachmayr
Mündliche Prüfung am:	28.08.2019

To my family

CONTENTS

Contents

List of Figures

List of Tables

ABSTRACT

Abstract

Metastatic cancer accounts for 90% of all cancer related deaths and is still considered incurable by reason of insufficient antimetastatic drugs and absence of therapeutically addressable targets. Specific therapeutic targeting of tumor cell motility could present a promising strategy to limit metastasis of solid tumors, considering that cell migration is a crucial step in the metastatic cascade.

The natural compound Neocarzilin A (NCA) was discovered decades ago, but so far no mode of action studies have been performed. Within the framework of this thesis, we elucidated the antitumor effects of NCA and identified the compound as potent inhibitor of cancer cell motility (Figure 1). By applying activity-based protein profiling (ABPP) using *in situ* labeling of proteins with the specifically designed activity-based probe NC-1 and subsequent LC-MS/MS analysis, we identified the synaptic vesicle membrane protein 1 (VAT-1) as target of NCA in cooperation with the group of Prof. Dr. Stephan Sieber (Chair of Organic Chemistry II, Technical University (TU) of Munich, Germany). A functional role of VAT-1 in cancer cell migration was confirmed by knockdown and CRISPR-Cas9 knockout studies. In depth investigation revealed that VAT-1 interacts with a complex network of key migration mediators, involved in extracellular matrix (ECM) composition, regulation of cell migration, and cell-ECM adhesion. Talin-1, the main activator of integrins and important mediator of adhesion, was identified as most prominent binding partner of VAT-1, providing a link between the antimigratory phenotype and the integrin mediated cell adhesion process. Consequently, we hypothesize that binding of NCA to its target VAT-1 influences its interaction with Talin-1, resulting in alternation of integrin mediated adhesion leading to impaired cell detachment and reduced migration.

In conclusion, we introduce the natural compound NCA as promising novel antimigratory drug and potential lead compound and VAT-1 as an innovative target for the development of cancer cell migration inhibitors for treatment of metastatic tumors.
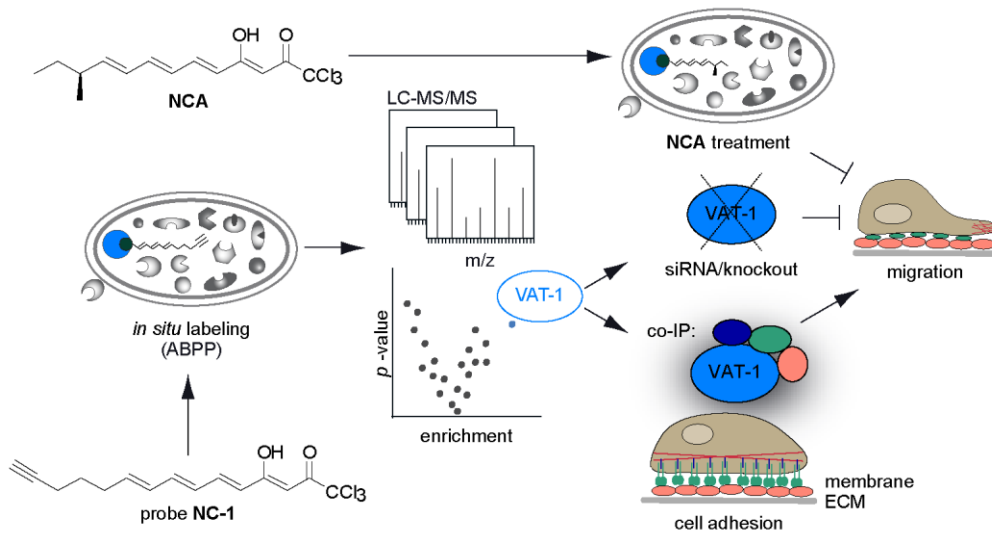
Figure 1. The project at a glance.

INTRODUCTION

1 Introduction

1.1 Metastatic breast cancer – an overview

1.1.1 Facts and figures

The global cancer burden continues to increase with 18.1 million new cases and 9.6 million cancer related deaths in 2018, primarily attributed to aging and growth of the population as well as adoption of a cancer promoting lifestyle.[1] Together with lung cancer, breast cancer shows the highest number of new cases worldwide with approximately 2.1 million diagnoses in 2018 (Figure 2) and presents the leading cause of cancer related death in women of all races.[1]
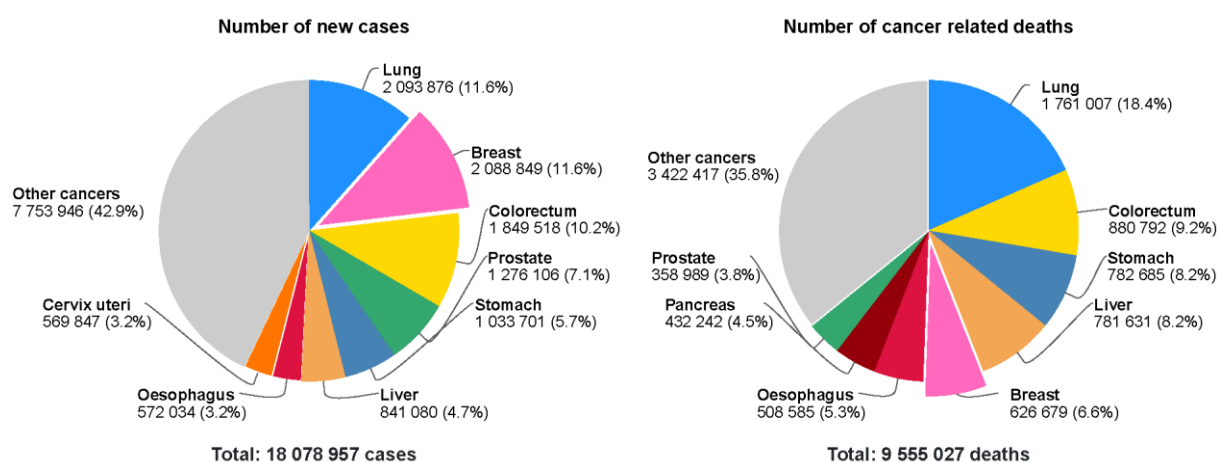
Figure 2. Global cancer burden in 2018. Data for all ages and both sexes is shown. Adapted from Bray *et al.*[2]

1.1.2   Classification of breast cancer

Breast cancer can be divided into a non-invasive and an invasive subclass.[3] Non-invasive breast cancer is localized either at the ducts or the lobules and therefore termed ductal carcinoma in situ (DCIS) or lobular carcinoma in situ (LCIS). These types of breast cancer are characterized by proliferation of malignant epithelial cells, but do not invade through the basal membrane.[3] In contrast, invasive breast cancer spreads into the breast tissue and in the worst case, metastasizes to lymph nodes and other parts of the body by cancer cells disseminating from the primary tumor.[4] Metastatic breast cancer is still considered incurable[5] and circulating tumor cells can already be detected in early stages of tumor development[6]. In metastatic cancer, mortality rates are primarily driven by metastases and invasion of migrating tumor cells into the surrounding tissue instead of the primary tumor itself.[4]

Breast cancer can be further classified according to the size of a tumor, whether it has invaded adjacent organs, if and how many regional lymph nodes it has spread to, and whether it has metastasized to distant locations. This classification is referred to as *cancer staging* in agreement with the TNM Classification of Malignant Tumors (TNM).[7] Whereas stage 0 describes DCIS and LCIS as pre-cancerous or marker conditions, tumors of stages 1-3 are located within the breast or regional lymph nodes. Stage 4 describes metastatic cancer, the most severe form with the least favorable prognosis.[7] A very aggressive and complex subtype of metastatic breast cancer is triple negative breast cancer, which is characterized by a lack of estrogen receptors, progesterone receptors and HER2 overexpression making therapeutic targeting particularly difficult.[8]

1.1.3   Treatment options for metastatic cancer

Cancer treatment can generally be divided in local and systemic treatment. Local cancer treatment comprises surgical removal of tumors and regional radiotherapy.[9] However, metastatic cancer calls for systemic treatment strategies to treat tumors which have spread throughout the body. In systemic cancer treatment cytotoxic chemotherapy, hormonal therapy, targeted therapy, and immunotherapy are used[10]:

- o   *Cytotoxic chemotherapeutics*: intervene with the cell division process leading to reduced proliferation and cell death. Well-known representatives are Doxorubicin, Paclitaxel and 5-Fluorouracil.[10, 11]

- o   *Hormonal therapeutics*: selective estrogen receptor modulators (SERMs) which specifically antagonize estrogen action leading to suppression of estrogen-stimulated tumor growth as present in estrogen-positive invasive breast cancer. This substance class includes e.g. Tamoxifen and Fulvestrant.[12, 13]

- o   *Targeted and immunotherapeutics:* block the growth of cancer cells by interfering with specific molecular targets that are involved in growth, progression, and spread of cancer, e.g. overexpressed oncogenes. Most targeted and immunotherapeutics are either small molecule drugs (e.g. Gefitinib) or monoclonal antibodies (e.g. Trastuzumab) which show less severe side effects as conventional chemotherapeutics due to directed targeting of cancer cells.[10, 14]

The success of each therapeutic option varies in between tumor types and depends on previous treatments. Moreover, current systemic therapy is often accompanied by severe short and long term side effects or becomes ineffective through development of chemoresistance of the cancer cells.[10] Considering that 90% of all cancer related deaths are caused by metastasizing tumors, targeting the process of metastasis could emerge as valuable additional treatment option to control metastatic spread of aggressive cancers and enhance overall survival of affected patients.[15] However, most of the so far investigated therapeutics targeting cancer cell metastasis have failed in clinical research. Therefore, up to date systemic chemotherapy targeting cancer cell proliferation remains the treatment option of choice despite its shortcomings.[16]

1.2 Shedding light on cancer cell migration and metastasis

1.2.1 Metastasis and the cell migration process

The formation of metastasis is a highly complex process in which cancer cells leave the primary tumor and invade into the surrounding tissue. For this purpose, loss of cellular adhesion, increased tumor cell motility and invasiveness, entry and survival in circulation, exit into new tissue, and colonization at a distant site are required.[17, 18] A schematic overview of the metastasis model is presented in Figure 3.
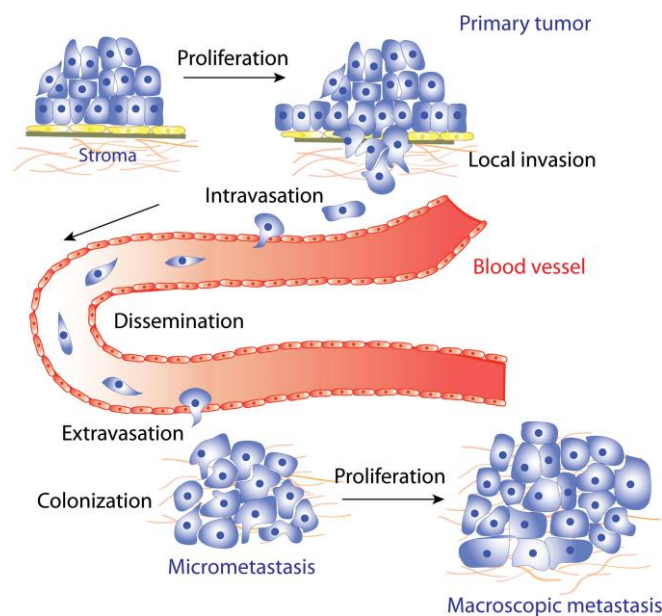
Figure 3. Schematic representation of the metastatic process. Tumor cells disseminate from the primary tumor by invading into the surrounding stroma and the blood vessel. Following circulation, the cells extravasate into a distant organ where they colonize and form macroscopic metastasis after proliferation. Adapted from Saxena *et al.*[19]

To achieve metastasis, cancer cells must show increased motility. Cell migration is a multi-step process which is initiated by the polarization of the cell including the formation of lamellipodia and filopodia at the leading edge of the migrating cell. Lamellipodia are broad membrane protrusions which are assembled of condensed F-actin initiated by the small Rho GTPase Rac1. In contrast, the small Rho GTPase Cdc42 stimulates filopodia formation, thin protrusions that act as antennae for the cell to probe the surrounding environment and establish the directionality of the movement. After polarization, activation of transmembrane receptors named integrins at the leading edge leads to

formation of focal adhesion complexes which attach the cell to the extracellular matrix (ECM) and allow extension of the cell body and translocation of the nucleus in the direction of migration. In the final step of the migration process, myosin II and the Rho GTPase RhoA trigger the contraction of actin stress fibers leading to retraction of the cell rear and forward movement. Simultaneously, focal adhesions at the rear are disassembled to allow detachment from the ECM. After contraction, the cycle starts again with the polarization and formation of the leading edge.[20, 21] The cell migration process is depicted in Figure 4.
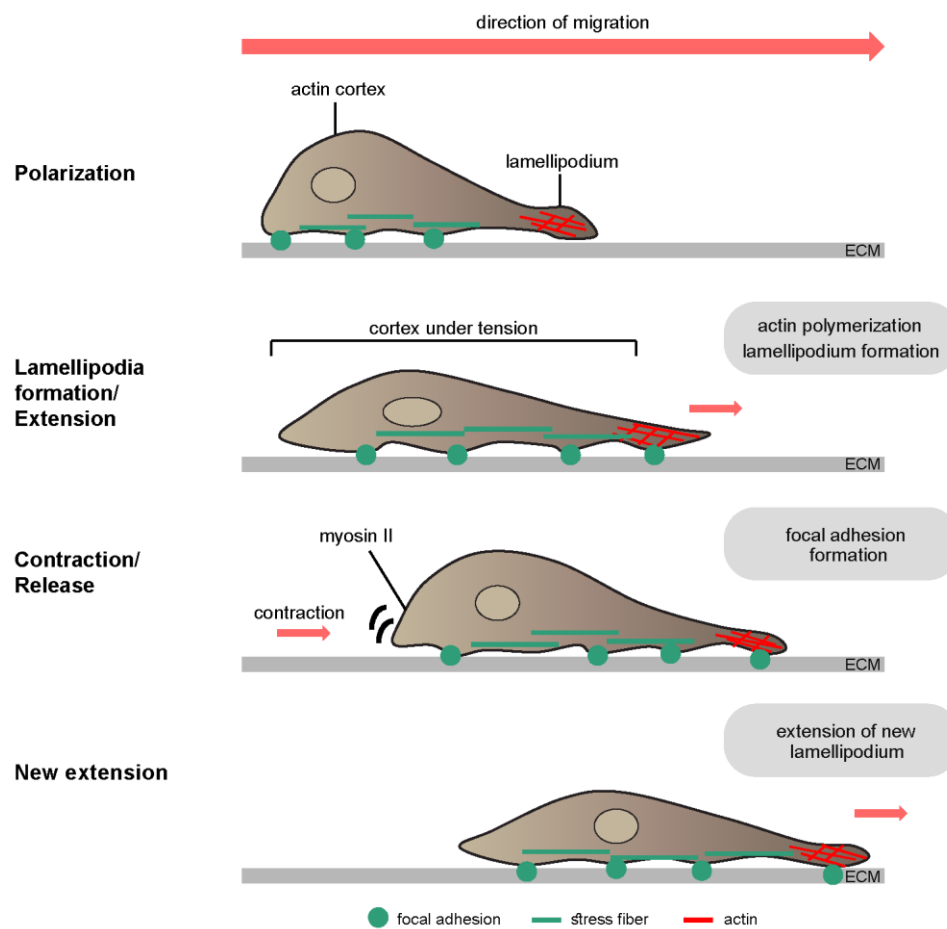
Figure 4. Cell migration process. Reorganization of the actin cytoskeleton leads to formation of lamellipodia and filopodia resulting in polarization of the cell. Focal adhesions are assembled at the leading edge to attach the cell to the extracellular matrix (ECM). Contraction of actin stress fibers via myosin II leads to forward movement of the cell with simultaneous disassembly of focal adhesions and detachment of the cell rear. Adapted from Weinberg[20]

1.2.2   Integrins and Talin-1: key regulators of cell adhesion and migration

Cell adhesion to the ECM plays a pivotal role in the cell migration process, turning it into a critical parameter in the progression of metastatic cancers. The ECM is an intricate network of various proteins with distinct physical and biochemical properties.[22] Some major components of the ECM are collagens, fibronectin, laminin glycoproteins, and vitronectin. The interaction of cells with these proteins determines multiple cellular functions and alternations in the ECM structure can contribute to pathological conditions.[23] For example, the high density of collagen fibers in breast tissue is associated with increased cancer cell migration and promotion of invasive behavior.[24]

Cell adhesion to the ECM is mediated by specific cell surface receptors. The most common and best characterized cell adhesion receptors are the integrins, which are bidirectional transmembrane receptors composed of an α and β subunit which connect the ECM to the cytoskeleton. In mammals 18 α and 8 β subunits can be combined to build 24 different heterodimers, each with specific ligand-binding properties.[25, 26] As typical transmembrane receptors, integrins feature an extracellular domain which is responsible for ligand binding, as well as an intracellular domain which binds to cytoskeletal proteins. The extracellular domain additionally possesses a metal ion dependent adhesion site (MIDAS) which is capable of binding divalent cations required for binding of glycoproteins.[26]

Integrins exist in two different conformational states which define their affinity for ECM proteins. They are inactive when being in a closed (bend) conformation showing low affinity for ECM ligands. In contrast, in their extended (open) conformation integrins are activated, able to engage with ligands, and capable of signal transduction.[25, 26] The signaling of integrins is bidirectional, which means that they can transfer signals from inside the cell to the extracellular environment (inside-out signaling) and *vise versa* (outside-in signaling) (Figure 5).[25]
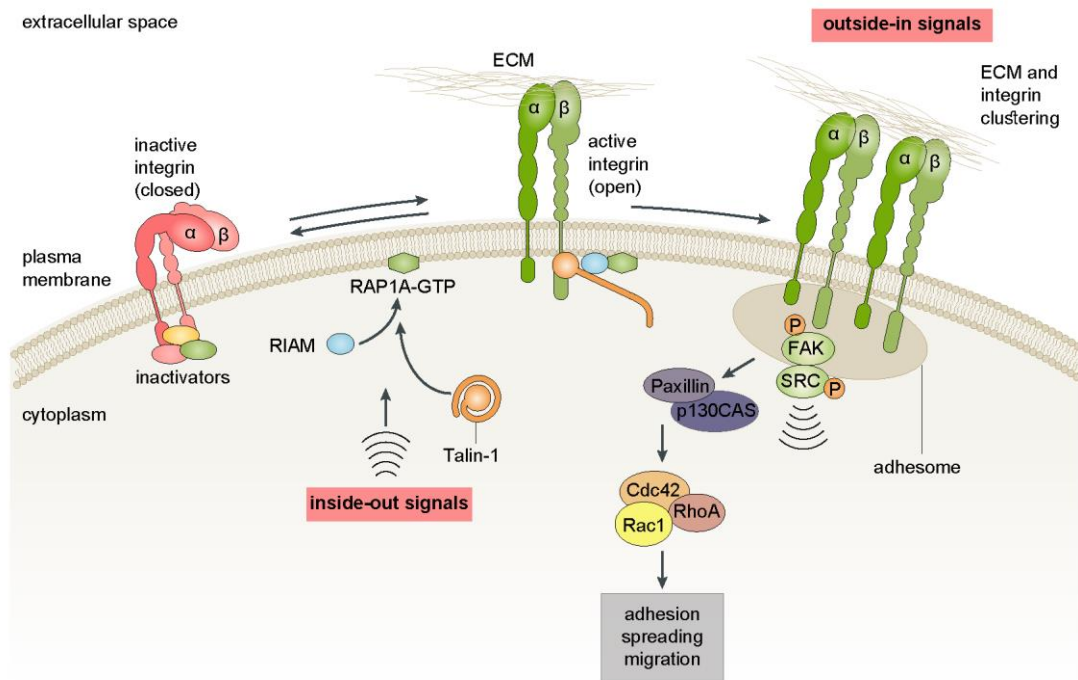
Figure 5. Bidirectional integrin signaling. Integrins can switch between an inactive (closed) and an active (open) conformational state. Activation is mediated by Talin-1 which itself is recruited to the plasma membrane and activated by the small GTPase RAP1A and RAP1-GTP-interacting adapter molecule (RIAM). Upon activation, integrins can engage with proteins of the ECM resulting in signal transduction. In the case of inside-out signaling, intracellular signals are transmitted to the extracellular environment upon binding of Talin-1 to the integrin β subunit. After ligand binding and adhesion, extracellular signals can be transferred into the cell via the assembly of the adhesome complex comprising focal adhesion kinase (FAK) and Src family kinases (outside-in signaling). Subsequently, the downstream effectors paxillin and p130Cas are phosphorylated which promote the activity of the small Rho GTPases Rac1, RhoA, and Cdc42 resulting in regulation of cell migration. Adapted from Hamidi *et al.*[25]

Inside-out signaling – Talin-1 as a key player

Many integrins need to be activated by inducing a conformational change from the closed to the opened conformation prior to binding to the ECM.[27] For this purpose, the small GTPase RAP1A recruits RAP1-GTP-interacting adapter molecule (RIAM) to the plasma membrane in order to activate Talin-1. Talin-1 is a well characterized cytoplasmic protein which shows three actin binding sites by which the protein can link integrins to actin filaments.[28] Talin-1 can thereby serve as adaptor protein which passes on signals, caused by changes in the cytoskeletal structure, to integrins, resulting in modulation of ECM-ligand binding and cell adhesion.[29, 30] In particular, activated Talin-1 binds to the integrin β subunit and induces a conformational change to generate the active high affinity state.[31] In

contrast, inactivating proteins such as integrin cytoplasmic domain-associated protein 1 (ICAP-1), filamin A and proteins of the SH3 family can counterbalance this activation.[32]

Outside-in signaling – induction of Rho GTPase signaling cascades

Upon ECM-ligand binding and adhesion, integrins cluster on the plasma membrane provoking the assembly of the adhesome, a multimeric integrin adhesion complex which triggers downstream adhesion signaling (outside-in signaling). The transmitted signals depend on the engaged integrin heterodimer, the ECM ligands involved, and also on the cell type.[25] In the context of cell migration, outside-in signaling results in recruitment and autophosphorylation of focal adhesion kinase (FAK) which itself recruits Src family kinases. The FAK-Src complex has two main phosphorylation targets, namely the adaptor proteins paxillin and p130Cas. Both proteins serve as downstream effectors by promoting the activity of the small Rho GTPases Rac1, RhoA, and Cdc42. Rac1 plays a key role in actin polymerization during lamellipodia formation and initiates the assembly of focal adhesions at the leading edge of the cell.[33] RhoA induces the formation of stress fibers during the contraction process, whereas Cdc42 regulates filopodia formation.[34] It has been shown that abnormal regulation of Rho GTPase signaling can severely impact the cell migration process and Rac1 and RhoA were found to be overexpressed or hyperactive in breast cancer tissue.[35, 36] In pathological conditions, Rac1 can induce invasion and metastasis by upregulating cell migration via increased actin polymerization and lamellipodia formation.[37] Overexpression or hyperactivation of RhoA leads to increased activation of the downstream effector kinase ROCK, which promotes migration by triggering stress fiber and focal adhesion formation.[38]

Taken together, cell adhesion to the ECM plays a crucial role in the cell migration process. Therapeutic targeting of adhesion mediating proteins could therefore protrude as promising option to prevent cancer metastasis and improve overall survival rates, considering that 90% of all cancer related deaths are caused by metastasizing tumors.[15]

1.3   Neocarzilins: a promising natural compound class in cancer therapy?

Natural products remain an important source of biologically active compounds for modern drug development.[39] In cancer medicine, for example, almost 50% of all anticancer drugs approved between 1981 and 2014 are either unaltered natural products or natural product derived.[40] These compounds, derived from plants, microorganisms or marine organisms, include various structural classes like isoprenoids, alkaloids, non-ribosomal peptides or polyketides.[39, 41] Besides functioning as lead structures in drug development, one major advantage of natural products is their use as chemical tools to understand biological and pharmacological systems.

The natural products Neocarzilin A (NCA) and Neocarzilin B (NCB) were first isolated by Nozoe *et al.* in 1992 from an extract of the mycelium of the actinomycete *Streptomyces carzinostaticus* var. F41.[42] The structures were determined by mass spectrometry and nuclear magnetic resonance (NMR) spectroscopy (Figure 6). Neocarzilins are long chain polyenones bearing a terminal chloromethyl group. The enolic hydroxyl group, which is stabilized by an intramolecular hydrogen bond, grants them a slightly acidic character. In 2004, years after the first total synthesis by Nozoe *et al.*[43], the biosynthetic pathway, involving a novel type I polyketide synthase system, was elucidated by analysis of the responsible gene cluster.[44] In course of the investigation, a third Neocarzilin derivative, named Neocarzilin C (NCC), containing a dichloromethyl instead of a trichloromethyl group, was identified and proposed to be a biosynthetic precursor (Figure 6).

First investigations into the biological activity of NCA, the only compound tested so far, revealed a potent cytotoxic activity against K562 chronic myelogenous leukemia cells with an IC_{50} of 0.06 µg/mL (185 nM).[42] NCA can therefore be considered to be as potent as neocarzinostatin (IC_{50} 0.09 µg/mL), a highly potent DNA damage agent derived from the same actinomycete which was used in Japan as anticancer agent to treat liver cancer until 2009.[44, 45] Up to date, no structure-activity relationship (SAR) studies of Neocarzilins in human cancer cells have been published. However, the acidic hydroxyl group seems to be crucial for the biological activity of NCA,

since the corresponding methylether showed only moderate cytotoxic activity with an IC_{50} of 2 μg/mL (6 μM).[42] Due to its potent cytotoxic activity and its good synthetic accessibility the natural compound NCA protrudes as interesting object for further research.
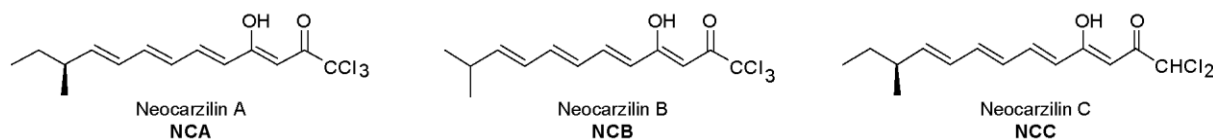
Figure 6. Structures of Neocarzilins A-C.

1.4   The synaptic vesicle membrane protein 1 (VAT-1)

1.4.1   Origin of VAT-1 and function in *T. californica*

The synaptic vesicle membrane protein 1 (VAT-1) was first discovered in the electric organ of the marine ray *Torpedo californica (T. californica)* by Linial *et al.* in 1989.[46] The 42 kDa protein was isolated from synaptic vesicle membranes and proposed to be an integral membrane protein due to its copurification with vesicles and its hydrophobic character.[46] During further investigations, Linial *et al.* discovered an ATPase activity for VAT-1 which was supported by divalent cations like Mg^{2+} and Ca^{2+}.[47] Moreover, they revealed that VAT-1 forms a high-molecular-mass complex of 170-180 kDa consisting of 3-4 VAT-1 homomers within the synaptic vesicle membrane.[48] Due to partial dissociation of VAT-1 subunits from the complex upon chelating Ca^{2+} ions, it was proposed that the stability of the complex is Ca^{2+} dependent[48]. Supporting this, Levius *et al.* discovered that VAT-1 overexpressed in *E.coli* binds Ca^{2+} with low affinity.[49] Although computational homology studies did not lead to the discovery of a relationship between VAT-1 and other proteins concerning ancestry and function, sequence similarities for the protein were found with the highest scores in translocases, protein kinase C, nucleotide binding proteins, ATPases, and especially alcohol dehydrogenase.[46] In addition, VAT-1 showed properties of oxidoreductases as a member of a reductase subgroup of the same protein super-family of medium-chain dehydrogenases/reductases (MDR). Interestingly, a homology to ζ-crystallin, a major protein in the lens of guinea pig which is included in the same subgroup of the MDR super-family, was found.[50, 51] Although VAT-1 had been

reported to be an integral membrane protein by Linial *et al.* upon its discovery, Persson *et al.* challenged this assumption based on conducted homology studies. The authors identified the suggested membrane bound segment as the coenzyme region of VAT-1, which makes it highly unlikely for this region to be membrane associated.[50] Furthermore the authors claimed that the corresponding region of alcohol dehydrogenase had possibly been detected as false positive when predicting membrane-spanning segments due to its hydrophobic character.[50] However, membrane binding of VAT-1 could also be explained by a possible interaction with other membrane bound proteins.

1.4.2   The function of VAT-1 in mammals

In 1998, the mammalian homolog of VAT-1 was first isolated from the murine breast cancer cell line Ehrlich ascites carcinoma and additionally detected in human T47D breast cancer cells.[52] Research has been focused on the human VAT-1 homolog because its gene has been localized on chromosome locus 17q21 neighboring the breast cancer gene BRCA1.[53] Chromosomal instability and inherited predisposition for breast and ovarian cancer are characteristic for this gene region giving rise to the question, whether VAT-1 as well might feature critical mutations with possible implications for cancer.[54] However, first studies on the expression pattern of VAT-1 in normal and malignant epithelial cells of the mammary gland and ovary found no dysregulation of VAT-1.[55]

Although VAT-1 was originally described as an integral membrane protein by Linial *et al.*, the localization of the mammalian VAT-1 homolog is still unclear. Recent studies showed that the protein is mainly localized in the cytoplasm[55, 56, 57] and to a small extend also associated with the endoplasmatic reticulum (ER) and the outer mitochondrial membrane[57]. Eura *et al.* proposed that both, hydrophobic and ionic interactions are involved in membrane association.[57] In conclusion, the localization of VAT-1 in mammalian cells is not limited to a single cell compartment.

Regarding the function of VAT-1 in mammals only limited data is available so far. Koch *et al.* showed that human VAT-1 is involved in calcium regulated processes in keratinocyte physiology.[55]

Moreover, they discovered that VAT-1 expression is decreased with increasing Ca^{2+} concentration in the human keratinocyte cell line HaCaT, supporting the finding of Linial *et al.* that the function of VAT-1 from *T. californica* is calcium dependent.[55, 58] Eura *et al.* suggested an involvement of VAT-1 in the regulation of mitochondrial dynamics.[57] They identified the VAT-1 rat homolog mitofusin binding protein (MIB) as binding partner of mitofusin protein 1 (Mfn1)[57], which is a key driver of mitochondrial fusion located at the outer mitochondrial membrane[59]. Knockdown of MIB led to large extension of mitochondrial network structures and exogenous expression of MIB induced mitochondrial fragmentation, which was prevented by coexpression of Mfn1.[57] On the assumption that the rat homolog MIB features the same functions as human VAT-1, a role of the protein in mitochondrial processes could be presumed. This hypothesis was also supported by Junker *et al.* which showed that VAT-1 is involved in the transport of phosphatidylserine (PS) from the ER to mitochondria where it can be decarboxylated to phosphatidylethanolamine (PE).[56]

1.4.3   The role of VAT-1 in cancer: *status quo*

Taking into consideration that the VAT-1 gene is located on chromosome locus 17q21 in direct proximity to the breast cancer gene BRCA1[53], it is of interest to investigate VAT-1's implication in cancer. Mori *et al.* demonstrated an influence of VAT-1 on proliferation of normal prostatic stromal cells (PrSC) and prostate cancer cells (PCa), since knockdown of VAT-1 inhibited proliferation of both, normal and cancerous cell lines.[60] Moreover, the protein was upregulated in benign prostatic hyperplasia (BPH) indicating that VAT-1 could be a pathogenic factor in BPH associated with cell proliferation.[60] In contrast, Mertsch *et al.* found no antiproliferative effect of VAT-1 knockdown in different glioma cell lines, but observed significant reduction of cell migration and general upregulation of VAT-1 in glioblastoma tissue.[61] However, the mode of action has remained unknown up to date.

Taken together, VAT-1 displays interesting functions in both normal as well as cancerous tissue. Considering its effects on cancer cells, VAT-1 emerges as interesting subject for further investigations.

1.5   Aims of the study

The natural compound Neocarzilin A (NCA) was discovered decades ago, but despite its potent cytotoxic effect no mode of action studies have been performed up to date. Considering the emergence of proteomic methods for target identification, we aimed to unravel its mode of action by identifying cellular interaction partners and investigate its antitumor effects to decipher its potential as anticancer lead structure.

The precise goals of this thesis can be summarized as follows:

1. assess the antitumor effects of NCA on cell proliferation, apoptosis, and migration

2. identify the cellular target protein of NCA by proteomic activity-based protein profiling (ABPP) in cooperation with Carolin Gleißner (Sieber Research Group, Department of Chemistry, Technical University of Munich, Germany)

3. validate the identified target protein and decipher its physiological role in cancer cells by investigating its protein interaction network

4. elucidate the mode of action of NCA by examining its effect on the target protein interaction network

MATERIALS AND METHODS

2 Materials and Methods

2.1 Materials

2.1.1 Compounds

All members of the Neocarzilin family (NCA, NCA', NCB, NCC) as well as the activity-based probe NC-1 were synthesized and kindly provided by the lab of Prof. Dr. Stephan Sieber (Chair of Organic Chemistry II, Technical University of Munich, Germany) (Figure 7). All compounds were dissolved in DMSO to 10 mM stock solutions, aliquoted á 2 µL, and stored at -20 °C. For experimental use, compounds were diluted to the appropriate concentration in growth medium, containing DMSO at a maximum of 0.1% (v/v) to prevent side effects.
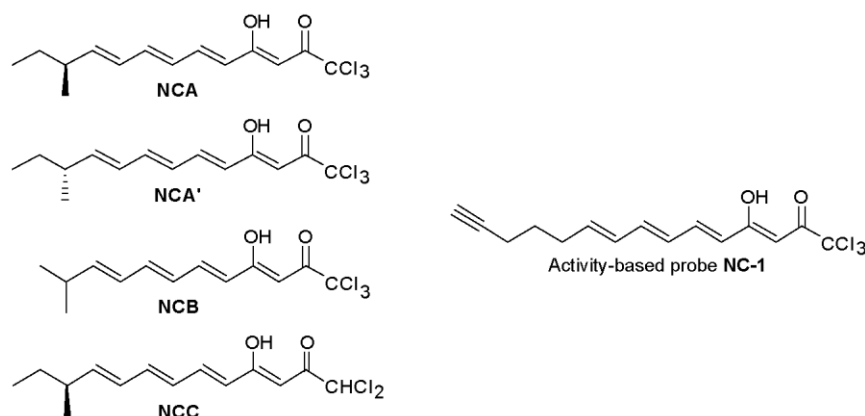
Figure 7. Chemical structure of Neocarzilins and the activity-based probe NC-1.

2.1.2 Chemicals and reagents

Table 1. Chemicals, reagents, dyes, and kits

Reagent	Source
5x siRNA buffer	Dharmacon, Lafayette, CO, USA
Active Rac1 pull-down and detection kit (16118)	Thermo Scientific, Waltham, MA, USA
Adenosine triphosphate (ATP) 25 mM	Epicentre, Madison, WI, USA
Agarose	VWR, Radnor, PA, USA
Ammoniumpersulfate (APS)	Sigma Aldrich, Taufkirchen, Germany
Ampicillin	Sigma Aldrich, Taufkirchen, Germany
BC assay reagent A	Interchim, Mannheim, Germany
BC assay reagent B	Interchim, Mannheim, Germany
Blasticidin S HCl	Thermo Scientific, Waltham, MA, USA
Bovine serum albumin (BSA)	Anprotec, Bruckberg, Germany
Bradford reagent Roti® Quant	Bio-Rad, Munich, Germany
Calcein-AM	Santa Cruz, Dallas, TX, USA
Calcium chloride dihydrate ($CaCl_2$ x 2 H_2O)	Sigma Aldrich, Taufkirchen, Germany
CellTiter-Blue® reagent	Promega, Mannheim, Germany
Collagen G	Biochrom AG, Berlin, Germany
Complete® protease inhibitor	Roche Diagnostics, Basel, Switzerland
Coumaric acid	Fluka, Buchs, Switzerland
Crystal violet	Carl Roth, Karlsruhe, Germany
Dimethylsulfoxide (DMSO)	AppliChem, Darmstadt, Germany
Di-sodiumhydrogenphosphate (Na_2HPO_4)	VWR, Radnor, PA, USA
Dithiothreitol (DTT)	Molekula, Munich, Germany
dNTPs mix	MP Biomedicals, Santa Ana, CA, USA
Dulbecco's Modified Eagle Medium (DMEM)	PAN Biotech, Aidenbach, Germany
ECL Plus WB detection reagent	GE Healthcare, Munich, Germany
EndoFree plasmid maxi kit	QIAGEN, Hilden, Germany
Epidermal growth factor (EGF)	Peprotech, Rocky Hill, NJ, USA
Ethylene diamine tetraacetic acid (EDTA)	Carl Roth, Karlsruhe, Germany
Ethylene glycol tetraacetic acid (EGTA)	Sigma Aldrich, Taufkirchen, Germany
FACS flow	BD Biosciences, Franklin Lakes, NJ, USA
FACS rinse	BD Biosciences, Franklin Lakes, NJ, USA
FACS shutdown solution	BD Biosciences, Franklin Lakes, NJ, USA
FastDigest Bpil	Thermo Scientific, Waltham, MA, USA
FastDigest green buffer (10x)	Thermo Scientific, Waltham, MA, USA
Fetal calf serum (FCS)	PAN Biotech, Aidenbach, Germany
Fibronectin	Corning, New York, NY, USA
FluorSave™ reagent mounting medium	Merck, Darmstadt, Germany

Formaldehyde 16%	Polysciences, Eppelheim, Germany
GeneRuler 1 kb Plus DNA ladder	Thermo Scientific, Waltham, MA, USA
Gibco® Versene solution	Thermo Scientific, Waltham, MA, USA
Glutaraldehyde 50%	Fluka Biochem, Taufkirchen, Germany
Glycerol	Applichem, Darmstadt, Germany
Hoechst 33342	Sigma Aldrich, Taufkirchen, Germany
Hydroxyethyl-piperazineethane-sulfonic acid buffer (HEPES)	AppliChem, Darmstadt, Germany
Igepal CA 630 (Nonidet P 40)	Sigma Aldrich, Taufkirchen, Germany
Kolliphor® EL	Sigma Aldrich, Taufkirchen, Germany
LB agar powder	Invitrogen, Carlsbad, CA, USA
LB broth powder	Invitrogen, Carlsbad, CA, USA
Lipofectamine™ 3000 transfection reagent	Thermo Scientific, Waltham, MA, USA
Luminol	Carl Roth, Karlsruhe, Germany
Magnesium chloride ($MgCl_2$)	Applichem, Darmstadt, Germany
Magnesium chloride hexahydrate ($MgCl_2$ x 6 H_2O)	Grüssing, Filsum, Germany
Matrigel®	VWR, Radnor, PA, USA
Methanol	Fisher Scientific, Waltham, MA, USA
Mitomycin C	Sigma Aldrich, Taufkirchen, Germany
Mitotracker® Green FM	Molecular Probes, Darmstadt, Germany
Non-fat dry milkpowder (Blotto)	Carl Roth, Karlsruhe, Germany
PAGE GelRed® nucleic acid gel stain 10,000x	Biotium, Fremont, CA, USA
Page Ruler™ Plus prestained protein ladder	Thermo Scientific, Waltham, MA, USA
Page Ruler™ prestained protein ladder	Thermo Scientific, Waltham, MA, USA
Penicillin/Streptomycin 100x	PAN Biotech, Aidenbach, Germany
Phenylmethylsulfonyl fluoride (PMSF)	Sigma Aldrich, Taufkirchen, Germany
Phusion Hot Start II DNA polymerase (2 U/µL)	Thermo Scientific, Waltham, MA, USA
Piperazine-1,4-bis(2-ethanesulfonic acid) (PIPES)	Sigma Aldrich, Taufkirchen, Germany
PlasmidSafe buffer (10x)	Epicentre, Madison, WI, USA
PlasmidSafe™ ATP-dependent DNase	Epicentre, Madison, WI, USA
Potassium chloride (KCl)	VWR, Radnor, PA, USA
Potassium dihydrogen phosphate (KH_2PO_4)	Merck, Darmstadt, Germany
Primers	Metabion, Planegg, Germany
Propidium iodide	Carl Roth, Karlsruhe, Germany
Protein A/G PLUS-agarose	Santa Cruz, Dallas, TX, USA
Puromycin	Sigma Aldrich, Taufkirchen, Germany
Pyronin Y	Sigma Aldrich, Taufkirchen, Germany
QIAGEN plasmid maxiprep kit	QIAGEN, Hilden, Germany
QIAprep spin miniprep kit	QIAGEN, Hilden, Germany

QIAquick gel extraction kit	QIAGEN, Hilden, Germany
QuickExtract™ DNA extraction solution	Epicentre, Madison, WI, USA
Rhodamine/Phalloidin	Sigma Aldrich, Taufkirchen, Germany
Roswell Park Memorial Institute Medium (RPMI-1640)	PAN Biotech, Aidenbach, Germany
Rotiphorese® Gel 30	Carl Roth, Karlsruhe, Germany
Sodium borohydride ($NaBH_4$)	Carl Roth, Karlsruhe, Germany
Sodium chloride (NaCl)	Sigma Aldrich, Taufkirchen, Germany
Sodium deoxycholate	Carl Roth, Karlsruhe, Germany
Sodium dihydrogen phosphate dihydrate (NaH_2PO_4 x H_2O)	Grüssing, Filsum, Germany
Sodium fluoride (NaF)	Merck, Darmstadt, Germany
Sodium glycerophosphate ($C_3H_7Na_2O_6P$)	Sigma Aldrich, Taufkirchen, Germany
Sodium glycerophosphate pentahydrate ($Na_2C_3H_7O_6$ x 5 H_2O)	Merck, Darmstadt, Germany
Sodium orthovanadate (Na_3VO_4)	ICN Biomedicals, Aurora, CO, USA
Sodium pyrophosphate decahydrate ($Na_4P_2O_7$ x 10 H_2O)	Sigma Aldrich, Taufkirchen, Germany
Sodiumdodecylsulfate (SDS)	Carl Roth, Karlsruhe, Germany
T4 DNA ligase	Thermo Scientific, Waltham, MA, USA
T4 ligation buffer (10x)	Thermo Scientific, Waltham, MA, USA
T7 Endonclease	New England Biolabs, Ipswich, MA, USA
Tetramethylethylenediamine (TEMED)	Thermo Scientific, Waltham, MA, USA
Trichloroethylene (TCE)	Sigma Aldrich, Taufkirchen, Germany
Tris/HCl	Carl Roth, Karlsruhe, Germany
Tri-sodium citrate	Carl Roth, Karlsruhe, Germany
Triton-X 100	Merck, Darmstadt, Germany
Trypsin	PAN Biotech, Aidenbach, Germany
Tween 20	Carl Roth, Karlsruhe, Germany

All commonly used acids, bases, buffer salts and organic solvents were either purchased from Merck (Darmstadt, Germany) or Sigma Aldrich (Taufkirchen, Germany).

2.1.3 Technical equipment

Table 2. Technical devices and lab equipment

Device	Source
C10 immersion thermostat with water bath	Thermo Haake, Waltham, MA, USA
Canon Eos 450 C camera	Canon, Krefeld, Germany
ChemiDoc™ touch imaging system	Bio-Rad, Munich, Germany
Clay adams nutator mixer	Marshall Scientific, Hampton, NH, USA
FACS Canto™ II	BD Biosciences, Franklin Lakes, NJ, USA
HBT 130-2 thermoblock	Haep Labor Consult, Bovenden, Germany
HeraCell 150i incubator	Heraeus, Hanau, Germany
HeraSafe laminar flow	Heraeus, Hanau, Germany
IVIS® Spectrum in vivo imaging system	PerkinElmer, Waltham, MA, USA
Leica DMi1	Leica, Wetzlar, Germany
Leica TCS SP8 confocal laser scanning microscope	Leica, Wetzlar, Germany
Megafuge 1.0 RS centrifuge	Thermo Scientific, Waltham, MA, USA
Mikro 22R microcentrifuge	Hettich, Tuttlingen, Germany
Mini PROTEAN 3 electrophoresis chambers	Bio-Rad, Munich, Germany
Mini Trans-Blot® system	Bio-Rad, Munich, Germany
MR 3001 K magnetic stirrer	Heidolph Instruments, Schwabach, Germany
Nanodrop® ND-100 spectrophotometer	PEQLAB Biotechnologie GmbH, Erlangen, Germany
Nikon Eclipse Ti inverted microscope	Nikon, Düsseldorf, Germany
Olympus CK30 inverted microscope	Olympus, Tokyo, Japan
Pipettes (0.5-10 µL, 10-100 µL, 100-1,000 µL, 500-5,000 µL)	Eppendorf, Hamburg, Germany
Power Pac 300 blotting device	Bio-Rad, Munich, Germany
Primus 25 advanced® thermocycler	PEQLAB Biotechnologie GmbH, Erlangen, Germany
Reax top vortex	Heidolph Instruments, Schwabach, Germany
Rotina 46R centrifuge	Hettich, Tuttlingen, Germany
SpectraFluor Plus™ plate reader	Tecan, Crailsheim, Germany
Vibrax VXR basic shaker	IKA, Staufen, Germany
Vi-Cell™ XR	Beckmann Coulter, Krefeld, Germany
xCELLigence dual purpose system	Roche Diagnostics, Penzberg, Germany
Zeiss LSM 510 Meta confocal laser scanning microscope	Zeiss, Oberkochen, Germany

2.1.4 Consumables

Table 3. List of consumables

Product	Source
Cell culture flasks, tubes, and plates	Sarstedt, Nümbrecht, Germany
Disposable plastic pipettes (5 mL, 10 mL, 25 mL)	Greiner Bio, Frickenhausen, Germany
Eppendorf tubes (0.5 mL, 1.5 mL, 2 mL)	Eppendorf, Hamburg, Germany
FACS tubes (5 mL)	Sarstedt, Nümbrecht, Germany
Falcon tubes (15 mL, 50 mL)	Greiner Bio, Frickenhausen, Germany
ibidi chemotaxis µ-slide	ibidi GmbH, Gräfelfing, Germany
ibiTreat µ-slides 8-well	ibidi GmbH, Gräfelfing, Germany
Nitrile gloves	VWR, Radnor, PA, USA
Pipette tips (10 µL, 100 µL, 1,000 µL)	Sarstedt, Nümbrecht, Germany
Polyvinylidene difluoride (PVDF) membrane (0.2 µm)	Amersham Bioscience, Freiburg, Germany
Transwell Boyden chamber inserts 8 µm pore size	Corning, New York, NY, USA
xCELLigence CIM-plates 16	ACEA Biosciences, San Diego, CA, USA
xCELLigence E-plates 16	ACEA Biosciences, San Diego, CA, USA

2.1.5 Software

Table 4. Software tools used for data acquisition and analysis

Software	Supplier
Adobe Creative Cloud	Adobe, San José, CA, USA
BD FACSDiva™	BD Biosciences, Franklin Lakes, NJ, USA
Chemotaxis and migration tool version 4.3.2	ibidi GmbH, Gräfelfing, Germany
FlowJo 7.6.5	Tree Star, Ashland, OR, USA
GraphPad Prism 7	GraphPad Software, San Diego, CA, USA
Image Lab 5.2	Bio-Rad, Hercules, CA, USA
ImageJ	NIH, Bethesda, MD, USA
Leica LAS X	Leica, Wetzlar, Germany
Living Image 4.4	PerkinElmer, Waltham, MA, USA
Microsoft Office 2010	Microsoft, Redmont, WA, USA
RTCA software 2.0	ACEA Biosciences, San Diego, CA, USA
Zeiss LSM image Browser	Zeiss, Oberkochen, Germany

2.2 Cell culture

2.2.1 Solutions and reagents

The following solutions were used for the cultivation of MDA-MB-231, 4T1-luc2, T24, HEK293, and

CRISPR VAT-1 knockout (k.o.) clones.

Table 5. Commonly used media, solutions, and buffers for cell culture

PBS (pH 7.4)		PBS+Ca^{2+}/Mg^{2+} (pH 7.4)	
NaCl	132.2 mM	NaCl	137 mM
Na$_2$HPO$_4$	10.4 mM	KCl	2.68 mM
KH$_2$PO$_4$	3.2 mM	Na$_2$HPO$_4$	8.10 mM
H$_2$O		KH$_2$PO$_4$	1.47 mM
		MgCl$_2$	0.25 mM
		CaCl$_2$	0.5 mM
		H$_2$O	

1x Trypsin/EDTA (1x T/E)		2x Trypsin/EDTA (2x T/E)	
Trypsin	0.05% (w/v)	Trypsin	0.1% (w/v)
EDTA	0.02% (w/v)	EDTA	0.02% (w/v)
PBS		PBS	

Growth medium		Growth medium	
DMEM	500 mL	RPMI-1640	500 mL
FCS	10% (v/v)	FCS	10% (v/v)
Penicillin/Streptomycin 100x	1% (v/v)	Penicillin/Streptomycin 100x	1% (v/v)

Starvation medium DMEM		Starvation medium RPMI-1640	
DMEM	500 mL	RPMI-1640	500 mL
Penicillin/Streptomycin 100x	1% (v/v)	Penicillin/Streptomycin 100x	1% (v/v)

Collagen G	
Collagen G	0.001% (v/v)
PBS	

2.2.2 Cell lines

Highly invasive human triple negative breast adenocarcinoma MDA-MB-231 cells, human urinary bladder carcinoma T24 cells, and human embryonic kidney HEK293 cells were obtained from the German Collection of Microorganisms and Cell Cultures GmbH (DSMZ, Braunschweig, Germany) and cultured in Dulbecco´s Modified Eagle´s Medium (DMEM) supplemented with 10% (v/v) fetal calf serum (FCS) and 1% (v/v) penicillin/streptomycin (P/S) (100 U/mL penicillin and 100 µg/mL streptomycin). The murine breast carcinoma cell line 4T1-luc2 was purchased from PerkinElmer (Waltham, MA, USA) and maintained in Roswell Park Memorial Institute Medium (RPMI-1640). RAEW glioblastoma multiforme cells established from a patient isolate in Linz were kindly provided by the MedUni Vienna and cultivated in RPMI-1640 medium supplemented with 10% (v/v) FCS and 1% (v/v) P/S. U87 human primary glioblastoma cells were kindly provided by the Weatherall Institute of Molecular Medicine of the University of Oxford and cultivated in RPMI-1640 medium supplemented with 10% (v/v) FCS and 1% (v/v) P/S. The HEK293-derived VAT-1 knockout (k.o.) cell lines were generated as described in section 2.4 and cultivated in DMEM medium supplemented with 10% (v/v) FCS and 1% (v/v) P/S. All cells were cultured at 37 °C with 5% CO_2 in constant humidity in an incubator and routinely tested for mycoplasma contamination. Before cell seeding of HEK293 or HEK293-derived clonal cell lines, all culture flasks, multiwell-plates, and dishes were coated with 0.001% (v/v) collagen G in PBS for 30 min.

2.2.3 Passaging

Cells were cultivated in growth medium until reaching 90% confluence and subsequently either seeded for experimental purposes or passaged every three to four days. For this purpose, the medium was removed, and the cells were washed twice with pre-warmed PBS. To detach the adherent cells, 1.0 mL 2x trypsin/EDTA (2x T/E) was added for all cell lines except HEK293 cells and HEK293-derived clonal cell lines which were detached with 1x T/E. After 3-5 min of incubation at 37 °C tryptic digestion was stopped by the addition of growth medium containing 10% (v/v) FCS and 1% (v/v) P/S. Cells were counted using a ViCell® XR Cell Viability Analyzer (Beckman Coulter,

Fullerton, CA, USA). For sub-cultivation, appropriate cell numbers were seeded in 75 cm^2 culture flasks adding 10.0 mL growth medium.

2.2.4 Freezing and thawing

For long term storage, cells were detached as described previously and resuspended in ice cold freezing medium (Table 6). Aliquots of 1.5 mL (equal to 2x10^6 cells) were added to cryovials. After an initial storage at -80 °C for 24 h, cryovials were transferred to liquid nitrogen for long term storage. For thawing, the content of a cryovial was dissolved in prewarmed culture medium. Through centrifugation (1,000 rpm, 5 min, 20 °C) excessive DMSO was removed by replacing freezing medium with fresh growth medium. Finally, the cell suspension was transferred to a culture flask and the medium was exchanged 24 h after thawing.

Table 6. Media for cell freezing

Freezing medium		Freezing medium	
MDA-MB-231, T24, HEK293, CRISPR VAT-1 k.o. clones		4T1-luc2, RAEW, U87	
DMEM	70% (v/v)	RPMI-1640	70% (v/v)
FCS	20% (v/v)	FCS	20% (v/v)
DMSO	10% (v/v)	DMSO	10% (v/v)

2.3 Transient transfection with small-interfering RNA (siRNA)

For silencing experiments, MDA-MB-231 and 4T1-luc2 cells were transfected with ON-TARGETplus SMARTpool small interfering RNA (siRNA) targeting human VAT-1 protein (Dharmacon, GE Healthcare, Munich, Germany) for 48 h using DharmaFECT™ transfection reagent according to manufacturer's protocol (Dharmacon, GE Healthcare, Munich, Germany). ON-TARGETplus non-targeting control siRNA (nt siRNA) served as control to determine baseline cellular responses in RNA interference experiments. siRNAs were resuspended according to Dharmacon instructions in 1x siRNA buffer (diluted from Dharmacon 5x siRNA buffer in RNase-free water) to a stock concentration of 20 µM and stored at -20 °C.

2.4 Genome editing using the CRISPR-Cas9 system

The CRISPR-Cas9 system was used to knock out VAT-1 in HEK293 cells by removing exon 2 of the gene following the procedure described by Ran *et al.*[62] using plasmid-based sgRNA delivery technique.

2.4.1 Guide RNA design

For the generation of single guide RNAs (sgRNAs) the CRISPOR-Tefor online designing tool was used as described previously.[63, 64] For experiments, the two highest ranked sgRNAs were used (Table 7).

Table 7. sgRNA sequences

sgRNA	Sequence
sgRNA-5'_1 top	5'-CACCGAAAGCACTTGAAATCGGGCT-3'
sgRNA-5'_1 bottom	5'-AAACAGCCCGATTTCAAGTGCTTTC-3'
sgRNA-5'_2 top	5'-CACCGTAGGGCAGCATGAAGTATTG-3'
sgRNA-5'_2 bottom	5'-AAACCGGCAACTACACAGCAGAGGC-3'
sgRNA 3' top	5'-CACCGCCTCTGCTGTGTAGTTGCCG-3'
sgRNA 3' bottom	5'-AAACCGGCAACTACACAGCAGAGGC-3'

2.4.2 Cloning and transformation of *E.coli*

To prepare the sgRNA-delivery plasmid construct, the sgRNAs were cloned into the eCas9_Puro2.0 plasmid (c = 455.9 ng/µL), which was kindly provided by Dr. Phuong Nguyen, via the BbsI restriction site using T4 DNA ligase according to the manufacturer's instructions (Thermo Scientific, Waltham, MA, USA). For this purpose, sgRNA oligomers were annealed using a PCR cycler (5 min at 95 °C, ramp down to 25 °C) and diluted 1:200 (v/v) in H_2O for further use (Table 8).

Table 8. sgRNA oligomer annealing mix

Reagent	Volume [µL]
sgRNA_top (100 µM)	1
sgRNA_bottom (100 µM)	1
T4 ligation buffer (10x)	1
H_2O	7

To insert the annealed sgRNA oligomers into the eCas9_Puro2.0 plasmid, the plasmid was digested for 30 min at 37 °C using a restriction enzyme mix (Table 9).

Table 9. Restriction enzyme mix

Reagent	Volume [µL]
eCas9_Puro2.0 plasmid (150 ng)	0.329
FastDigest green buffer (10x)	1.5
FastDigest Bpil restriction enzyme	1
H_2O	ad 15

For ligation of annealed sgRNA oligomers and digested plasmid, a ligation mix containing T4 DNA ligase was prepared and incubated at RT for 30 min (Table 10). Non-ligated plasmid was removed with PlasmidSafe™ ATP-Dependent DNase according to the manufacturer's protocol (Epicentre, Madison, WI, USA) by incubation at 37 °C for 30 min and 70 °C for 30 min (Table 11). Obtained plasmids were stored at -20 °C before transformation of *E.coli*.

Table 10. Ligation mix

Reagent	Volume [µL]
Restricted eCas9_Puro2.0 plasmid	10
Annealed sgRNA oligomers (diluted 1:200)	2
T4 ligation buffer (10x)	2
T4 DNA ligase	1
H_2O	5

Table 11. PlasmidSafe™ ATP-Dependent DNase mix

Reagent	Volume [µL]
Ligation product	11
PlasmidSafe buffer (10x)	1.5
ATP (25 mM)	0.6
PlasmidSafe™ ATP-dependent DNase	1
H_2O	ad 15

In order to replicate plasmid-DNA, competent DH5α-*E.coli* were transformed with the respective sgRNA plasmids. In brief, 3 µL of plasmid-DNA were added and *E.coli* were first kept on ice for 10 min before being heat-shocked at 42 °C for 45 s and returned to ice for 2 min. The bacterial

suspension was then plated on an agar plate with ampicillin and stored at 37 °C overnight. Afterwards, 3-5 colonies per plasmid were picked and amplified in 5 mL LB medium supplemented with 100 μg/mL ampicillin. Subsequently, plasmids were isolated using the QIAprep Spin Miniprep Kit (Qiagen, Hilden, Germany) according to the manufacturer's instructions. To validate correct insertion, plasmids were sequenced starting from the U6 promotor (U6-F-primer: 5'-GAGGGCCTATTTCCCATGATTCC-3') before selected plasmids were amplified and isolated using the QIAGEN plasmid Maxiprep Kit (Qiagen, Hilden, Germany) according to the manufacturer's protocol.

2.4.3 Transfection and evaluation of genome targeting efficiency

HEK293 were cultured in 6-well plates to a confluency of 70-80% before being transfected with respective plasmids using Lipofectamine™ 3000 (Thermo Scientific, Waltham, MA, USA) as described by the manufacturer. Transfection efficiency was monitored after 48 h using eGFP-plasmid, before puromycin (0.6 μg/mL) and blasticidin S (8.0 μg/mL) were added for another 72 h. After removal of selection media, cells were cultured in growth medium and allowed to recover. After reaching sufficient confluency, genome targeting efficiency of the different sgRNA pairs was assessed using T7 Endonuclease I (New England Biolabs, Ipswich, MA, USA) according to the manufacturer's instructions. Cells transfected with the sgRNA plasmid with the highest genome targeting efficiency were subjected to clonal selection.

2.4.4 Selection of clonal cell lines and knockout verification

To isolate clonal cell lines, single-cell dilution was performed by dissociation of cells via a cell strainer and dilution to a final concentration of 0.5 cells per 100 µL. Cells were plated in multiple 96-well plates and allowed to grow for 7 days. Wells were inspected under a microscope and wells that had been seeded with multiple cells were marked off. After expansion of colonies for 2-3 weeks they were transferred to 12-well plates and a sample of each colony was collected for DNA and whole cell protein isolation for verification of successful knockout. DNA was isolated with QuickExtract™ DNA Extraction Solution (Epicentre, Madison, WI, USA) according to the manufacturer's protocol.

Subsequently, successful deletion of exon 2 was verified by PCR product size analysis using primer pairs in which either both primers anneal outside of the deleted region, yielding a PCR product of specific length in case of successful knockout, or one primer anneals outside and one within the deleted region (no PCR product is to be expected) (Table 12). Knockout of VAT-1 in identified clones was additionally confirmed by sequencing and Western blot. Sequencing services, sequencing primers, cloning oligomers and PCR primers were provided by Eurofins Genomics GmbH (Ebersberg, Germany). Additionally to HEK293 WT cells, the clone cell line *CRISPR control* was isolated which was subjected to the complete CRISPR-Cas9 procedure, but did not result in successful knockout of VAT-1 and used as control in all experiments.

Table 12. Primers used for PCR product size analysis and sequencing

Primer	Sequence
Out-fwd primer	5'-GCTCAAACACACTTCTCCCG-3'
Out-rev primer	5'-CTCCCTACCCCCTCCCATAT-3'
In-fwd primer	5'-ATGTGGCAGGAAGAGGTGAC-3'
Out-rev primer	5'-CCATTCTCCTTCAGTGCCTC- 3'
Sequencing primer	5'-AACTGGAGCTGGAAAAGTGG-3'

2.5 Proliferation and viability assays

Depending on the cell line and purpose of the experiment different proliferation or viability assays were conducted and listed below.

2.5.1 Crystal violet proliferation assay

To determine the antiproliferative effect of Neocarzilins, 5.0×10^3 (MDA-MB-231, 4T1-luc2, T24) or 1.0×10^4 (RAEW, U87) cells were incubated in triplicate with the indicated concentrations of compounds for 72 h and stained with 0.5% crystal violet solution (Table 13) for 10 min. After careful washing with water to remove excess staining solution the plate was allowed to dry. Afterwards, crystal violet was redissolved with trisodium citrate solution (Table 13) to measure absorption at 550 nm at a SpectraFluor Plus™ plate reader (Tecan, Crailsheim, Germany). For statistical analysis,

values of the day zero control were subtracted, and results of each biological replicate were normalized to the corresponding DMSO control which was set to 100% proliferation.

Table 13. Solutions for crystal violet assay

Crystal violet solution		Trisodium citrate solution	
Crystal violet	0.5% (w/v)	0.1 M Trisodium citrate dihydrate	50% (w/v)
Methanol	20% (v/v)	Ethanol (95-98%)	50% (v/v)
H_2O		H_2O	

2.5.2 CellTiter-Blue® (CTB) viability assay

The metabolic activity of cells can be employed as an indicator for their viability. Therefore, CellTiter-Blue® (CTB) cell viability assay (Promega, Mannheim, Germany), which uses the indicator dye resazurin (Figure 8), was performed to measure the influence of NCA on the viability of HEK293 cells and CRISPR-Cas9 VAT-1 k.o. clones. CTB assay was chosen in the first place, since HEK293 cells are fairly adherent and therefore very sensitive to the washing protocol applied in crystal violet proliferation assay.
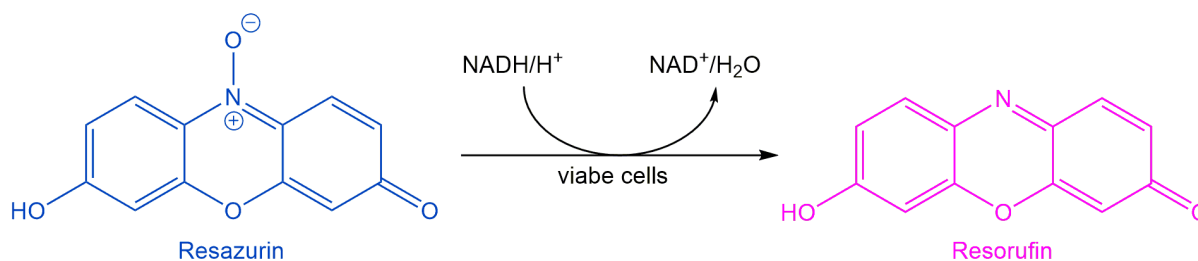
Figure 8. CellTiter-Blue® cell viability assay reaction. In viable cells resazurin is reduced to resorufin which emits fluorescence at 590 nm.

Experiments were carried out following the manufacturer's protocol (Promega, Mannheim, Germany). Therefore, 5.0×10^3 cells per well were seeded in 96-well plates and allowed to adhere overnight. Before cells were treated with NCA or DMSO for controls for 72 h, the initial metabolic activity was determined (day zero control). On day three, CellTiter-Blue® reagent was added 3 h before terminating the experiment to allow reduction of the indicator dye. Fluorescence at 590 nm was measured using a SpectraFluor Plus™ (Tecan, Crailsheim, Germany). For statistical analysis, values of the day zero

control were subtracted, and results of each biological replicate were normalized to the corresponding DMSO control which was set to 100% viability.

2.5.3 xCELLigence proliferation assay

To monitor the time-dependent effect of silencing of VAT-1 on cell proliferation, cellular growth was investigated using real-time impedance measurements performed on a xCELLigence dual purpose system (Roche Diagnostics, Penzberg, Germany) according to the manufacturer's instructions. MDA-MB-231 cells were silenced with siRNA targeting VAT-1 for 48 h as described in section 2.3. Prior to addition of cells, a background measurement was performed. Subsequently, 5.0×10^3 cells were seeded in triplicate in 100 µL growth medium in equilibrated 16-well E-plates (ACEA Biosciences, San Diego, CA, USA) and proliferation was monitored over 72 h. Through impedance measurement, the xCELLigence system evaluates the cell index, a dimensionless parameter, which is proportional to the cell number and recorded every hour. For interpretation of results, background values were subtracted, and data was normalized to the cell index at the starting point of treatment. Further data evaluation was performed with the RTCA xCELLigence software (ACEA Biosciences, San Diego, CA, USA). For statistical analysis, results of each biological replicate were normalized to the corresponding nt siRNA control which was set to 100% proliferation.

2.6 Migration and invasion assays

To measure the effect of Neocarzilins or silencing of VAT-1 protein on cell migration and invasion, different assays for endpoint- and time-dependent analysis of directed migration were performed.

2.6.1 Boyden chamber assay

To investigate the migratory potential of different cell lines after treatment with Neocarzilins or knockdown of VAT-1 protein via silencing, transwell migration/invasion assays using Boyden chamber inserts were performed. The assay uses a chemoattractant gradient and inserts with a permeable membrane of defined pore size which can be penetrated by migrating cells either directly

(migration assay) or after successful invasion into a layer of Matrigel® (VWR, Radnor, PA, USA) on top of the membrane (invasion assay). In detail, 4.0×10^5 cells were seeded in 6-well plates, allowed to adhere overnight and subsequently treated with indicated concentrations of compounds for 24 h or silenced with siRNA targeting VAT-1 under nutrient deprivation. HEK293 CRISPR-Cas9 VAT-1 k.o. clones were additionally treated with 10 µg/mL mitomycin for 2 h prior to harvest to inhibit proliferation. 1.6×10^5 cells (MDA-MB-231, 4T1-luc2) or 1.4×10^5 cells (HEK293, CRISPR-Cas9 VAT-1 k.o. clones) were resuspended in media without FCS and added on top of the Boyden chamber membrane (8 µm; Corning, New York, NY, USA) in duplicate. Culture medium containing 10% FCS (MDA-MB-231, 4T1-luc2) or fibroblast-conditioned medium (HEK293, CRISPR-Cas9 VAT-1 k.o. clones) was used as chemoattractant. After 4 h (MDA-MB-231), 6 h (4T1-luc2) or 42 h (HEK293, CRISPR-Cas9 VAT-1 k.o. clones) migrated cells were fixed and stained with crystal violet solution (Table 14) for 10 min. Non-migrated cells on top of the membrane were removed with a cotton swab. For invasion assays, membranes were coated with Matrigel® (VWR, Radnor, PA, USA) according to manufacturer's instructions. For every condition 5 pictures of the membrane were taken with an Axiovert 25 microscope (Zeiss, Oberkochen, Germany) and a Canon Eos 450 C camera (Canon, Krefeld, Germany) and cells were counted manually using ImageJ software (NIH, Bethesda, MD, USA). For statistical analysis, results of each biological replicate were normalized to the corresponding DMSO control which was set to 100% migration.

Table 14. Staining solution for Boyden chamber assay

Crystal violet solution	
Crystal violet	0.5% (w/v)
Methanol	20% (v/v)
H_2O	

2.6.2 Chemotaxis assay

Chemotaxis describes the directed migration of cells towards a chemoattractant. By seeding cells in an ibidi chemotaxis µ-slide (ibidi GmbH, Gräfelfing, Germany) the motility of living single cells can be monitored in real time by using inverted microscopy. Chemotaxis assay allows the investigation of general forward migration as well as its directness and velocity. In detail, 4.0×10^5 MDA-MB-231 cells were seeded in 6-wells, allowed to attach overnight and treated with NCA for 24 h in serum-free DMEM medium. Afterwards cells were detached and seeded in ibidi Chemotaxis µ-Slides (ibidi GmbH, Gräfelfing, Germany) at a concentration of 3.0×10^6 cells/mL in DMEM medium containing FCS for better adhesion. After cell attachment, channels were washed with serum-free DMEM medium and a FCS-gradient was established by filling one reservoir of the slide with FCS negative medium and the other with medium containing 10% FCS. Images were taken every 10 min for 20 h using a Nikon Eclipse Ti inverted microscope (Nikon, Düsseldorf, Germany) and the indicated migration parameters were calculated using the chemotaxis and migration tool Open Source Edition version 4.3.2 (ibidi GmbH, Gräfelfing, Germany).

2.6.3 xCELLigence migration assay

For real time monitoring of cell migration, a xCELLigence CIM-plate 16 was assembled and equilibrated according to manufacturer's protocol (ACEA Biosciences, San Diego, CA, USA). MDA-MB-231 cells were transfected with nt siRNA or siRNA targeting VAT-1 for 48 h as described in section 2.3. Cells were starved overnight, resuspended in medium without FCS and 4.0×10^4 cells were seeded in triplicate per 100 µL in the equilibrated CIM-plate. After cells were allowed to settle onto the bottom for 30 min at RT, the CIM-plate was placed into the xCELLigence instrument and migration towards growth medium containing 10% FCS as chemoattractant was monitored over 16 h. By impedance measurement, the xCELLigence device evaluates the cell index, a dimensionless parameter, which is proportional to the number of migrated cells. Data evaluation was performed with the RTCA xCELLigence software (ACEA Biosciences, San Diego, CA, USA). For statistical analysis,

results of each biological replicate were normalized to the corresponding nt siRNA control which was set to 100% migration

2.7   Plate-and-wash adhesion assay

To investigate the impact of NCA on cell adhesion of MDA-MB-231 cells to collagen I and fibronectin a plate-and-wash adhesion assay was performed. For this purpose, the protocol for cell-substrate adhesion assays by Martin J. Humphries[65] was adapted and optimized for MDA-MB-231 cells as well as for the used extracellular matrix ligands. In detail, 4.0×10^5 cells were seeded in 6-wells, allowed to attach overnight and subsequently treated with NCA for 24 h. On the day of stimulation an untreated 96-well plate was coated with 100 µL collagen I (5 µg/mL) or fibronectin (10 µg/mL) diluted in coating buffer (Table 15) overnight at 4 °C. Afterwards, the coating solution was removed, and the wells were washed with 100 µL PBS. Non-specific binding sites were blocked with 100 µL of 3% (w/v) BSA in PBS for 30-60 min at RT. Simultaneously, treated cells were washed once with PBS and incubated with 1 mL of a 2 µM calcein acetoxymethyl ester (calcein-AM) solution in PBS at 37 °C for 30 min. Calcein-AM is a cell-permeant non-fluorescent dye which is converted to green-fluorescent calcein in living cells by hydrolysis of acetoxymethyl ester through intracellular esterases. In this assay setup, calcein-AM staining was used for quantification of living cells. After incubation, suspensions of cells were centrifuged (1,000 rpm, 5 min, RT), the supernatants were discarded and the pellets once washed with PBS. After removal of PBS by another centrifugation step the cell pellets were resuspended in 1.5 mL FCS reduced medium (Table 15) and the cell density was adjusted to 4.0×10^4 cells/100 µL. To ensure optimal CO_2 equilibration as well as a recovery from the detachment and centrifugation process, cells were incubated for 10 min at 37 °C in falcon tubes without lid. Meanwhile, the previously coated and blocked 96-well plate was prepared for cell addition. The blocking solution was aspirated, and the wells were washed once with 100 µL PBS. Prior to cell addition, 100 µL PBS per well were added to minimize the formation of a meniscus, which leads to uneven distribution of cells on the bottom of the well. Subsequently, 4.0×10^4 cells in

100 µL were rapidly transferred to the coated wells in triplicate with a multichannel pipette and fluorescence of calcein at 485 nm was measured immediately for quantification of initial seeding density using a SpectraFluor Plus™ (Tecan, Crailsheim, Germany). Afterwards plates were incubated at 37 °C without lid for 25 min. Subsequently, medium containing non-adherent cells was carefully removed with a multichannel pipette and wells were washed twice with 100 µL PBS+Ca^{2+}/Mg^{2+}. To prevent attached cells from being detached due to an increased force of the stream of liquid in regular pipet tips with narrow bores, cut-off pipet tips were used. Finally, fluorescence of calcein at 485 nm was measured again using a SpectraFluor Plus™ (Tecan, Crailsheim, Germany). For statistical analysis, the fluorescent signal obtained for each well was normalized to the initial signal detected after plating and obtained values were normalized to the DMSO control which was set to 100%.

Table 15. Buffers and medium for plate-and-wash adhesion assay

Coating buffer		FCS reduced medium	
Tris-HCl (pH 9.0)	20 mM	FCS	0.1% (v/v)
NaCl	150 mM	HEPES buffer	25 mM
$MgCl_2$	2 mM	DMEM	
H_2O			

HEPES buffer	
NaCl	125 mM
KCl	3 mM
NaH_2PO_4 x H_2O	1.25 mM
$CaCl_2$ x 2 H_2O	2.5 mM
$MgCl_2$ x 6 H_2O	1.5 mM
Glucose	10 mM
HEPES	10 mM
H_2O	

2.8   Active Rac1 pulldown

To evaluate the effect of NCA-treatment on the activation level of the small Rho GTPase Rac1, the Active Rac1 Pull-Down and Detection Kit #16118 (Thermo Scientific, Waltham, MA, USA) was used according to the manufacturer's instructions. In detail, per condition 2.5 x 10^6 MDA-MB-231 cells

were seeded in 100 mm dishes, allowed to adhere overnight and treated with NCA for 24 h. Rac1 activation was induced by adding 100 ng/mL epidermal growth factor (EGF) for 5 min prior to harvest. Afterwards, the medium was removed, and cells were washed with ice-cold PBS before addition of the provided Lysis/ Binding/ Wash Buffer. Cells were scraped off, centrifuged (14,000 x g, 4° C, 15 min) and the supernatant was collected. After protein quantification by Pierce BCA assay as described in section 2.13.1, 1.5 mg of total protein were incubated with glutathione resin and GST-Pak1-PBD, which specifically binds to active (GTP-bound) Rac1. The reaction mixture was transferred to the provided spin cup with collection tube and incubated at 4 °C for 1 h under constant agitation. After three washing steps reducing sample buffer was added to the resin and the eluted samples were subjected to SDS-PAGE and Western blot analysis as described in section 2.13 using a Rac1 mouse monoclonal antibody provided by the manufacturer of the kit. Anti-mouse IgG_{2b}, HRP-linked antibody (1090-05; Southern Biotec, Birmingham, AL, USA) diluted 1:1,000 (v/v) in 1% (w/v) non-fat dry milkpowder (Blotto) was used as secondary antibody. For statistical analysis, results of each biological replicate were normalized to the corresponding DMSO control which was set to 1.0-fold Rac1 activation.

2.9 In vivo dissemination assay

The *in vivo* animal experiment was approved by the District Government of Upper Bavaria in accordance with the German animal welfare and institutional guidelines and performed by Dr. C. Atzberger and K. Loske. 16 female Balb/c "Balb/cOlaHsd" mice, six weeks old, purchased from Envigo (Huntingdon, Cambridgeshire, United Kingdom) were used. The mice were pretreated intraperitoneally with 10 mg/kg NCA or solvent (5% DMSO, 10% Kolliphor® EL, 85% PBS) three times (48, 24, and 0.5 h) before 1.0×10^5 4T1-luc2 cells were injected into the tail vein. Imaging of the mice after intraperitoneal injection of 6 mg luciferin/mouse was performed on day five after cell injection using the IVIS® Spectrum In Vivo Imaging System (PerkinElmer, Waltham, MA, USA). The tumor signal per defined region of interest was calculated with the Living Image 4.4 software (PerkinElmer, Waltham, MA, USA) as photons/second/cm2 (total flux/area).

2.10 Confocal imaging

2.10.1 Microtubule staining

For microtubule staining 1.0×10^4 MDA-MB-231 cells were seeded in 8-well ibiTreat µ-slides (ibidi GmbH, Gräfelfing, Germany) and allowed to adhere overnight. Cells were stimulated with the indicated concentration of NCA for designated periods of time. Subsequently, cells were washed once with ice-cold PBS+Ca^{2+}/Mg^{2+} and extraction buffer (Table 16) was added for 2 min prior to the addition of 5% glutaraldehyde. After 10 min incubation, the suspension was discarded and a 0.1% (w/v) $NaBH_4$ in PBS solution was added for 7 min. Cells were washed three times with PBS, blocked for 10 min with 0.2% (w/v) BSA in PBS and incubated for 30 min with anti-α-tubulin antibody (ab18251; Abcam, Cambridge, UK) diluted 1:400 in 0.2% (w/v) BSA in PBS. Thereafter, cells were washed three times with PBS and incubated with AlexaFluor® 488 secondary antibody (A-11001; Molecular Probes, Eugene, OR, USA) diluted 1:200 (v/v) in 0.2% (w/v) BSA in PBS for 2 h at RT in the dark. For nuclei staining, Hoechst 33342 was added at a final concentration of 5 µg/mL for 30 min and cells were finally washed three times with PBS for 10 min and one time with H_2O to remove access antibody solution. Each well was sealed with FluorSave™ reagent mounting medium (Merck, Darmstadt, Germany) and glass coverslips. Images were taken with a Zeiss LSM 510 Meta confocal laser scanning microscope (Zeiss, Oberkochen, Germany) and analyzed using Zeiss LSM Image Browser software (Zeiss, Oberkochen, Germany) and Image J (NIH, Bethesda, MD, USA).

Table 16. Extraction buffer for microtubule staining

Extraction buffer 5x	
PIPES	400 mM
$MgCl_2$	5 mM
EGTA	5 mM
Triton-X	0.5% (v/v)
H_2O	

2.10.2 Immunofluorescence staining of migrating cells

Immunofluorescence staining of migrating cells was performed for localization of the small Rho GTPase Rac1 as well as investigation of colocalization of VAT-1 and Talin-1. For this purpose, 7.5×10^4 T24 cells per well were seeded in 8-well ibiTreat µ-slides (ibidi GmbH, Gräfelfing, Germany) and allowed to adhere overnight. After treatment of cells with NCA for 24 h, confluent cells were wounded with a pipette tip, washed twice with PBS and treated as indicated for additional 8 h with NCA. Afterwards, cells were fixed with 4% (v/v) paraformaldehyde in PBS for 10 min, permeabilized with 0.2% (v/v) Triton X-100 in PBS for 10 min and blocked with 1% (w/v) BSA in PBS for 2 h at RT. Depending on the experimental purpose, cell were either incubated with a 1:200 (v/v) dilution of Rac1 antibody (05-389; Upstate, Lake Placid, NY, USA) in 1% (w/v) BSA in PBS or with a mixture of VAT-1 (sc-515705; Santa Cruz, Dallas, TX, USA) and Talin-1 (#4021, Cell Signaling, Danvers, MA, USA) primary antibodies diluted 1:100 (v/v) in 1% (w/v) BSA in PBS overnight at 4 °C under gentle agitation. Subsequently, cells were washed three times with PBS and incubated with AlexaFluor® 647 and/or 488 (647: A-21443; 488: A-11001, Thermo Scientific, Waltham, MA, USA) secondary antibodies diluted 1:200 (v/v) together with rhodamine/phalloidin diluted 1:300 (v/v) in 1% (w/v) BSA in PBS for 2 h at RT in the dark. To stain nuclei, Hoechst 33342 was added at a final concentration of 5 µg/mL for 30 min and cells were finally washed three times with PBS for 10 min and one time with H_2O. Cells were covered with FluorSave™ reagent mounting medium (Merck, Darmstadt, Germany) and glass coverslips. Images were taken with a Leica SP8 confocal laser scanning microscope (Leica, Wetzlar, Germany) and analyzed using Leica LAS X software (Leica, Wetzlar, Germany) and Image J (NIH, Bethesda, MD, USA).

2.11 Flow cytometry

All FACS experiments were performed on a FACS Canto™ II instrument (BD Biosciences, Franklin Lakes, NJ, USA) using BD FACSDiva™ software (BD Biosciences, Franklin Lakes, NJ, USA) measuring 1.0×10^4 events per sample with medium flow rate.

2.11.1 Apoptosis and cell cycle assay

Apoptosis rate and cell cycle analysis were determined by propidium iodide (PI) staining and flow cytometry according to Nicoletti et al.[66, 67] In brief, 4.0×10^4 cells (MDA-MB-231 cells) or 2.0×10^4 cells (4T1-luc2, HEK293, CRISPR VAT-1 k.o. clones) were seeded in 24-well plates and allowed to adhere overnight. For determination of apoptosis cells were treated with indicated concentrations of NCA for 24 h or 72 h or transfected with nt siRNA or siRNA targeting VAT-1 for 48 h as described in section 2.3, whereas cells for cell cycle analysis were treated for 48 h. Cells were harvested on ice and permeabilized in fluorochrome solution (Table 17) for at least 30 min at 4 °C. The fluorescence intensity was recorded at Ex 488 nm/ Em 585 nm and is indicative for the extent of DNA fragmentation of the cells, which can be used to determine the rate of apoptosis. PI intercalates in intact DNA structures, however, in apoptotic cells the DNA is fragmented, therefore less PI is taken up resulting in lower fluorescence signals (sub-G1 peak). For the determination of the percentage of apoptotic cells and the populations in different cell cycle phases the FlowJo 7.6.5 analysis software using the Watson pragmatic model for cell cycle analysis (Tree Star, Ashland, OR, USA) was used.

Table 17. Fluorochrome solution

Fluorochrome solution	
Propidium iodide	50 µg/mL
Sodium citrate	0.1% (w/v)
Trition-X 100	0.1% (v/v)
PBS	

2.11.2 Assessment of integrin expression and activation

To investigate the influence of NCA on the surface expression of integrin β1, β3, and α5 as well as the activation level of integrin β1 in MDA-MB-231 cells antibody staining and FACS analysis was performed. In detail, 2.0×10^4 MDA-MB-231 cells were seeded in 12-well plates, allowed to adhere overnight and treated with indicated concentrations of NCA for 24 h. For harvesting, cells were washed once with PBS and subsequently incubated with 1 mL Gibco® Versene solution (Thermo Scientific, Waltham, MA, USA) at 37 °C for 30 min for non-enzymatic cell detachment. Subsequently, the cell suspension was transferred to FACS tubes and incubated with 500 µL 4% PFA in PBS for 10 min for fixation. Cells were washed twice by adding 1 mL FACS staining buffer (Table 18), centrifugation (400 x g, 4° C, 5 min) and removal of the supernatant. Primary antibodies against total integrin β1, α2β1, β3, and α5 as well as active integrin β1 were added according to Table 19 and incubated for 45 min at RT while gently shaking. Excess primary antibody was removed by washing twice with 1 mL FACS staining buffer, subsequent centrifugation (400 x g, 4° C, 5 min) and removal of the supernatant. Appropriate AlexaFluor® 488-conjugated secondary antibody was added according to Table 19 and samples were incubated for 45 min at 4 °C protected from light. Afterwards, cells were washed twice with 1 mL FACS staining buffer as described above and resuspended in 250 µL FACS staining buffer. FACS analysis was directly performed by measuring the fluorescence intensity at Ex 488 nm/ Em 530 nm. Data was analyzed using the FlowJo 7.6.5 analysis software (Tree Star, Ashland, OR, USA).

Table 18. FACS staining buffer

FACS staining buffer	
EDTA	20 mM
FCS	2% (v/v)
PBS	

Table 19. Antibodies used for FACS analysis of integrins

Name	Catalogue	Manufacturer	Concentration
Integrin α2β1	ab30483	Abcam	5 µg/mL
Integrin α5	ab23589	Abcam	5 µg/mL
Integrin β1 - active	ab30394	Abcam	5 µg/mL
Integrin β1 - total	sc-53711	Santa Cruz	2 µg/mL
Integrin β3	555752	BD Biosciences	2 µg/mL
AlexaFluor® 488, goat anti-mouse IgG	A-11001	Molecular Probes	5 µg/mL
Mouse IgG$_1$ kappa light chain isotype control	ab18443	Abcam	5 µg/mL

2.12 Co-Immunoprecipiation (co-IP)

For investigation of protein-protein interaction of VAT-1 and Talin-1, co-immunoprecipiation (co-IP) experiments were performed. In detail, 2.0 x 10^6 MDA-MB-231 cells were seeded in 100 mm dishes, allowed to adhere overnight and treated with NCA for 24 h. Subsequently, cells were washed with ice-cold PBS and lysed by incubation with co-IP lysis buffer (Table 20) for 30 min at 4 °C under constant agitation. After centrifugation (10,000 x g, 4° C, 10 min) the supernatant was collected, and the protein amount was quantified by Pierce BCA assay as described in section 2.13.1. Next, 1 mg of total protein was adjusted to 1 mL final volume with co-IP lysis buffer and pre-incubated with 2 µg VAT-1 pull-down antibody (ABIN2443750; antibodies online, Aachen, Germany) for 2 h at 4 °C under constant agitation before 40 µL of resuspended protein A/G PLUS-Agarose (sc-2003; Santa Cruz, Dallas, TX, USA) were added. Samples were incubated overnight at 4 °C and co-IP was subsequently performed according to the manufacturer's instructions (sc-2003; Santa Cruz, Dallas, TX, USA) using PBS for washing. A specific isotype control antibody served as control of heavy and light chains (#2729; Cell Signaling, Danvers, MA, USA). The amount of VAT-1 (antibody ABIN2443750; antibodies online, Aachen, Germany) and Talin-1 (antibody 4021; Chemicon International, Temecula, CA, USA) in eluted fractions was analyzed via SDS-PAGE and Western blot as described in section 2.13. For statistical analysis, results of each biological replicate were normalized to the corresponding DMSO control which was set to 1.0-fold VAT-1:Talin-1 ratio.

Table 20. Co-IP lysis buffer

Co-IP lysis buffer	
Tris HCl (pH 8.0)	50 mM
NaCl	150 mM
Triton-X	1% (v/v)
Igepal CA-630 (NP-40)	1% (v/v)
H_2O	
Before use:	
PMSF	1 mM
Complete® protease inh.	1:10

2.13   Immunoblotting

2.13.1   Sample preparation and protein quantification

To analyze cellular protein levels SDS-polyacrylamide gel electrophoresis (SDS-PAGE) and Western blot was performed. For sample preparation cells were washed with ice-cold PBS prior to addition of NP-40 lysis buffer or phospho lysis buffer for investigation of phosphorylated proteins (Table 21). Samples were frozen at -80 °C for a minimum of 30 min. Subsequently, cells were scraped off, transferred to an Eppendorf tube and centrifuged (14,000 rpm, 10 min, 4 °C) for removal of cell debris. To ensure equal amount of protein during further investigation, the protein concentration was measured using bicinchoninic acid (BCA) assay as described previously[68]. In brief, 10 µL of protein sample as well as bovine serum albumin (BSA) standards (0-2,000 µg/mL) were transferred to a 96-well plate in triplicate and diluted with 190 µL BC assay reagent. The reduction of Cu^{2+} to Cu^+ leading to BCA chelate formation and a purple-colored product is proportional to the amount of protein. After incubation at 37 °C for 30 min absorbance at 550 nm was measured using a SpectraFluor Plus™ (Tecan, Crailsheim, Germany). Sample protein concentration was determined by linear regression using BSA standards. Western blot samples were prepared by mixing a lysate volume corresponding to 30-40 µg protein with 1:5 (v/v) of 5x SDS sample buffer and 1x SDS sample buffer (Table 21) to a total volume of 40 µl. Samples were boiled at 95 °C for 5 min and stored at -20 °C until further use.

Table 21. Buffers for cell lysis and sample preparation used for Western blot

NP-40 lysis buffer		Phospho lysis buffer	
NaCl	150 mM	NaCl	137 mM
Igepal CA-630 (NP-40)	1% (v/v)	Triton-X	1% (v/v)
Tris HCl	50 mM	Tris Base	20 mM
Sodium deoxycholate	0.25% (w/v)	$Na_4P_2O_7$ x 10 H_2O	2 mM
EGTA	1 mM	EDTA	2 mM
H_2O		Na-Glycerolphosphate	20 mM
Before use:		NaF	10 mM
PMSF	1 mM	H_2O	
Complete® protease inh.	1:10	Before use:	
		PMSF	1 mM
		Complete® protease inh.	1:10
		Na_3VO_4	2 mM

5x SDS sample buffer		1x SDS sample buffer	
Tris HCl (pH 6.8)	3.125 M	5x SDS sample buffer	20% (v/v)
Glycerol	50% (v/v)	H_2O	
SDS	5% (w/v)		
DTT	2% (w/v)		
Pyronin Y	0.025% (w/v)		
H_2O			

2.13.2 SDS-polyacrylamide gel electrophoresis (SDS-PAGE)

For protein separation by molecular weight, discontinuous SDS-PAGE was performed as described by Laemmli[69]. In brief, equal amounts of adjusted protein samples were loaded on discontinuous polyacrylamide gels, which consist of a separation and a stacking gel (Table 22) and separated using a Mini PROTEAN 3 electrophoresis chamber (Bio-Rad, Munich, Germany). The polyacrylamid concentration was typically 12% but was adjusted in a range of 10-15% according the molecular weight of the protein of interest to guarantee optimal separation. At the start of the electrophoresis the proteins were stacked at a current of 100 V for 21 min before being separated at 200 V for 45 min in the second step. The total protein amount of each lane was quantified using stain-free technology[70] using a ChemiDoc™ touch imaging system (Bio-Rad, Munich, Germany). The molecular weight of the

resulting protein bands was assessed by comparison with the Page Ruler™ Prestained Protein Ladder or the PageRuler™ Plus Prestained Protein Ladder (Thermo Scientific, Waltham, MA, USA).

Table 22. Gels and buffer for SDS-PAGE

Stacking gel	
Rotiphorese® Gel 30	17% (v/v)
Tris HCl (pH 6.8)	125 mM
SDS	0.1% (w/v)
TEMED	0.2% (v/v)
APS	0.1% (w/v)
H$_2$O	

Separation gel 12%	
Rotiphorese® Gel 30	40% (v/v)
Tris HCl (pH 8.8)	375 mM
SDS	0.1% (w/v)
TEMED	0.1% (v/v)
APS	0.05% (w/v)
TCE	0.05% (v/v)
H$_2$O	

Electrophoresis buffer	
Tris base	4.9 mM
Glycin	38 mM
SDS	0.1% (w/v)
H$_2$O	

2.13.3 Protein transfer and detection

After separation, proteins were transferred to 0.2 µm polyvinylidene difluoride (PVDF) membranes (Amersham Bioscience, Freiburg, Germany) by electro tank blotting[71] after activation of membranes with methanol. Protein transfer was performed at 100 V and 4 °C for 90 min using a Mini Trans-Blot® system (Bio-Rad, Munich, Germany) filled with 1x tank buffer (Table 23). To block unspecific binding sites, membranes were incubated with 5% non-fat dry milkpowder (Blotto) for 2 h before incubation with the primary antibody (Table 24) overnight at 4 °C. Subsequently, membranes were washed four times with TBS-T (Table 26) in order to remove excess primary antibody solution, before incubation with an appropriate HRP-conjugated secondary antibody (Table 25) for 2 h at RT. Membranes were washed three times with TBS-T and once with H$_2$O before chemiluminescence was detected using ECL solution (Table 26) and a ChemiDoc™ touch imaging system (Bio-Rad, Munich, Germany). Western blot data was analyzed using Image Lab 5.2 (Bio-Rad, Hercules, CA, USA).

Table 23. Tank buffer used for proteins transfer

5x Tank buffer		1x Tank buffer	
Tris base	240 mM	5x Tank buffer	20% (v/v)
Glycin	195 mM	Methanol	20% (v/v)
H_2O		H_2O	

Table 24. Primary antibodies for Western blot

Name	Species	Catalogue	Manufacturer	Dilution
Gelsolin	Rabbit IgG	12953	Cell Signaling Technologies	1:1,000
Rac1	Mouse IgG$_{2b}$	05-389	Upstate	1:1,000
Talin-1	Mouse IgG$_1$	MAB1676	Chemicon International	1:1,000
Talin-1	Rabbit IgG	4021	Cell Signaling Technologies	1:1,000
Thrombospondin-1	Rabbit IgG	37879	Cell Signaling Technologies	1:1,000
VAT-1	Mouse IgG$_{2a}$	ab89138	Abcam	1:1,000
VAT-1	Mouse IgG$_{2b}$	sc-515705	Santa Cruz	1:500
VAT-1	Rabbit IgG	SAB1100727	Sigma Aldrich	1:1,000
VAT-1	Goat polycl.	sc-107348	Santa Cruz	1:200
VAT-1	Rabbit polycl.	ABIN2443750	Antibodies online	1:1,000
Vinculin	Mouse IgG$_{2a}$	sc-25336	Santa Cruz	1:1,000

Table 25. Secondary antibodies for Western blot

Name/Species	Catalogue	Manufacturer	Dilution
HRP, donkey-anti-goat IgG	ab97120	Abcam	1:1,000
HRP, goat-anti-mouse IgG$_1$	ab97240	Abcam	1:1,000
HRP, goat-anti-mouse IgG$_{2a}$	1080-05	Southern Biotec	1:1,000
HRP, goat-anti-mouse IgG$_{2b}$	1090-05	Southern Biotec	1:1,000
HRP, goat-anti-rabbit IgG	172-1019	Bio-Rad	1:1,000

Table 26. Solutions for protein visualization

ECL solution		TBS-T	
Tris (pH 8.5)	100 mM	Tris base (pH 8.0)	24.8 mM
Luminol	2.5 mM	Glycin	190 mM
Coumaric acid	1 mM	Tween 20	0.1% (v/v)
H_2O_2	17 µM	H_2O	
H_2O			

2.14   Statistical analysis

Results of at least three independent experiments (biological replicates, each performed in two or three technical replicates) are expressed as mean ± SEM or as percentage value. Statistical analysis was performed using GraphPad Prism 7 (GraphPad Software, San Diego, CA, USA) using either two-tailed unpaired Student's t test *P < 0.033, **P < 0.002, ***P < 0.001, or one-way ANOVA, Dunnett's test, *P < 0.033, **P < 0.002, ***P < 0.001 compared with DMSO control.

RESULTS

3 Results

3.1   Neocarzilins reduce cancer cell proliferation in various cell lines

In 1992 Nozoe *et al.* revealed a potent cytotoxic activity for NCA against K562 chronic myelogenous leukemia cells (IC_{50} of 185 nM).[42] However, up to date no further investigations into the antitumor activity of the Neocarzilins have been pursued. To gain more insight into the potential of this interesting compound class we performed crystal violet assays to determine the antiproliferative effect of all members of the Neocarzilin family (NCA, NCA', NCB, NCC) as well as the activity-based probe NC-1 (Figure 9) used for target identification experiments in a panel of cancer cell lines. NCA showed IC_{50} values ranging from about 300 to 800 nM for different cancer cell lines, affirming previous literature data (Figure 10 A-C).[42] In comparison, NCA', NCB, and NCC showed less pronounced effects with IC_{50} values ranging from about 1-6 µM for human MDA-MB-231 cells (Figure 10 A) and murine 4T1-luc2 cells (Figure 10 B). Whereas NCA' and NCB showed comparable potency, NCC emerged as the least active compound. The antiproliferative activity of the Neocarzilin probe NC-1 was significantly reduced in MDA-MB-231 and 4T1-luc2 cells (IC_{50}'s of 24-34 µM) compared to NCA (Figure 10 D).
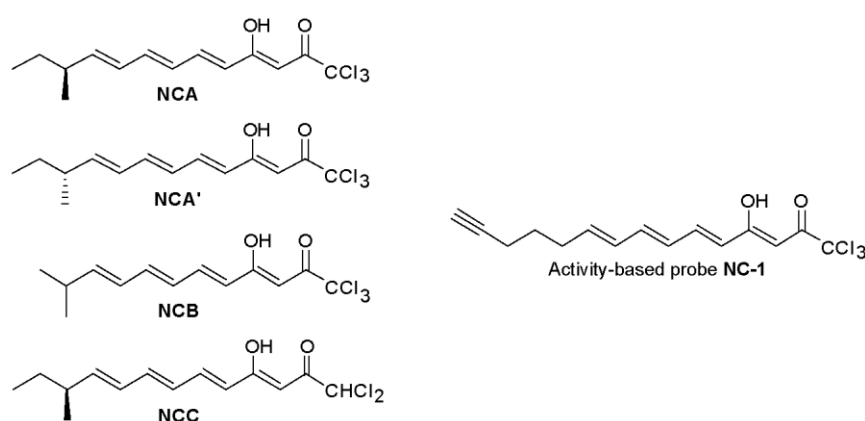
Figure 9. Chemical structure of Neocarzilins and the activity-based probe NC-1 used for ABPP.
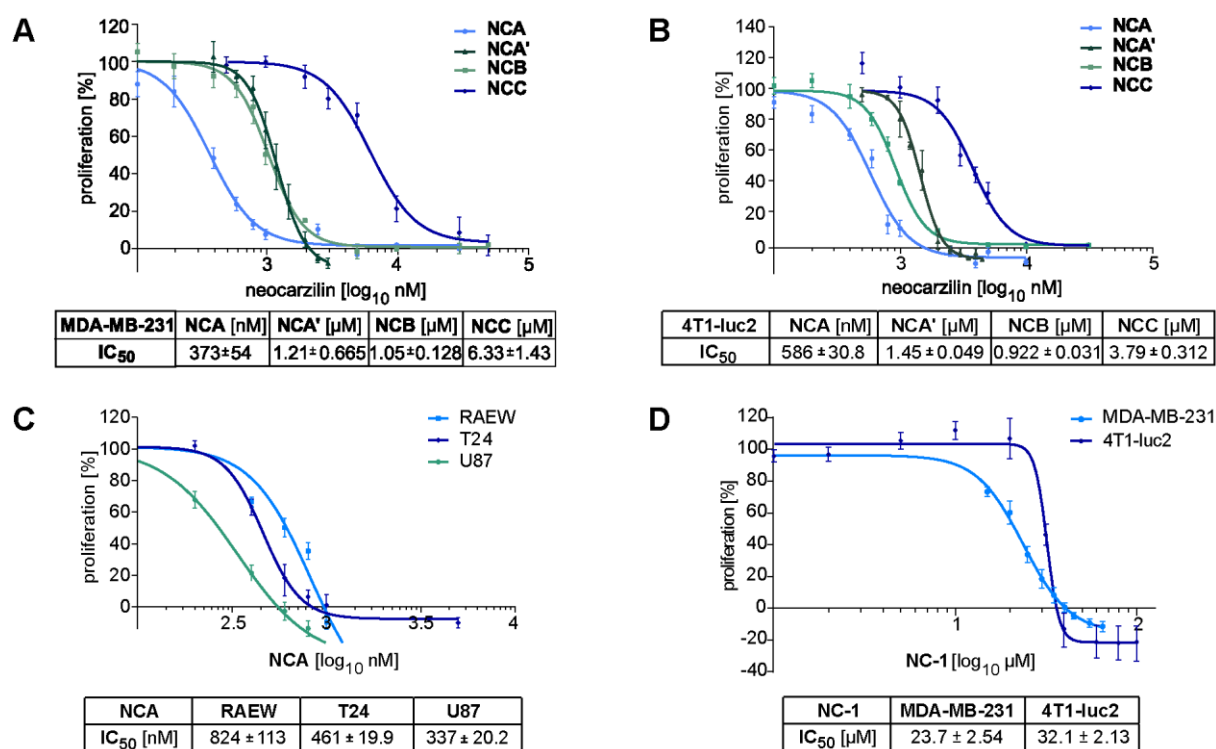
Figure 10. Antiproliferative effects of Neocarzilins in different cancer cell lines. (A, B) Proliferative capacity of human breast adenocarcinoma MDA-MB-231 cells (A) and murine breast cancer 4T1-luc2 cells (B) treated with NCA, NCA', NCB and NCC and IC$_{50}$ values determined by crystal violet staining after 72 h. **(C)** The antiproliferative effect of NCA on T24 human bladder carcinoma cells and the glioblastoma cell lines RAEW and U87 was determined by crystal violet staining after 72 h. **(D)** Proliferative capacity of human MDA-MB-231 and murine 4T1-luc2 breast cancer cells treated with the activity-based probe NC-1 determined by crystal violet staining after 72 h. **(A-D)** Bars represent the mean ± SEM of at least three independent experiments performed in triplicate.

3.2 Neocarzilin A induces apoptosis without influencing the cell cycle

Since NCA showed the strongest antiproliferative effect, we further characterized it by investigating its capability to induce apoptosis in human MDA-MB-231 and murine 4T1-luc2 cells according to Nicoletti *et al.*[66, 67] After 24 h and 48 h treatment, NCA induced apoptosis only at high concentrations in MDA-MB-231 cells (Figure 11 A). However, incubation for 72 h resulted in strong induction of apoptosis starting around 2.0 µM NCA (Figure 11 A). 4T1-luc2 cells generally showed a higher sensitivity towards NCA treatment indicated by elevated apoptosis starting already around 1.5 µM NCA after 24 h and a strong increase of apoptotic cells at 3.0 µM NCA after 48 h and 72 h incubation (Figure 11 B). In contrast, the probe NC-1 had no apoptotic effect on MDA-MB-231 cells after 24 h and 48 h incubation with concentrations up to 10 µM (Figure 11 C). Of note, NCA had no effect on cell cycle progression and microtubule network organization in MDA-MB-231 cells (Figure 11 D, E).
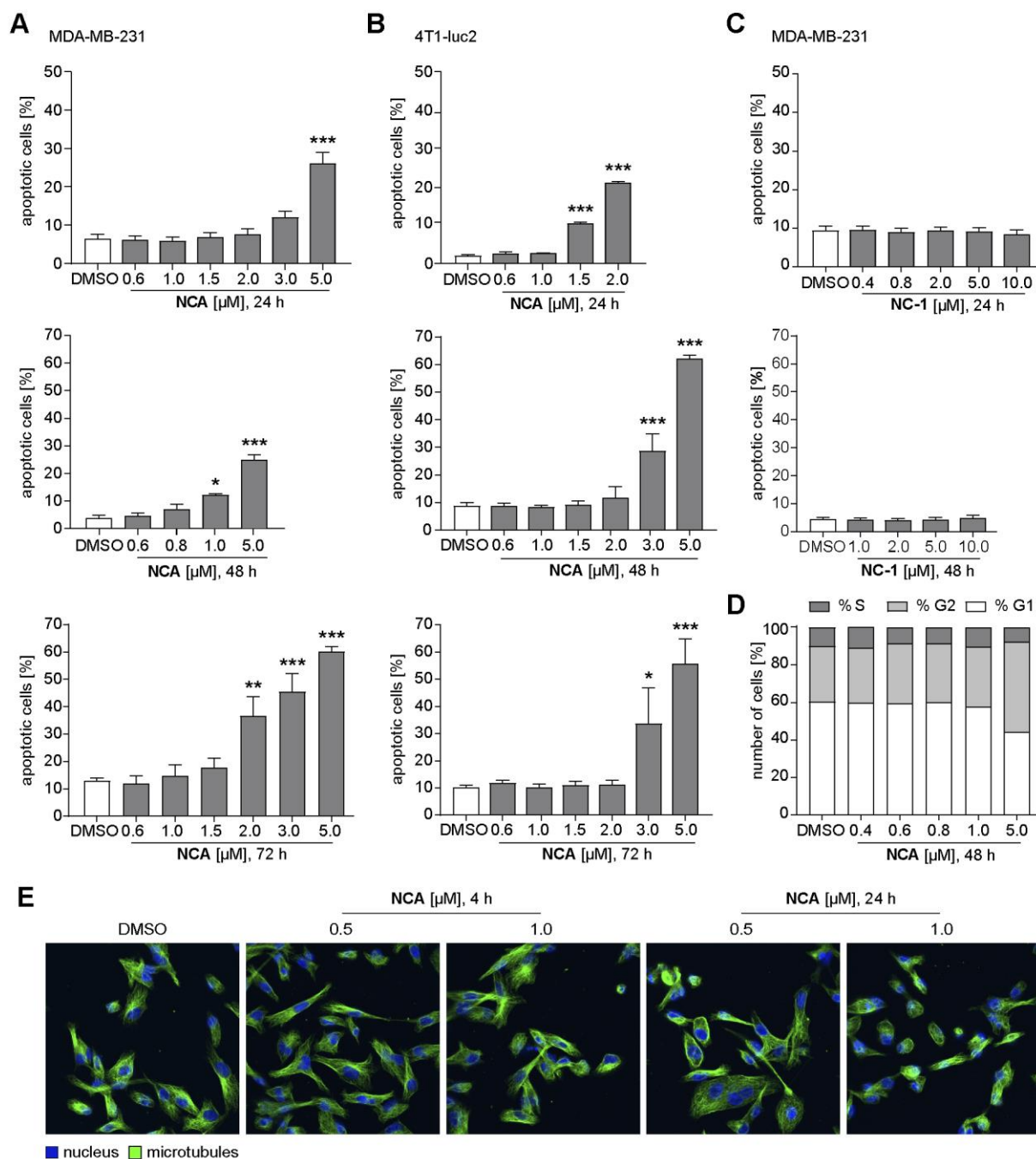
Figure 11. Effect of NCA on apoptosis and cell cycle. (A-B) MDA-MB-231 (A) or 4T1-luc2 cells (B) were treated with indicated concentrations of NCA for 24 h, 48 h or 72 h. Cells were permeabilized and stained with propidiumiodide using the method described by Nicoletti *et al.*[66, 67]. The percentage of dying cells was determined by flow cytometry. **(C)** The apoptotic effect of NC-1 on MDA-MB-231 cells was analyzed using propidiumiodide using the method described by Nicoletti *et al.*[66, 67] after 24 h and 48 h. The percentage of dying cells was determined by flow cytometry. **(A-C)** Bars represent the mean ± SEM of at least three independent experiments performed in triplicate, one-way ANOVA, Dunnett's test, *P < 0.033, **P < 0.002, ***P < 0.001 compared with DMSO control. **(D)** The effect of NCA on the cell cycle progression of MDA-MB-231 cells was determined by propidiumiodide staining using the method described by Nicoletti *et al.*[66, 67] The cell cycle analysis was performed with the FlowJo 7.6.5 program using the Watson pragmatic model. **(E)** Confocal images of MDA-MB-231 cells stimulated with NCA or DMSO as indicated. α-Tubulin (green) and nuclei (blue) were visualized by immunocytochemistry. Representative images out of three independent experiments are shown.

3.3 Neocarzilin A significantly reduces cancer cell motility

3.3.1 Cell migration and invasion are inhibited upon Neocarzilin A treatment

Targeting cell viability to fight cancer presents the major approach in cancer medicine. However, targeting cancer cell migration can present a supportive strategy to control metastatic spread of cancer. Therefore, we have investigated the effect of the Neocarzilins on cell migration and invasion *in vitro* as well as tumor cell dissemination *in vivo*. NCA significantly reduced the migration capacity of highly invasive human triple negative breast adenocarcinoma MDA-MB-231 cells, whereas NCA', NCB, and NCC only showed minor antimigratory effects (Figure 12 A, B). In murine 4T1-luc2 cells the same trend was observed although migration was inhibited less effectively compared to MDA-MB-231 cells (Figure 12 C). In contrast to proliferation inhibition, where the activity-based probe NC-1 showed strongly reduced activity, its effect on cell migration of MDA-MB-231 cells was only slightly reduced compared to NCA (Figure 12 D). Moreover, the antimigratory effect of NCA was confirmed in a Chemotaxis assay in which the motility of single cells can be monitored in real time by using inverted microscopy. NCA significantly reduced the directed migration of MDA-MB-231 cells towards FCS as chemoattractant which is defined by the forward migration index (Figure 12 E). Furthermore, the treatment resulted in less directed cell migration towards FCS (Figure 12 E).

The inhibitory effect of NCA was not only limited to cell migration, but was also present in cell invasion experiments. NCA reduced the invasiveness of highly invasive MDA-MB-231 cells in a Boyden chamber assay setup using Matrigel® coated transwell inserts (Figure 13 A). For investigation of the *in vivo* efficacy of NCA, a tumor cell dissemination assay was performed by Dr. Carina Atzberger and Kerstin Loske by injecting 4T1-luc2 cells into the tail vein of Balb/c mice as previously described.[72] After 5 days, luciferase tagged cells were located by bioluminescent imaging of the mice. Treatment with 10 mg/kg of NCA led to a clear trend towards reduced tumor cell dissemination into the mouse lungs compared to solvent control treated animals (Figure 13 B). However, due to two outliers within the control group, results were not significant. Of note, a suitable safety profile of NCA

can be presumed, since the body weight of the mice increased evenly in both groups throughout the

experiment (Figure 13 B).
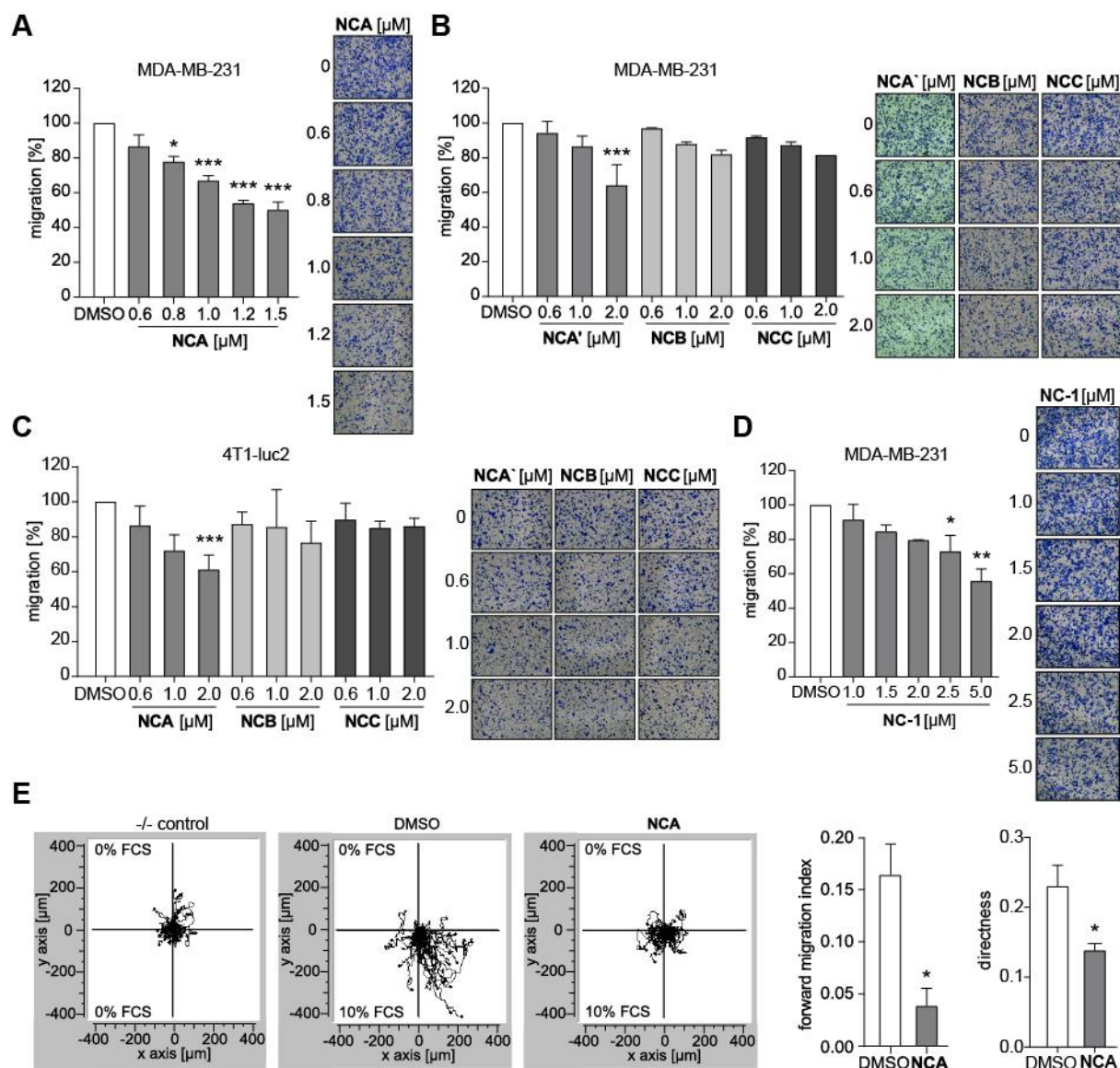
Figure 12. Inhibitory effect of NCA on cancer cell migration. (A, B) Transwell migration (4 h) of MDA-MB-231 cells pretreated with NCA (A), NCA', NCB or NCC (B) for 24 h determined by Boyden chamber assay. **(C)** Antimigratory effect of NCA, NCB or NCC on 4T1-luc2 cells after pretreatment for 24 h and migration time of 6 h determined by Boyden chamber assay. **(D)** Inhibition of transwell migration (4 h) of MDA-MB-231 cells pretreated with NC-1 for 24 h determined by Boyden chamber assay. **(A-D)** Bar diagrams showing the number of migrated cells normalized to the control as mean ± SEM of at least three independent experiments performed in duplicate are presented, one-way ANOVA, Dunnett's test, *$P < 0.033$, **$P < 0.002$, ***$P < 0.001$ compared with DMSO control. **(E)** Trajectory blots and forward migration index as measure of directed chemotactic migration of MDA-MB-231 cells towards FCS as chemoattractant as well as directness of migration after preincubation with NCA for 24 h determined by Chemotaxis assay. 30 cells per condition were monitored over 20 h. Bars represent the mean ± SEM of four independent experiments, two-tailed unpaired Student's t test, *$P < 0.033$.
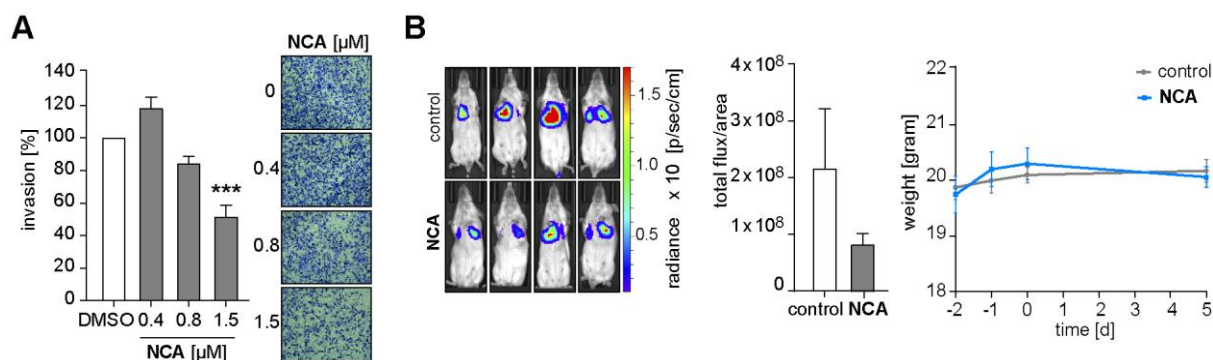
Figure 13. Reduction of cell invasion and tumor cell dissemination by NCA. (A) The effect of NCA on the invasiveness of MDA-MB-231 cells was determined via Boyden chamber assay using Matrigel®-coated membrane inserts. The bar diagram shows the number of invasive cells normalized to the control. Bars represent the mean ± SEM of at least three independent experiments performed in duplicate, one-way ANOVA, Dunnett's test, ***$P < 0.001$ compared with DMSO control. **(B)** Dissemination of 4T1-luc2 cells injected into the tail vein of control and NCA-treated Balb/c mice into the lungs and bodyweight changes in control and NCA-treated mice. Representative *in vivo* bioluminescent images on day 5 are shown. Bar diagram shows corresponding signal intensities with bars representing the mean ± SEM of 8 mice, two-tailed unpaired Student's t test, not significant.

3.3.2 Rac1 activation and localization in migrating cells is altered by Neocarzilin A

The small Rho GTPase Rac1 is a key player in cell migration by triggering actin polymerization and formation of lamellipodia at the leading edge of migrating cells.[73] Under pathological conditions activation of Rac1 can induce invasion and metastasis by augmenting migration. To investigate the effect of NCA on the activation of Rac1, which is active in the GTP-bound state, we performed a Rac1-GTP pulldown assay after inducing Rac1 activation via epidermal growth factor (EGF) addition. We were able to show that NCA treatment significantly reduced Rac1 activation (Figure 14 A). Moreover, confocal imaging revealed that fewer lamellipodia were formed and that Rac1 was no longer localized at the leading edge of migrating cells upon NCA treatment (Figure 14 B).
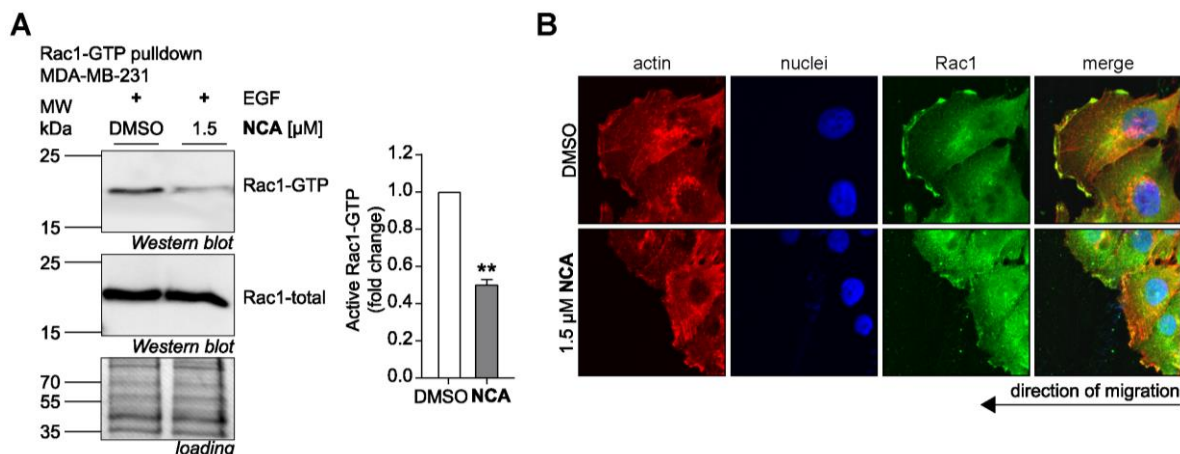
Figure 14. Influence of NCA on Rac1 activation and localization in migrating cells. (A) Active Rac1 pulldown assay was conducted upon 5 min EGF stimulation (100 ng/mL). A representative experiment out of three independent experiments is shown. Amount of Rac1-GTP determined by Western blot was normalized to total Rac1 and results were normalized to the DMSO control. Bars represent the mean ± SEM of three independent experiments, two-tailed unpaired Student's t test, **P < 0.002. **(B)** T24 cells treated with NCA were engaged in a Scratch assay and stained for Rac1 and F-actin. Nuclei were stained with Hoechst 33342. Representative images out of three independent experiments are shown.

3.3.3 Neocarzilin A activates integrin β1 and enhances cell-matrix adhesion

Adhesion of cells to the ECM via integrins plays a crucial role in cell migration and metastasis. To observe the effect of NCA on the surface expression of integrin β1, β3, and α5 and the activation level of integrin β1 in MDA-MB-231 cells, we performed antibody staining with subsequent FACS analysis. NCA significantly increased the cell surface expression of all investigated integrins in a dose dependent matter (Figure 15 A). Since integrin expression on the cell surface alone is no reliable indicator for adhesion strength, we additionally examined the activation status of integrin β1 by immunostaining with a primary antibody specifically detecting the activated form. We were able to show that NCA treatment led to a significant activation of integrin β1 in MDA-MB-231 cells (Figure 15 B). Integrin β1 is the most abundant β integrin and associates with a total of ten α integrin subunits.[74] Due to its high abundance and importance in cell adhesion we investigated whether activation of integrin β1 via NCA has an effect on cell adhesion to collagen I and fibronectin in a plate-and-wash adhesion assay. We were able to show that NCA treatment significantly increased cell adhesion of MDA-MB-231 cells to both extracellular ligands (Figure 15 C, D).
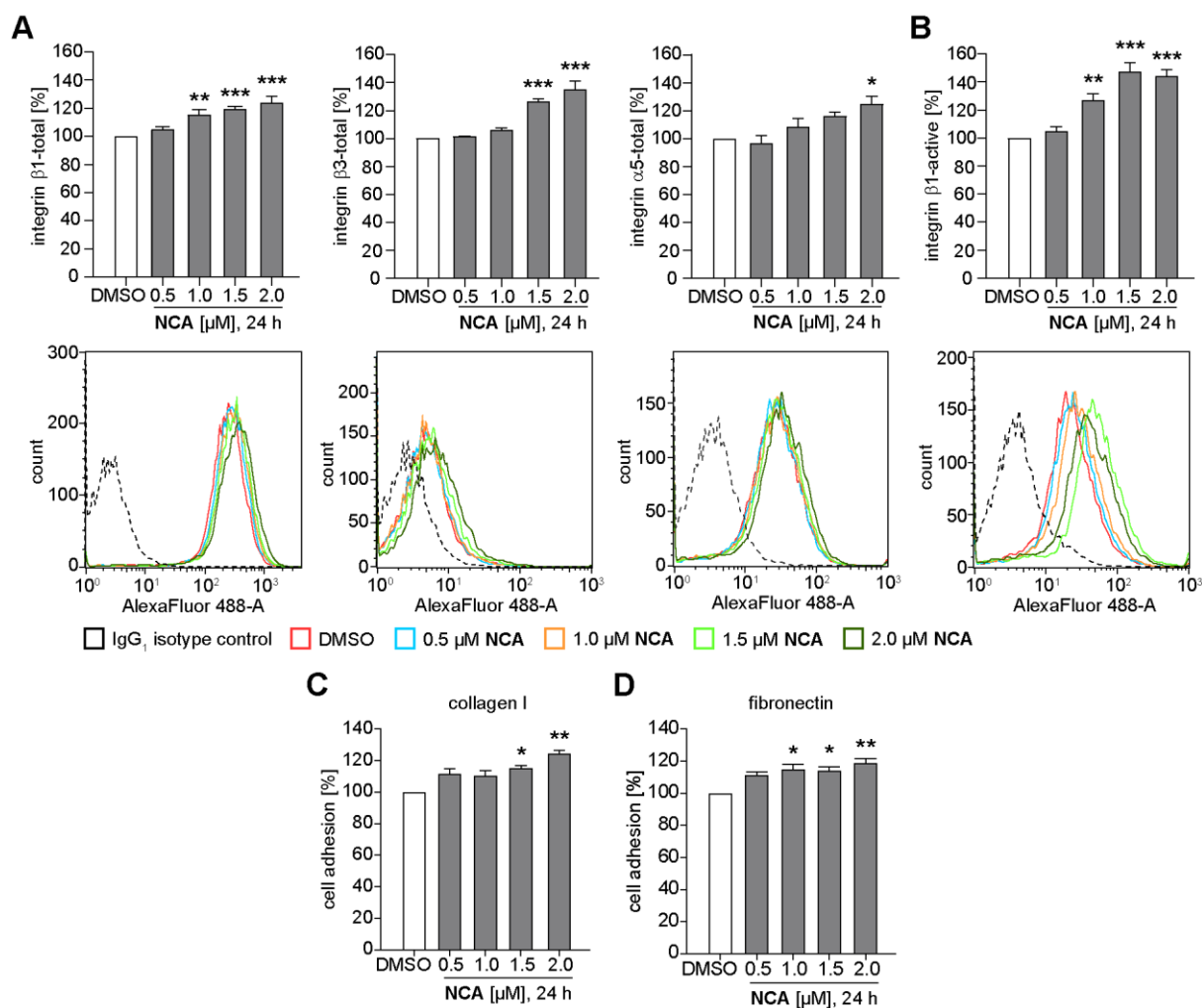
Figure 15. Impact of NCA on integrin expression and cell-matrix adhesion. (A) Surface expression of total integrin β1, β3, and α5 was determined via antibody staining and FACS analysis in MDA-MB-231 cells after 24 h treatment with NCA. **(B)** The effect of NCA on the activation of integrin β1 in MDA-MB-231 was analyzed by immunostaining and FACS analysis in MDA-MB-231 cells after 24 h. **(A, B)** Data was analyzed using FlowJo 7.6.5 software. **(C, D)** Influence of NCA on the adhesion of MDA-MB-231 cells to collagen I (C) and fibronectin (D) determined via plate-and-wash adhesion assay. **(A-D)** Bar diagrams showing results normalized to the DMSO control as mean ± SEM of at least three independent experiments performed in triplicate are presented, one-way ANOVA, Dunnett's test, *$P < 0.033$, **$P < 0.002$, ***$P < 0.001$ compared with DMSO control.

3.4 Chemical proteomics identify VAT-1 as cellular target of Neocarzilin A

To elucidate the mode of action of NCA, target identification and validation experiments were performed by Carolin Gleißner (Sieber Research Group, Department of Chemistry, TU Munich, Germany) using MS-based activity-based protein profiling (ABPP). Via ABPP the whole complement of target proteins of a compound can be identified in living cells by introducing only slight modifications to the initial structure.[75, 76, 77] ABPP has therefore become a widely applied method in cancer therapy to unravel targets of natural compounds.[78] For ABPP experiments the activity-based probe NC-1 (Figure 9) was synthesized according to Supplementary Scheme 4 starting from a NCA analog featuring a terminal alkyne at the polyene tail. This alkyne serves as important moiety for identification of protein targets enabling click chemistry to biotin azide, avidin enrichment, and quantitative LC-MS/MS analysis upon *in situ* protein binding and cell lysis (Figure 16 A). Before conducting MS studies, appropriate conditions for labeling of the target protein with NC-1 were established by SDS-PAGE analysis. Labeling yielded one intense band of approximately 40 kDa after 1 h, 24 h and 48 h incubation indicating sufficient stability upon protein binding (Supplementary Figure 1 A). To identify the targets of NCA in MDA-MB-231 cells using the probe NC-1, two proteomics-based methods were applied, namely stable isotope labeling of amino acids in cell culture (SILAC) and label-free quantification (LQF). Both methods revealed the synaptic vesicle membrane protein 1 (VAT-1) as most significant and highly enriched target, indicating reproducible readout of both methods (Figure 16 B, C and Supplementary Figure 1 B). Competitive studies with an excess of 5-fold NCA over NC-1 using LFQ further verified the result. VAT-1 still emerged as most prominent hit when plotting samples of competitive labeling experiments against NC-1 treated samples (Figure 16 D). This result and the decreasing VAT-1 band detected in competitive analytical labeling experiments (Figure 16 E) indicate that the probe NC-1 and the natural compound NCA compete for the same target. Of note, most of the other hits of the target identification experiments are proteins present in high concentration within the cell and show highly electrophile-sensitive cysteine residues (e.g. heme oxygenase HMOX2) or displayed insufficient competition (Supplementary Figure 1 C).
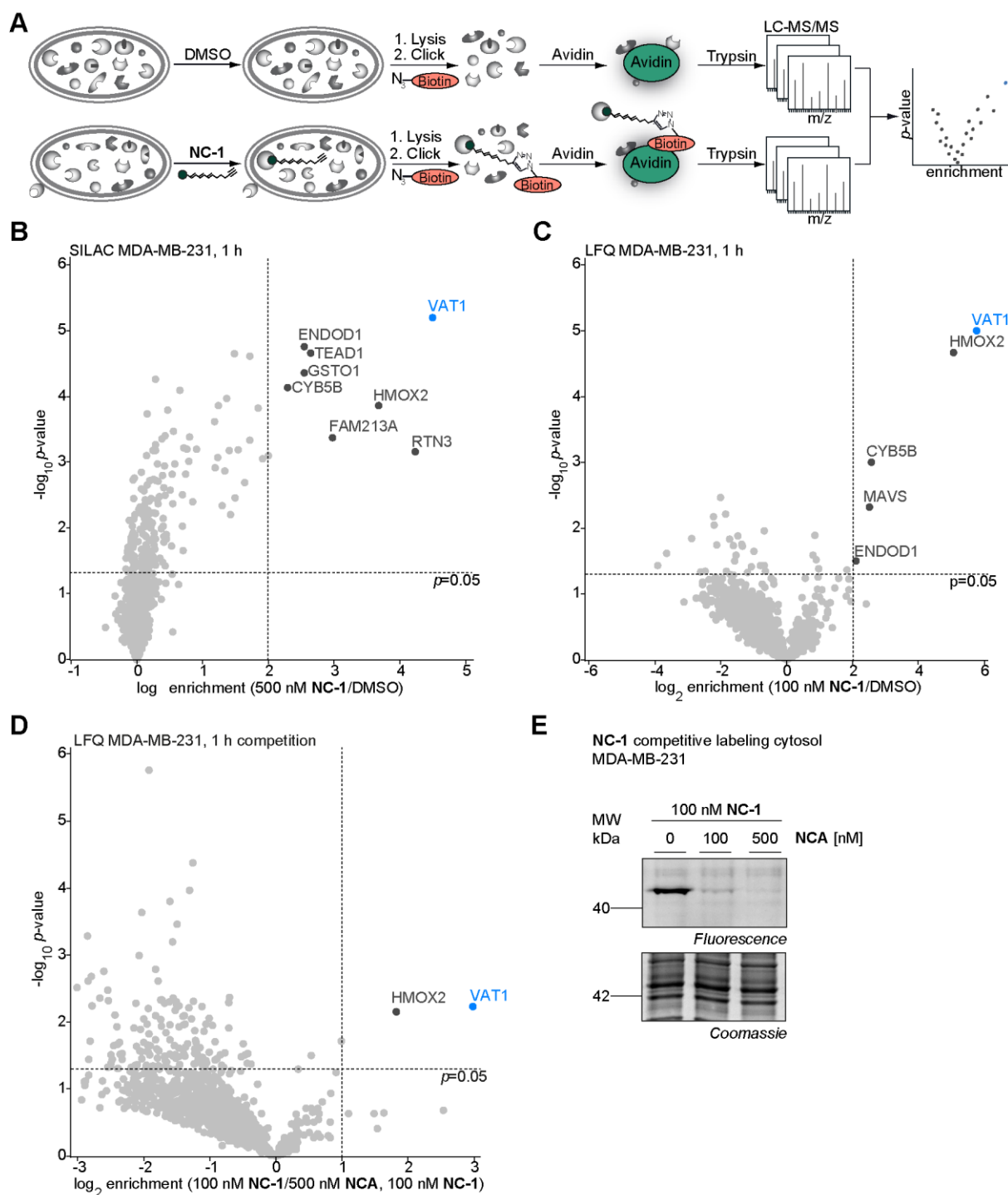
Figure 16. Identification of VAT-1 as cellular target protein of NCA. **(A)** Schematic overview of *in situ* ABPP approach with LFQ in cancer cells with MS/MS-based read-out**. (B)** Volcano plot of *in situ* SILAC ABPP experiment with 500 nM NC-1(n=6). **(C)** Volcano plot of *in situ* LFQ ABPP experiment with 100 nM NC-1 (n=5). **(B, C)** Hits (log$_2$(enrichment) > 2, p-value < 0.05) are highlighted and the protein with the highest enrichment factor (VAT-1) is shown in blue. Hits of volcano plots highlighted in dark grey are listed in the Supplementary Table 1 and Supplementary Table 2 in the Appendix. **(D)** Volcano plot of in situ competitive label-free ABPP experiment (n=5) ((log$_2$(enrichment) > 1.5, p-value < 0.05). Hits of volcano plots highlighted in dark grey are listed in Supplementary Table 4 in the Appendix. **(E)** SDS-PAGE of competitive analytical labeling for 1 h in MDA-MB-231 cells with natural product NCA and probe NC-1 in concentration ratios 1:1 and 5:1 (natural product:probe). (performed by Carolin Gleißner, Technical University of Munich)

For direct target validation VAT-1 was knocked down in MDA-MB-231 cells via transfection with siRNA prior to *in situ* labeling with NC-1 and subsequent cell lysis. Fluorescent SDS-PAGE did not show the characteristic 40 kDa band in siVAT-1 treated cells confirming VAT-1 as target protein of NCA (Figure 17 A, successful knockdown of VAT-1 in siRNA transfected cells is shown in Figure 18 A). To unravel the binding mode of NCA an ABPP-based approach was applied that uses click chemistry to label NC-1 with desthiobiotin after *in situ* probe labeling of cells, subsequent tryptic protein digestion, and enrichment on avidin beads to narrow down the binding site peptide (Supplementary Figure 2 A). For closer investigation, all nucleophilic amino acids within the peptide sequence were mutated and the resulting His-TEV-VAT-1 constructs were tested for labeling with NC-1 (Supplementary Figure 2 B). Only in the case of the E113Q mutant labeling failed, confirming correct identification of the binding position and importance of E113 for binding of NCA to VAT-1 (Figure 17 B). All describes experiments were performed by Carolin Gleißner (Sieber Research Group, Department of Chemistry, Technical University of Munich, Germany).
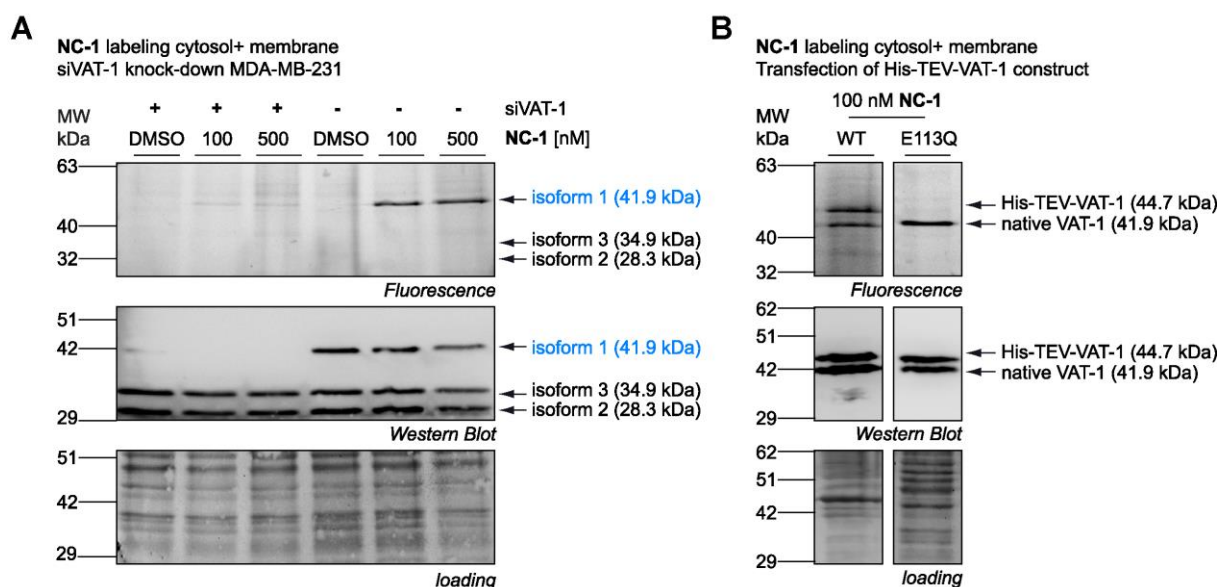
Figure 17. Validation of VAT-1 as cellular target protein of NCA. (A) Analytical labeling of siVAT-1 knockdown cells in comparison to control-treated cells. **(B)** *In situ* labeling of MDA-MB-231 which were transfected with His-TEV-VAT-1 construct expressing wildtype (WT) or the point mutant E113Q. (performed by Carolin Gleißner, Technical University of Munich)

3.5   VAT-1 plays an essential role in cancer cell migration

To provide a functional link between VAT-1 and the observed antitumor effects of NCA, migration, proliferation, and apoptosis experiments were performed in cells after knockdown or knockout (k.o.) of VAT-1. Successful knockdown of VAT-1 in MDA-MB-231 and 4T1-luc2 was achieved using siRNA (Figure 18 A). Additionally, we generated VAT-1 k.o. clones by deleting exon 2 of VAT-1 in HEK293 cells using the CRISPR-Cas9 method (Figure 18 B). Knockdown of VAT-1 caused 50-80% inhibition of migration in both cell lines compared to cells transfected with non-targeting (nt) siRNA (Figure 18 C, D). In contrast to wildtype (WT) HEK293 cells and mock-transfected CRISPR control cells, knockout of VAT-1 resulted in inhibition of migration to a comparable extent as observed with NCA (Figure 18 E). While these results indicate that the inhibitory effect of NCA on cell motility is predominantly mediated by VAT-1, proliferation and apoptosis were not affected by knockdown or knockout of the protein (Figure 18 F-H). This provides evidence that the antiproliferative and apoptotic effect of NCA could be attributed to a different target.
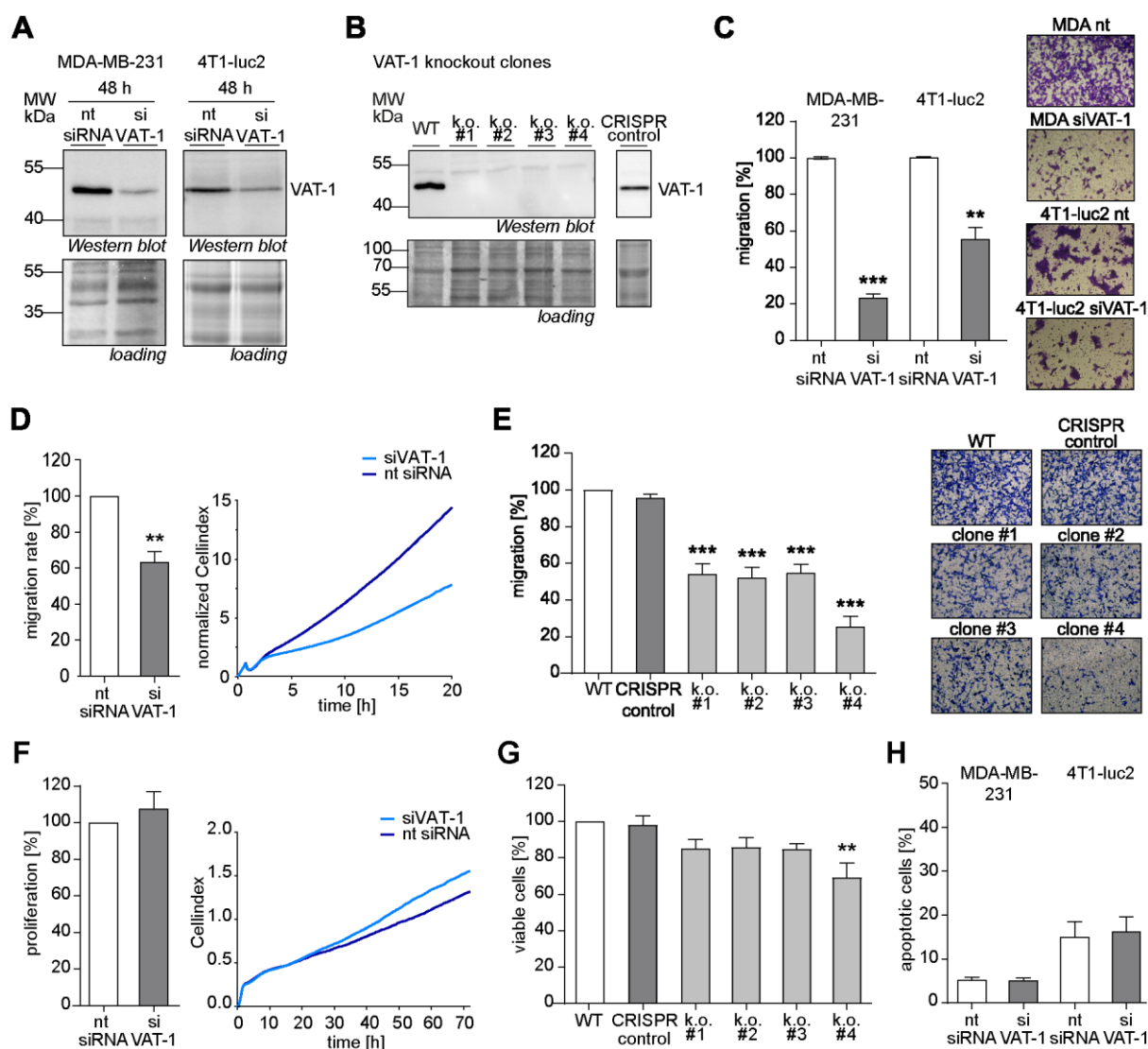
Figure 18. Functional link between VAT-1 and antitumor effects of NCA. (A, B) Western blot of VAT-1 protein levels in non-targeting (nt) and VAT-1 siRNA MDA-MB-231 and 4T1-luc2 cells after 48 h transfection (A) or in HEK293 WT cells and HEK293 VAT-1 k.o. clones generated via the CRISPR-Cas9 method (B). **(C)** Transwell migration of nt and VAT-1 siRNA transfected MDA-MB-231 and 4T1-luc2 cells determined by Boyden chamber assay. **(D)** Dynamic real time monitoring of migration of nt and VAT-1 siRNA transfected MDA-MB-231 cells using the xCELLigence migration assay. Representative graph out of three independent experiments is shown. **(E)** Transwell migration of HEK293 CRISPR-Cas9 VAT-1 k.o. clones determined by Boyden chamber assay. Unsuccessfully altered WT cells were included as additional control (CRISPR control). **(F)** Proliferation of nt and VAT-1 siRNA transfected MDA-MB-231 cells determined by crystal violet staining after 72 h (left) and dynamic real time xCELLigence proliferation assay (right). Representative xCELLigence graph out of three independent experiments is shown. **(G)** Proliferative capacity of WT and VAT-1 k.o. clones determined by CellTiter-Blue® viability assay after 72 h. Unsuccessfully altered WT cells were included as additional control (CRISPR control). **(H)** Apoptosis of nt and siVAT-1 MDA-MB-231 or 4T1-luc2 cells after 48 h transfection was measured as described by Nicoletti *et al.*[66, 67]. The percentage of dying cells was determined by flow cytometry. **(C-G)** Bar diagrams show results normalized to nt siRNA cells (C, D, F) or WT HEK293 cells (E, G). **(C-H)** Bars represent the mean ± SEM of at least three independent experiments performed in duplicate/triplicate, two-tailed unpaired Student's t test, **P < 0.002, ***P < 0.001 (C, D, F, H), one-way ANOVA, Dunnett's test, **P < 0.002, ***P < 0.001 compared with DMSO control (E, G).

3.6   VAT-1 interaction partners are involved in cell adhesion and migration

To unravel the functional role of VAT-1 in cell migration, proteomics-based co-immunoprecipitation (co-IP) experiments were performed by Carolin Gleißner (Sieber Research Group, Department of Chemistry, Technical University of Munich, Germany). VAT-1 was immunoprecipitated from MDA-MB-231 whole cell lysates with an immobilized anti-VAT-1 antibody together with the use of a disuccinimidyl sulfoxide (DSSO) crosslinker for detection of transient protein-protein interactions as shown by Fux *et al.*[79] Pulled down proteins were analyzed via LC-MS/MS and several significantly enriched hits were obtained (Figure 19). Strikingly, Gene Ontology (GO) enrichment analysis performed with the Cytoscape[80] BINGO app[81] revealed that many identified hits are involved in cell adhesion (e.g. gelsolin, GSN; fibronectin, FN1), integrin activation (e.g. Talin-1, TLN), and lamellipodium organization (e.g. RAC2), all playing a crucial role in the cell migration process (Figure 20).
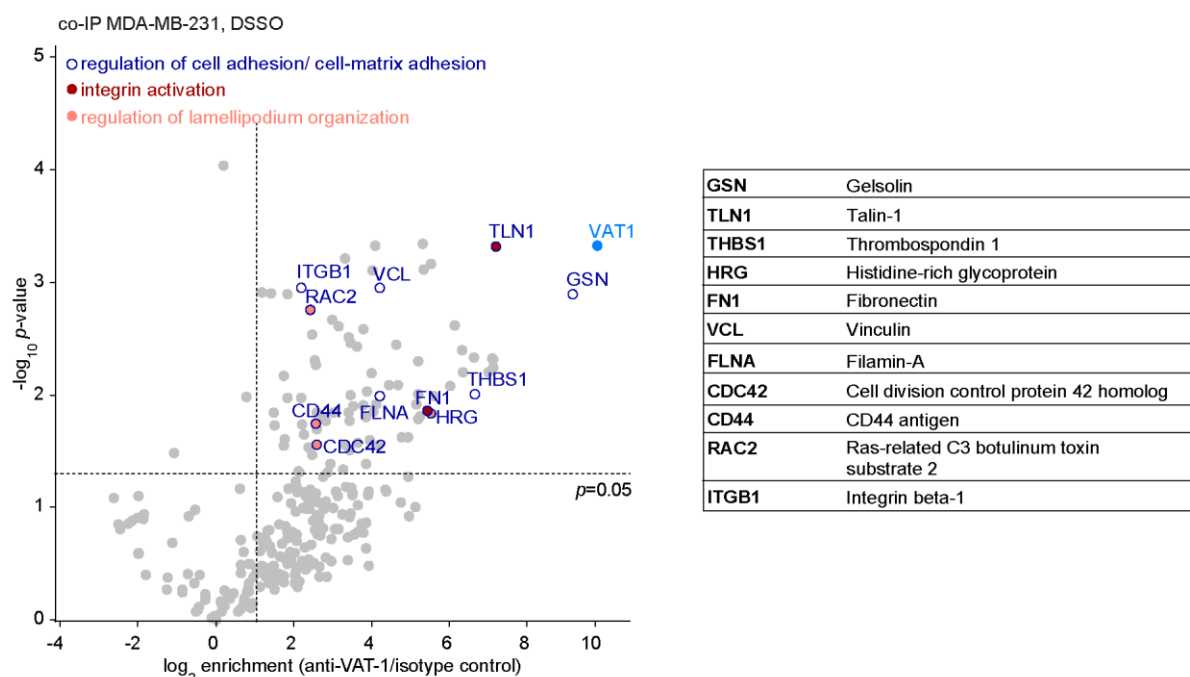
Figure 19. Interaction partners of VAT-1 identified by co-IP. Volcano plot of co-IP of VAT-1 with 2 mM DSSO in MDA-MB-231 (n=3). Hits of volcano plot are listed in Supplementary Table 5 in the Appendix. (performed by Carolin Gleißner, Technical University of Munich)

GO enrichment analysis	corr. *p*-value			GO ID
extracellular vesicle	1.16E-33		cellular component	(GO:1903561)
focal adhesion	6.17E-10			(GO:0005925)
cell-substate adherens junction	6.55E-10			(GO:0005924)
secretory vesicle	9.41E-05			(GO:0099503)
collagen containing extracellular matrix	2.53E-04			(GO:0062023)
actin cytoskeleton	1.49E-03			(GO:0015629)
lamellipodium	7.67E-03			(GO:0030027)
cell-cell contact zone	1.74E-03			(GO:0044291)
actin-based cell projection	3.65E-02			(GO:0098858)
clathrin coated vesicle membrane	3.44E-02			(GO:0030665)
oxidoreductase activity	2.88E-06		molecular function	(GO:0016491)
cytoskeletal protein binding	2.72E-03			(GO:0008092)
cell adhesion molecule binding	1.42E-04			(GO:0050839)
actin binding	2.88E-03			(GO:0003779)
endopeptidase inhibitor activity	2.66E-05			(GO:0004866)
collagen binding	4.72E-04			(GO:0005518)
integrin binding	4.90E-03			(GO:0005178)
fibronectin binding	4.05E-02			(GO:0001968)
collagen V binding	4.08E-02			(GO:0070052)
vesicle mediated transport	1.23E-03		biological process	(GO:0016192)
actin cytoskeleton organization	2.50E-04			(GO:0030036)
regulation of cell adhesion	8.34E-03			(GO:0030155)
wound healing	2.75E-03			(GO:0042060)
extracellular matrix organization	1.22E-03			(GO:0030198)
regulation of cell-substrate adhesion	2.32E-03			(GO:0010810)
cell projection assembly	4.31E-02			(GO:0030031)
regulation of lamellipodium organization	2.32E-02			(GO:1902743)
cell-matrix adhesion	3.45E-02			(GO:0007160)
collagen fibril organization	2.00E-02			(GO:0030199)
integrin activation	1.40E-02			(GO:0033622)
basement membrane organization	3.25E-02			(GO:0071711)

☐ global human proteome
■ interaction partner of VAT-1

frequency [%] — 0 10 20 30 40 50 60 70 80 90 100

Figure 20. GO enrichment analysis of co-IP hits. GO enrichment analysis of hits (($\log_2$(enrichment) > 1, p-value < 0.05) was performed with Cytoscape[80] BINGO app[81] whereas frequencies of enriched GO terms are compared between the co-IP and the global proteome. (performed by Carolin Gleißner, Technical University of Munich)

To verify the overall effect of NCA on protein regulation, global proteome analysis was performed. However, the effect of NCA on the total proteome was rather limited and NCA treatment did not result in significant regulation of the expression of co-IP hits (Figure 21 A). This result was verified by Western blot analysis of selected interaction partners of VAT-1 after different time points of incubation (Figure 21 B, C).
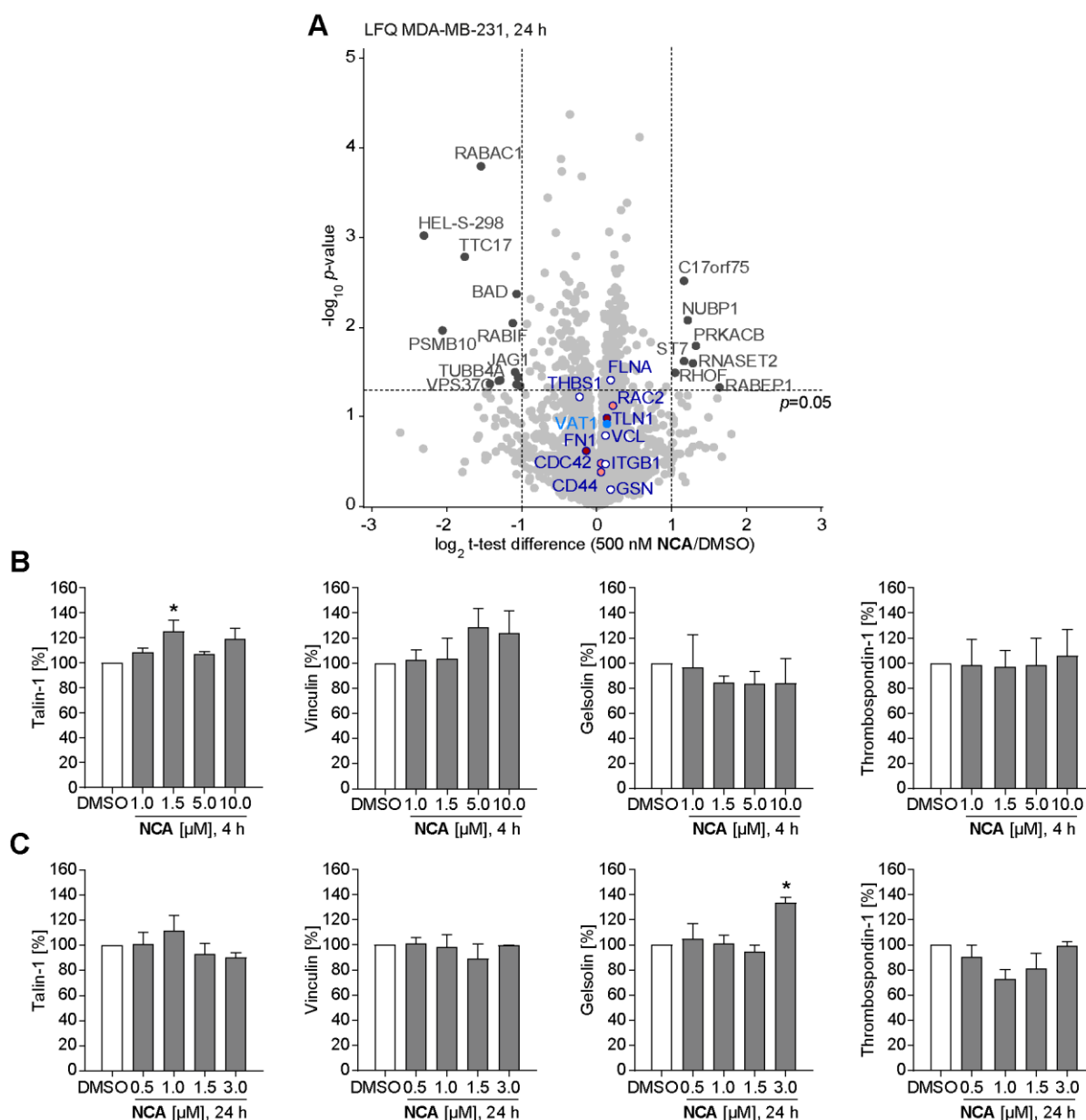
Figure 21. Influence of NCA on total proteome and selected co-IP hits. (A) Volcano plot of global proteome analysis with LFQ in MDA-MB-231 treated with 500 nM NCA for 24 h (n=6). Proteins identified in the co-IP are shown in the same color code (Figure 19). Hits of volcano plots are listed in Supplementary Table 6 in the Appendix. (Carolin Gleißner, Technical University of Munich) **(B, C)** MDA-MB-231 cells were treated with the indicated concentrations of NCA for 4 h (B) or 24 h (C). Cellular protein levels were detected by Western blot analysis and results normalized to DMSO treated cells. Bars represent the mean ± SEM of three independent experiments, one-way ANOVA, Dunnett's test, *P < 0.033 compared with DMSO control.

3.6.1 Neocarzilin A enhances the interaction of VAT-1 with Talin-1

The protein Talin-1 was identified as one of the strongest hits in MS-based co-IP experiments. The cytoplasmic protein regulates integrin adhesion to the ECM by linking integrins directly to the actin cytoskeleton and mediating integrin activation, which is a crucial step of cell migration and metastasis.[28, 29] To investigate the influence of NCA on the interaction of VAT-1 with Talin-1, Western blot-based co-IP was performed after NCA treatment with the same anti-VAT-1 antibody as used for MS-based co-IP. We were able to reproduce the results obtained by MS-based co-IP and moreover showed that NCA significantly enhanced the interaction of VAT-1 with Talin-1 (Figure 22 A). Furthermore, immunostaining revealed a colocalization of both proteins in lamellipodia at the leading edge of migrating cells, indicating that the interaction of both proteins could be important for cell migration (Figure 22 B, exemplarily indicated with white arrows). However, upon NCA treatment no colocalization of VAT-1 and Talin-1 was observed at the leading edge contradicting the results obtained by co-IP. Crystallography or computational studies will help to further elucidate and interpret the effect of NCA on the interaction of VAT-1 and Talin-1.
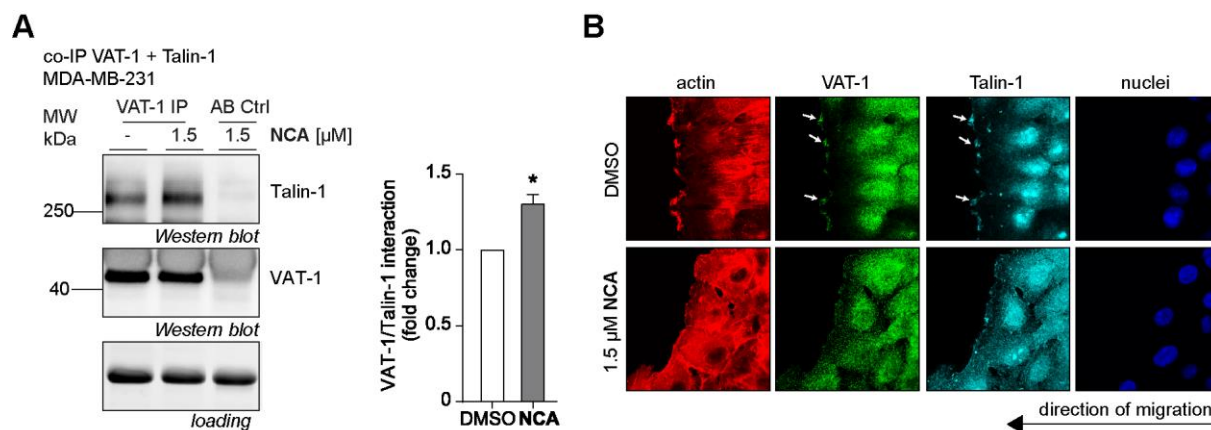
Figure 22. Effect of NCA on the interaction of VAT-1 with Talin-1. (A) Co-IP of VAT-1 and Talin-1. VAT-1 was precipitated from MDA-MB-231 cell lysates after 24 h stimulation with NCA. Amount of Talin-1 determined by Western blot was normalized to VAT-1 and results were normalized to the DMSO control. Bars represent the mean ± SEM of three independent experiments, two-tailed unpaired Student's t test, *P < 0.033. **(B)** T24 cells treated with NCA were engaged in a Scratch assay and co-stained for VAT-1 (green), Talin-1 (cyan) and actin (red). Nuclei were stained with Hoechst 33342. White arrows exemplarily indicate areas of colocalization. **(A, B)** A representative experiment out of three independent experiments is shown.

3.7   Summary

The main finding of this work is the identification of NCA as an inhibitor of tumor cell motility by interacting with VAT-1 protein, which was identified as cellular target of Neocarzilins via proteomics-based ABPP experiments. In summary, NCA reduced directed migration and invasion *in vitro* as well as cell dissemination *in vivo.* Moreover, treatment with NCA led to impaired activation of Rac1 and lamellipodia formation in migrating cells, while upregulating integrin surface expression and activation and increasing cell adhesion to collagen I and fibronectin. Facilitating these results, proteomics-based co-IP experiments identified an intricate network of key migration mediators, such as Talin-1, as interaction partners of VAT-1. While we were able to attribute the strong antimigratory effect of NCA to its interaction with VAT-1, the responsible target for antiproliferative and apoptotic effects still needs to be defined, leaving room for further investigations of this promising newly defined potent therapeutic lead structure.

DISCUSSION

4 Discussion

4.1 Neocarzilins as structure-dependent antitumor agents

Since their discovery in the 1990s by Nozoe *et al.,* the Neocarzilins have attracted only little attention. Only Neocarzilin A (NCA) was shown to exhibit potent cytotoxic activity against K562 chronic myelogenous leukemia cells.[42] To gain more insight into this interesting natural compound class, we performed detailed analysis of their antitumor activities and recognized them as antitumor agents showing the most prominent effects on inhibition of cell migration, invasion, and tumor cell dissemination. Strikingly, the Neocarzilins showed diverse potency depending on their chemical structure and stereochemistry. Comparison of the effects of NCA with its opposite enantiomer NCA' and NCB revealed that changes in the stereochemistry of NCA result in reduced antiproliferative and antimigratory effects. Moreover, exchange of the trichloromethyl group with a dichloromethyl group in NCC resulted in an even more radical drop of potency. This suggests that both, stereochemistry and the trichloromethyl group with its electrophilic character, determine the biological activity by interacting with the target protein.

Moreover, it is worth mentioning that the Neocarzilins not only stand out due to their strong antimigratory and antiproliferative effects, but that they also distinguish themselves from other therapeutically active natural compounds through their comparably simple chemical structure as well as synthesis. Many natural products are structurally complex making total synthesis extremely challenging, resulting in low yields and supply problems.[82] Due to their simple structure, Neocarzilins can easily be chemically modified. Based on further investigations of the binding mode of NCA to its target VAT-1, NCA can therefore be undertaken further optimization to increase its pharmacological activity and selectivity towards its target. Considering that NCA additionally fulfills Lipinski's rule of

five for prediction of drug-likeness and estimation of the potential as orally active drug in humans[83], it emerges as promising new drug lead compound.

Taken together, the Neocarzilins were identified as a promising natural compound family and potential drug leads exhibiting structure-dependent antitumor effects with great potential in inhibition of cell migration and proliferation. In all conducted experiments, NCA protruded as the most active compound and was therefore chosen for in depth investigations.

4.2 Chemical proteomics as powerful tool in the target identification of Neocarzilin A

Over the last decades, natural products have emerged as valuable source of biologically active compounds for drug discovery.[40, 84] However, in numerous cases the cellular target and mode of action of the compound are not identified, which is even the case for natural products in clinical trials or approved pharmaceuticals.[85] The same applies for the natural compound NCA, which up to date was not undertaken any mode of action studies, despite its early discovery. With the advent of chemical proteomics-based methods for drug target identification, readdressing of previously identified, but so far neglected structures has evolved as viable strategy for the identification of new anticancer leads and enables detailed mode of action studies. One major strategy applied is activity-based protein profiling (ABPP).[86, 87] The key component to successful target identification via ABPP is the design of an activity-based probe based on the original structure of the natural product which is used for *in situ* labeling of target proteins in living cells.[78] ABPP using the activity-based probe NC-1 resulted in identification of the synaptic vesicle membrane protein 1 (VAT-1) as target protein of NCA. The result was further verified by competitive labeling approaches with NCA and NC-1, which underline the high specificity of NCA to its target VAT-1. Moreover, the nucleophilic amino acid E113 of the VAT-1 sequence was identified as the likely point of drug attachment by point mutation and labeling experiments, supporting the assumption that the electrophilic trichloromethyl

group of NCA determines the biological activity by interacting with the target protein. As discussed by Gersch *et al.*, electrophilic natural products are typically characterized by covalent interaction with their target protein.[76] Therefore, we suggest that NCA covalently attaches to VAT-1, however, this remains to be elucidated.

The other hits identified via ABPP either represented proteins known to be often targeted by electrophilic compounds which are present in great abundance (e.g. heme oxygenase HMOX2) or showed insufficient competition. For this reason, these proteins were not included in further investigations.

The identification of VAT-1 as target protein of NCA decades after its discovery, illustrates the power of chemical proteomics in drug target identification. However, chemical proteomics-based drug target identification methods also show certain limitations. During the design of the activity-based probe NC-1, the methyl stereocenter was removed, which was proven to have an impact on the biological activity of NCA. Indeed, the antiproliferative capacity of NC-1 was drastically reduced compared to NCA whereas the antimigratory potential was only slightly decreased. This result suggests that the probe NC-1 is suitable for binding the NCA target protein VAT-1, which is involved in the mediation of the antimigratory effect, but that supposedly one or more other proteins are responsible for the antiproliferative effect which cannot interact with NC-1 due to the loss of the stereocenter. This hypothesis is also supported by our finding that the antiproliferative effect could not be attributed to VAT-1 as shown in knockdown and knockout experiments. This leads to the conclusion that NCA most likely has multiple cellular targets which mediate the different antitumor effects of the compound. However, up to date we were not able to identify the responsible target for proliferation inhibition, since VAT-1 was presented as the only prominent hit in target identification experiments, showing the limitations of proteomics-based ABPP in drug target identification. To overcome this deficit, an alternative method for target identification which does not require chemical modification of the natural compound could be applied to identify so far unknown target proteins of NCA. One

possible option is mass spectrometry-based cellular thermal shift assay (MS-CETSA), which is modification-independent, works in live cells and determines target proteins by stabilizing effects on proteins upon compound binding resulting in a change in thermal denaturation temperature.[88]

4.3   Targeting tumor cell motility as a strategy against metastasis

In detailed investigations of its antitumor effects, we identified NCA as potent inhibitor of cell migration, a key element of cancer cell metastasis. By causing 90% of all cancer related deaths, metastasis is the major contributor to patient mortality and still considered incurable due to deficient treatment options.[15, 89] The development of antimetastatic drugs has therefore emerged as one of the main prospects of cancer therapy with the central goal to identify potent therapeutics and therapeutically viable targets. Nguyen *et al.* presented that the molecular mechanisms of cell migration and the progression of cancer to a systemic disease are strongly connected.[90] Specific therapeutic targeting of tumor cell motility therefore presents a promising strategy to limit metastasis of solid tumors, considering that cell migration is a crucial step in the metastatic cascade.[91] It also aims at reducing the need for aggressive cytotoxic therapy with strong side effects, which is currently used to avoid the risk of metastatic spread of tumors, to increase survival rates and quality of life of patients.[89]

4.3.1   The *status quo* of metastatic cancer treatment

Up to date, no therapeutics targeting cell motility have entered the market, however several promising candidates are in clinical trial targeting different elements of the cell migration process like actin polymerization, cell contractility, cell-ECM adhesion or matrix remodeling enzymes[92, 93, 94]. The regulation of the actin cytoskeleton was shown to play a crucial role in cancer cell migration.[95] Actin targeting substances like latrunculins[96] or chondramide A[97], showing either actin destabilizing or stabilizing properties, inhibit migration and invasion in highly invasive MDA-MB-231 breast cancer cells. By interfering with cell contractility, the myosin inhibitor blebbistatin was shown to inhibit

invasiveness in a panel of cancer cell lines *in vitro* [92], whereas the specific ROCK inhibitor Y-27632 inhibited tumor invasion *in vivo*[98]. However, targeting the actin cytoskeleton remains challenging, due to its high abundance and involvement in numerous important processes like gene expression and cell division. Moreover, matrix metalloproteinases (MMPs), which are capable of cleaving components of the ECM, contributing to metastatic progression, have emerged as interesting addressable targets.[94] Endostatin[99] and curcumin[100], two MMP targeting compounds, are currently in phase II clinical trials. Another strategy in the development of antimetastatic drugs is addressing of the cell-ECM interface. As main mediators of cell adhesion, integrins have protruded as potential therapeutic targets.[93] The monoclonal antibodies abituzumab and intetumumab as well as the cyclic peptide cilengitide are the most advanced molecules studied in clinical trials. However, they show only moderate efficacy and none of them have been approved for cancer treatment, emphasizing the persistent need for novel antimetastatic drugs.[101]

4.3.2 Neocarzilin A as novel antimetastatic drug targeting the cell-ECM interface

In depth investigation of the antitumor effects of NCA presented the compound as an inhibitor of cell migration, invasion, and tumor cell dissemination. Strikingly, NCA showed an upregulating effect on integrin surface expression and activation, as well as on cell adhesion to collagen I and fibronectin. Integrin-mediated cell adhesion is a highly dynamic process which plays a key role in cancer cell migration by linking the cell to the ECM.[25] It has previously been shown that overexpression and increased activation of integrins can reduce cell motility. Palecek *et al.* discovered that the cell migration rate is strongly determined by both, ECM ligand and integrin expression levels. Already small changes in these two parameters resulted in significant changes in migration speed.[102] Investigations by Huttenlocher *et al.* revealed that stable artificial activation of integrin α2bβ3 via mutation or antibody-based activation results in a significant drop of the cell migration speed.[103] Both groups claim that the reduced migration rate can be attributed to inhibited release of adhesion at the cell rear during the migration process, preventing cell contraction for forward movement.[102, 103] Consequently, cell detachment protrudes as limiting factor of cell migration speed under conditions of

high cell-ECM adhesiveness. Based on these findings we propose that NCA has a high potential as antimetastatic drug lead by increasing cell adhesion strength due to upregulation of integrin expression and activity, leading to impaired detachment of the cell's rear and finally resulting in reduced migration.

However, a major challenge which must be overcome during the development of novel antimetastatic drugs is toxicity. According to Steeg *et al.*, the most promising treatment outcome can be expected when antimetastatic drugs are given continuously and at an early stage of tumor progression.[104] Palmer *et al.* also call for continuous antimetastatic treatment, since it is currently not predictable when a tumor becomes metastatic.[89] Therefore, low toxicity of antimetastatic drugs is an indispensable requirement to prevent cytotoxic side effects during long-term treatment of patients. In the case of NCA, no induction of apoptosis was observed at concentrations and time points relevant for migration inhibition and a suitable safety profile was confirmed *in vivo* by a comparable increase of the bodyweight of mice of the control and NCA-treated group. However, investigations of the toxic effects of NCA on non-tumorous cells and long-term cytotoxicity studies are urgently needed to evaluate its potential as cancer therapeutic.

Besides its prominent antimigratory effect, NCA also showed antiproliferative activity in a panel of different cancer cell lines. As discussed by Gandalovičová *et al.*, synergy of antimigratory and antiproliferative cancer therapeutics evolves as promising approach for treatment of metastasis, emphasizing the great potential of NCA as treatment option of metastatic cancer.[92]

Taken together, targeting cell migration and metastasis has become a major interest of cancer research, showing great potential as supportive strategy to conventional antiproliferative treatment. However, most of the so far investigated therapeutics and target pathways have failed in clinical research resulting in the urgent need of novel therapeutics and target strategies. Therefore, we here introduce the natural compound NCA as promising novel antimetastatic drug and potential lead compound which significantly reduces cell migration and proliferation in invasive breast cancer cell lines.

4.3.3   VAT-1 as innovative drug target for therapy of metastatic cancer

In context of this thesis, we present the synaptic vesicle membrane protein 1 (VAT-1) as novel drug target for cell migration inhibition in the fight against metastatic cancer. Proteomics-based target identification methods have identified VAT-1 as target of NCA, mediating the antimigratory effect of the novel drug. A role of VAT-1 in cell migration has further been confirmed by siRNA knockdown and CRISPR-Cas9 mediated knockout studies, resulting in impaired migration. In accordance, Mertsch *et al.* showed that VAT-1 knockdown significantly reduced glioma cell migration.[61]

Proteomics-based co-IP experiments identified a complex network of VAT-1 interaction partners associated with cell motility. For example, the interaction partners gelsolin[105], vitronectin[106], and fibronectin[107] are directly involved in regulation of ECM composition. Cdc42 and Rac2 are key players in the migration process, whereas CD44 and integrin β1 present important glycoproteins, involved in the cell adhesion process.[108] Strikingly, Talin-1 was identified as most prominent binding partner of VAT-1 and both proteins were shown to colocalize at the leading edge of migrating cells. Upon activation, Talin-1 binds to the integrin β subunit and induces a conformational change to generate the active high affinity state of the integrin, enabling interaction with ECM ligands.[29, 31] This link between VAT-1 and the cell adhesion process suggests that the involvement of VAT-1 in cell migration could be mediated by direct interaction with Talin-1 and alternation of integrin balance. Incubation with NCA led to a significant enhancement of the interaction of VAT-1 with Talin-1, most likely resulting in increased activation of integrins and strengthened cell adhesion to collagen I and fibronectin, as determined during in depth analysis of cell adhesion parameters. Further investigations including crystallography and computational modeling will have to elucidate how NCA influences the interaction of VAT-1 with the cell adhesion network on a molecular level.

In summary, VAT-1 was identified as so far unknown player in regulation of cancer cell migration with possible impact in tumor metastasis by direct interaction with key migration mediators such as Talin-1. Moreover, the identification of NCA as potent inhibitor of migration opens the door to

chemically easily accessible VAT-1 probes allowing further in depth analysis of its physiological function and exploitability in antimetastatic cancer research. Hence, VAT-1 is set on stage as innovative anticancer drug target preventing migration and metastasis.

4.4 Summary and Conclusion

Metastatic cancer remains the primary cause of cancer related deaths[2]. Metastasis is strongly driven by tumor cell migration and specific targeting of this cellular process could significantly improve cancer treatment. However, up to date there are only limited therapeutic options available. Therefore, the identification of novel antimigratory drugs and therapeutically addressable targets has evolved as urgent need for treatment of metastatic cancer and attracted the attention of researchers in this field.

Within the framework of this thesis, we propose the natural compound Neocarzilin A (NCA) as potent inhibitor of cancer cell motility. By activity-based protein profiling (ABPP) we identified the synaptic vesicle membrane protein 1 (VAT-1) as target of NCA in cooperation with the group of Prof. Dr. Stephan Sieber (Chair of Organic Chemistry II, Technical University of Munich, Germany). In depth investigation revealed that VAT-1 interacts with an intricate network of key migration mediators such as Talin-1, the main activator of integrins. Moreover, VAT-1's involvement in the cancer cell migration process was confirmed by knockdown and knockout studies (Figure 23). We suggest that binding of NCA to its target VAT-1 alters its interaction with Talin-1, resulting in increased integrin-mediated adhesion strength leading to impaired cell detachment and reduced migration.

In conclusion, we introduce the natural compound NCA as potent antimigratory drug and potential lead compound and VAT-1 as a promising novel target for development of cancer cell migration inhibitors for treatment of metastatic tumors.
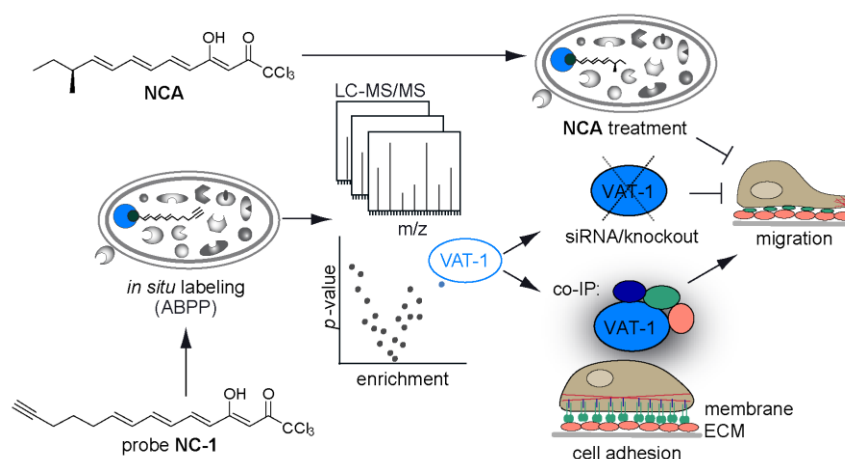
Figure 23. Summary and conclusion.

REFERENCES

5 References

[1] International Agency for Research on Cancer (IARC), *Latest global cancer data: Cancer burden rises to 18.1 million new cases and 9.6 million cancer deaths in 2018.* **2018**.

[2] Bray, F.; Ferlay, J.; Soerjomataram, I.; Siegel, R. L.; Torre, L. A.; Jemal, A., Global cancer statistics 2018: GLOBOCAN estimates of incidence and mortality worldwide for 36 cancers in 185 countries. *CA Cancer J. Clin.* **2018,** *68* (6), 394-424.

[3] Richie, R. C.; Swanson, J. O., Breast cancer: a review of the literature. *J. Insur. Med.* **2003,** *35* (2), 85-101.

[4] Bogenrieder, T.; Herlyn, M., Axis of evil: molecular mechanisms of cancer metastasis. *Oncogene* **2003,** *22* (42), 6524-36.

[5] Sledge, G. W., Jr., Curing Metastatic Breast Cancer. *J. Oncol. Pract.* **2016,** *12* (1), 6-10.

[6] Manel Gasent Blesa, J.; Alberola Candel, V.; Esteban, E.; Vidal Martínez, J.; Gisbert-Criado, R.; Provencio, M.; Laforga, J.; Pachmann, K., Circulating tumor cells in breast cancer: Methodology and clinical repercussions. *Clin. Transl. Oncol.* **2008,** *10*, 399-406.

[7] O'Sullivan, B.; Brierley, J.; Byrd, D.; Bosman, F.; Kehoe, S.; Kossary, C.; Pineros, M.; Van Eycken, E.; Weir, H. K.; Gospodarowicz, M., The TNM classification of malignant tumours-towards common understanding and reasonable expectations. *Lancet Oncol.* **2017,** *18* (7), 849-851.

[8] Rastelli, F.; Biancanelli, S.; Falzetta, A.; Martignetti, A.; Casi, C.; Bascioni, R.; Giustini, L.; Crispino, S., Triple-negative breast cancer: current state of the art. *Tumori* **2010,** *96* (6), 875-88.

[9] Punglia, R. S.; Morrow, M.; Winer, E. P.; Harris, J. R., Local therapy and survival in breast cancer. *N. Engl. J. Med.* **2007,** *356* (23), 2399-405.

[10] Palumbo, M.; Kavan, P.; Miller, W.; Panasci, L.; Assouline, S.; Johnson, N.; Cohen, V.; Patenaude, F.; Pollak, M.; Jagoe, R.; Batist, G., Systemic cancer therapy: achievements and challenges that lie ahead. *Front. Pharmacol.* **2013,** *4* (57).

[11] Swanton, C.; Szallasi, Z.; Brenton, J. D.; Downward, J., Functional genomic analysis of drug sensitivity pathways to guide adjuvant strategies in breast cancer. *Breast Cancer Res.* **2008,** *10* (5), 214.

[12] Castrellon, A. B.; Gluck, S., Chemoprevention of breast cancer. *Expert Rev. Anticancer Ther.* **2008,** *8* (3), 443-52.

[13] Osborne, C. K.; Wakeling, A.; Nicholson, R. I., Fulvestrant: an oestrogen receptor antagonist with a novel mechanism of action. *Br. J. Cancer* **2004,** *90 Suppl 1*, S2-6.

[14] Masoud, V.; Pages, G., Targeted therapies in breast cancer: New challenges to fight against resistance. *World J. Clin. Oncol.* **2017,** *8* (2), 120-134.

[15] Hanahan, D.; Weinberg, R. A., The hallmarks of cancer. *Cell* **2000,** *100* (1), 57-70.

[16] Lee, A.; Djamgoz, M. B. A., Triple negative breast cancer: Emerging therapeutic modalities and novel combination therapies. *Cancer Treatment Rev.* **2018,** *62*, 110-122.

[17] Chambers, A. F.; Groom, A. C.; MacDonald, I. C., Dissemination and growth of cancer cells in metastatic sites. *Nat. Rev. Cancer* **2002,** *2* (8), 563-72.

[18] Gupta, G. P.; Massague, J., Cancer metastasis: building a framework. *Cell* **2006,** *127* (4), 679-95.

[19] Saxena, M.; Christofori, G., Rebuilding cancer metastasis in the mouse. *Mol. Oncol.* **2013,** *7* (2), 283-296.

[20] Weinberg, R. A., *The biology of cancer* Garland Science: New York, **2014**.

[21] Vicente-Manzanares, M.; Webb, D. J.; Horwitz, A. R., Cell migration at a glance. *J. Cell. Sci.* **2005,** *118* (Pt 21), 4917-9.

[22] Yue, B., Biology of the extracellular matrix: an overview. *J. Glaucoma* **2014,** *23* (8 Suppl 1), S20-3.

[23] Egeblad, M.; Rasch, M. G.; Weaver, V. M., Dynamic interplay between the collagen scaffold and tumor evolution. *Curr. Opin. Cell Biol.* **2010,** *22* (5), 697-706.

[24] Provenzano, P. P.; Eliceiri, K. W.; Campbell, J. M.; Inman, D. R.; White, J. G.; Keely, P. J., Collagen reorganization at the tumor-stromal interface facilitates local invasion. *BMC Med.* **2006,** *4* (1), 38.

[25] Hamidi, H.; Ivaska, J., Every step of the way: integrins in cancer progression and metastasis. *Nat. Rev. Cancer* **2018**.

[26] Moser, M.; Legate, K. R.; Zent, R.; Fassler, R., The tail of integrins, talin, and kindlins. *Science* **2009,** *324* (5929), 895-9.

[27] Calderwood, D. A., Integrin activation. *J. Cell. Sci.* **2004,** *117* (Pt 5), 657-66.

[28] Critchley, D. R.; Gingras, A. R., Talin at a glance. *J. Cell Sci.* **2008,** *121* (9), 1345-1347.

[29] Klapholz, B.; Brown, N. H., Talin - the master of integrin adhesions. *J. Cell Sci.* **2017,** *130* (15), 2435-2446.

[30] Rossier, O.; Octeau, V.; Sibarita, J. B.; Leduc, C.; Tessier, B.; Nair, D.; Gatterdam, V.; Destaing, O.; Albiges-Rizo, C.; Tampe, R.; Cognet, L.; Choquet, D.; Lounis, B.; Giannone, G., Integrins beta1 and beta3 exhibit distinct dynamic nanoscale organizations inside focal adhesions. *Nat. Cell Biol.* **2012,** *14* (10), 1057-67.

[31] Tadokoro, S.; Shattil, S. J.; Eto, K.; Tai, V.; Liddington, R. C.; de Pereda, J. M.; Ginsberg, M. H.; Calderwood, D. A., Talin binding to integrin beta tails: a final common step in integrin activation. *Science* **2003,** *302* (5642), 103-6.

[32] Bouvard, D.; Pouwels, J.; De Franceschi, N.; Ivaska, J., Integrin inactivators: balancing cellular functions in vitro and in vivo. *Nat. Rev.Mol. Cell Biol.* **2013,** *14*, 430.

[33] Etienne-Manneville, S.; Hall, A., Rho GTPases in cell biology. *Nature* **2002,** *420* (6916), 629-35.

[34] Jiang, P.; Enomoto, A.; Takahashi, M., Cell biology of the movement of breast cancer cells: intracellular signalling and the actin cytoskeleton. *Cancer Lett.* **2009,** *284* (2), 122-30.

[35] Fritz, G.; Just, I.; Kaina, B., Rho GTPases are over-expressed in human tumors. *Int. J. Cancer* **1999,** *81* (5), 682-7.

[36] Fritz, G.; Brachetti, C.; Bahlmann, F.; Schmidt, M.; Kaina, B., Rho GTPases in human breast tumours: expression and mutation analyses and correlation with clinical parameters. *Br. J. Cancer* **2002,** *87* (6), 635-44.

[37] Wertheimer, E.; Gutierrez-Uzquiza, A.; Rosemblit, C.; Lopez-Haber, C.; Sosa, M. S.; Kazanietz, M. G., Rac signaling in breast cancer: A tale of GEFs and GAPs. *Cell. Signal.* **2012,** *24* (2), 353-362.

[38] Riento, K.; Ridley, A. J., Rocks: multifunctional kinases in cell behaviour. *Nat. Rev. Mol. Cell Biol.* **2003,** *4* (6), 446-56.

[39] Harvey, A. L., Natural products in drug discovery. *Drug Discov. Today* **2008,** *13* (19-20), 894-901.

[40] Newman, D. J.; Cragg, G. M., Natural Products as Sources of New Drugs from 1981 to 2014. *J. Nat. Prod.* **2016,** *79* (3), 629-61.

[41] Santos, R.; Ursu, O.; Gaulton, A.; Bento, A. P.; Donadi, R. S.; Bologa, C. G.; Karlsson, A.; Al-Lazikani, B.; Hersey, A.; Oprea, T. I.; Overington, J. P., A comprehensive map of molecular drug targets. *Nat. Rev. Drug Discov.* **2017,** *16* (1), 19-34.

[42] Nozoe, S.; Ishii, N.; Kusano, G.; Kikuchi, K.; Ohta, T., Neocarzilins A and B, Novel Polyenones from Streptomyces Carzinostaticus. *Tetrahedron Lett.* **1992,** *33* (49), 7547-7550.

[43] Nozoe, S.; Kikuchi, K.; Ishii, N.; Ohta, T., Synthesis of neocarzilin A: An absolute streochemistry. *Tetrahedron Lett.* **1992,** *33* (49), 7551-7552.

[44] Otsuka, M.; Ichinose, K.; Fujii, I.; Ebizuka, Y., Cloning, Sequencing, and Functional Analysis of an Iterative Type I Polyketide Synthase Gene Cluster for Biosynthesis of the Antitumor Chlorinated Polyenone Neocarzilin in "Streptomyces carzinostaticus". *Antimicrob. Agents Chemother.* **2004,** *48* (9), 3468-3476.

[45] Ishida, N.; Miyazaki, K.; Kumagai, K.; Rikimaru, M., Neocarzinostatin, an Antitumor Antibiotic of High Molecular Weight. Isolation, Physiochemical Properties and Biological Activities. *J. Antibiot.* **1965,** *18*, 68-76.

[46] Linial, M.; Miller, K.; Scheller, R. H., VAT-1: an abundant membrane protein from Torpedo cholinergic synaptic vesicles. *Neuron* **1989,** *2* (3), 1265-73.

[47] Linial, M.; Levius, O., The protein VAT-1 from Torpedo electric organ exhibits an ATPase activity. *Neurosci. Lett.* **1993,** *152* (1-2), 155-7.

[48] Linial, M., VAT-1 from Torpedo electric organ forms a high-molecular-mass protein complex within the synaptic vesicle membrane. *Eur. J. Biochem.* **1993,** *216* (1), 189-97.

[49] Levius, O.; Linial, M., VAT-1 from Torpedo synaptic vesicles is a calcium binding protein: a study in bacterial expression systems. *Cell Mol. Neurobiol.* **1993,** *13* (5), 483-92.

[50] Persson, B.; Zigler, J. S., Jr.; Jornvall, H., A super-family of medium-chain dehydrogenases/reductases (MDR). Sub-lines including zeta-crystallin, alcohol and polyol dehydrogenases, quinone oxidoreductase enoyl reductases, VAT-1 and other proteins. *Eur. J. Biochem.* **1994,** *226* (1), 15-22.

[51] Linial, M.; Levius, O., VAT-1 from Torpedo is a membranous homologue of zeta crystallin. *FEBS Lett.* **1993,** *315* (1), 91-4.

[52] Hayess, K.; Kraft, R.; Sachsinger, J.; Janke, J.; Beckmann, G.; Rohde, K.; Jandrig, B.; Benndorf, R., Mammalian protein homologous to VAT-1 of Torpedo californica: isolation from Ehrlich ascites tumor cells, biochemical characterization, and organization of its gene. *J. Cell Biochem.* **1998,** *69* (3), 304-15.

[53] Friedman, L. S.; Ostermeyer, E. A.; Lynch, E. D.; Welcsh, P.; Szabo, C. I.; Meza, J. E.; Anderson, L. A.; Dowd, P.; Lee, M. K.; Rowell, S. E.; et al., 22 genes from chromosome 17q21: cloning, sequencing, and characterization of mutations in breast cancer families and tumors. *Genomics* **1995,** *25* (1), 256-63.

[54] Miki, Y.; Swensen, J.; Shattuck-Eidens, D.; Futreal, P. A.; Harshman, K.; Tavtigian, S.; Liu, Q.; Cochran, C.; Bennett, L. M.; Ding, W.; et al., A strong candidate for the breast and ovarian cancer susceptibility gene BRCA1. *Science* **1994,** *266* (5182), 66-71.

[55] Koch, J.; Foekens, J.; Timmermans, M.; Fink, W.; Wirzbach, A.; Kramer, M. D.; Schaefer, B. M., Human VAT-1: a calcium-regulated activation marker of human epithelial cells. *Arch. Dermatol. Res* **2003,** *295* (5), 203-10.

[56] Junker, M.; Rapoport, T. A., Involvement of VAT-1 in Phosphatidylserine Transfer from the Endoplasmic Reticulum to Mitochondria. *Traffic* **2015,** *16* (12), 1306-17.

[57] Eura, Y.; Ishihara, N.; Oka, T.; Mihara, K., Identification of a novel protein that regulates mitochondrial fusion by modulating mitofusin (Mfn) protein function. *J. Cell Sci.* **2006,** *119* (Pt 23), 4913-25.

[58] Linial, M.; Levius, O.; Ilouz, N.; Parnas, D., The effect of calcium levels on synaptic proteins. A study on VAT-1 from Torpedo. *J. Physiol. Paris* **1995,** *89* (2), 103-12.

[59] Chen, H.; Detmer, S. A.; Ewald, A. J.; Griffin, E. E.; Fraser, S. E.; Chan, D. C., Mitofusins Mfn1 and Mfn2 coordinately regulate mitochondrial fusion and are essential for embryonic development. *J. Cell Biol.* **2003,** *160* (2), 189-200.

[60] Mori, F.; Tanigawa, K.; Endo, K.; Minamiguchi, K.; Abe, M.; Yamada, S.; Miyoshi, K., VAT-1 is a novel pathogenic factor of progressive benign prostatic hyperplasia. *Prostate* **2011,** *71* (14), 1579-86.

[61] Mertsch, S.; Becker, M.; Lichota, A.; Paulus, W.; Senner, V., Vesicle amine transport protein-1 (VAT-1) is upregulated in glioblastomas and promotes migration. *Neuropathol. Appl. Neurobiol.* **2009,** *35* (4), 342-52.

[62] Ran, F. A.; Hsu, P. D.; Wright, J.; Agarwala, V.; Scott, D. A.; Zhang, F., Genome engineering using the CRISPR-Cas9 system. *Nat. Protoc.* **2013,** *8* (11), 2281-2308.

[63] Concordet, J.-P.; Haeussler, M., CRISPOR: intuitive guide selection for CRISPR/Cas9 genome editing experiments and screens. *Nucleic Acids Res.* **2018,** *46* (W1), W242-W245.

[64] Haeussler, M.; Schonig, K.; Eckert, H.; Eschstruth, A.; Mianne, J.; Renaud, J. B.; Schneider-Maunoury, S.; Shkumatava, A.; Teboul, L.; Kent, J.; Joly, J. S.; Concordet, J. P., Evaluation of off-target and on-target scoring algorithms and integration into the guide RNA selection tool CRISPOR. *Genome Biol.* **2016,** *17* (1), 148.

[65] Humphries, M. J., Cell-substrate adhesion assays. *Curr. Protoc. Cell Biol.* **2001,** *Chapter 9*, Unit 9 1.

[66] Nicoletti, I.; Migliorati, G.; Pagliacci, M. C.; Grignani, F.; Riccardi, C., A rapid and simple method for measuring thymocyte apoptosis by propidium iodide staining and flow cytometry. *J Immunol. Methods* **1991,** *139* (2), 271-9.

[67] Riccardi, C.; Nicoletti, I., Analysis of apoptosis by propidium iodide staining and flow cytometry. *Nat. Protoc.* **2006,** *1* (3), 1458-61.

[68] Smith, P. K.; Krohn, R. I.; Hermanson, G. T.; Mallia, A. K.; Gartner, F. H.; Provenzano, M. D.; Fujimoto, E. K.; Goeke, N. M.; Olson, B. J.; Klenk, D. C., Measurement of protein using bicinchoninic acid. *Anal. Biochem.* **1985,** *150* (1), 76-85.

[69] Laemmli, U. K., Cleavage of structural proteins during the assembly of the head of bacteriophage T4. *Nature* **1970,** *227* (5259), 680-5.

[70] Gurtler, A.; Kunz, N.; Gomolka, M.; Hornhardt, S.; Friedl, A. A.; McDonald, K.; Kohn, J. E.; Posch, A., Stain-Free technology as a normalization tool in Western blot analysis. *Anal. Biochem.* **2013,** *433* (2), 105-11.

[71] Kurien, B. T.; Scofield, R. H., Introduction to protein blotting. *Methods Mol. Biol.* **2009,** *536*, 9-22.

[72] Braig, S.; Kressirer, C. A.; Liebl, J.; Bischoff, F.; Zahler, S.; Meijer, L.; Vollmar, A. M., Indirubin derivative 6BIO suppresses metastasis. *Cancer Res.* **2013,** *73* (19), 6004-12.

[73] Lewis-Saravalli, S.; Campbell, S.; Claing, A., ARF1 controls Rac1 signaling to regulate migration of MDA-MB-231 invasive breast cancer cells. *Cell. Signal.* **2013,** *25* (9), 1813-9.

[74] Hynes, R. O., Integrins: Versatility, modulation, and signaling in cell adhesion. *Cell* **1992,** *69* (1), 11-25.

[75] Evans, M. J.; Cravatt, B. F., Mechanism-based profiling of enzyme families. *Chem. Rev.* **2006,** *106* (8), 3279-301.

[76] Gersch, M.; Kreuzer, J.; Sieber, S. A., Electrophilic natural products and their biological targets. *Nat. Prod. Rep.* **2012,** *29* (6), 659-82.

[77] Fonovic, M.; Bogyo, M., Activity-based probes as a tool for functional proteomic analysis of proteases. *Expert Rev. Proteomics* **2008,** *5* (5), 721-30.

[78] Liu, Y.; Guo, M., Chemical proteomic strategies for the discovery and development of anticancer drugs. *Proteomics* **2014,** *14* (4-5), 399-411.

[79] Fux, A.; Korotkov, V. S.; Schneider, M.; Antes, I.; Sieber, S. A., Chemical Cross-Linking Enables Drafting ClpXP Proximity Maps and Taking Snapshots of In Situ Interaction Networks. *Cell Chem. Biol.* **2019,** *26* (1), 48-59 e7.

[80] Shannon, P.; Markiel, A.; Ozier, O.; Baliga, N. S.; Wang, J. T.; Ramage, D.; Amin, N.; Schwikowski, B.; Ideker, T., Cytoscape: a software environment for integrated models of biomolecular interaction networks. *Genome Res.* **2003,** *13* (11), 2498-504.

[81] Maere, S.; Heymans, K.; Kuiper, M., BiNGO: a Cytoscape plugin to assess overrepresentation of gene ontology categories in biological networks. *Bioinformatics* **2005,** *21* (16), 3448-9.

[82] Li, C. J.; Trost, B. M., Green chemistry for chemical synthesis. *Proc. Natl. Acad. Sci. U.S.A.* **2008,** *105* (36), 13197-202.

[83] Lipinski, C. A.; Lombardo, F.; Dominy, B. W.; Feeney, P. J., Experimental and computational approaches to estimate solubility and permeability in drug discovery and development settings. *Adv Drug Deliv Rev* **2001,** *46* (1-3), 3-26.

[84] Harvey, A. L.; Edrada-Ebel, R.; Quinn, R. J., The re-emergence of natural products for drug discovery in the genomics era. *Nat. Rev. Drug Discov.* **2015,** *14*, 111.

[85] Piggott, A. M.; Karuso, P., Quality not Quantity: The Role of Marine Natural Products in Drug Discovery and Reverse Chemical Proteomics. *Marine Drugs* **2005,** *3* (2), 36-63.

[86] Schenone, M.; Dančík, V.; Wagner, B. K.; Clemons, P. A., Target identification and mechanism of action in chemical biology and drug discovery. *Nat. Chem. Biol.* **2013,** *9*, 232.

[87] Berger, A. B.; Vitorino, P. M.; Bogyo, M., Activity-based protein profiling: applications to biomarker discovery, in vivo imaging and drug discovery. *Am. J. Pharmacogenomics* **2004,** *4* (6), 371-81.

[88] Savitski, M. M.; Reinhard, F. B.; Franken, H.; Werner, T.; Savitski, M. F.; Eberhard, D.; Martinez Molina, D.; Jafari, R.; Dovega, R. B.; Klaeger, S.; Kuster, B.; Nordlund, P.; Bantscheff, M.; Drewes, G., Tracking cancer drugs in living cells by thermal profiling of the proteome. *Science* **2014,** *346* (6205), 1255784.

[89] Palmer, T. D.; Ashby, W. J.; Lewis, J. D.; Zijlstra, A., Targeting tumor cell motility to prevent metastasis. *Adv. Drug Deliv. Rev.* **2011,** *63* (8), 568-81.

[90] Nguyen, D. X.; Bos, P. D.; Massague, J., Metastasis: from dissemination to organ-specific colonization. *Nat. Rev. Cancer* **2009,** *9* (4), 274-84.

[91] Wells, A.; Grahovac, J.; Wheeler, S.; Ma, B.; Lauffenburger, D., Targeting tumor cell motility as a strategy against invasion and metastasis. *Trends Pharmacol. Sci.* **2013,** *34* (5), 283-289.

[92] Gandalovicova, A.; Rosel, D.; Fernandes, M.; Vesely, P.; Heneberg, P.; Cermak, V.; Petruzelka, L.; Kumar, S.; Sanz-Moreno, V.; Brabek, J., Migrastatics-Anti-metastatic and Anti-invasion Drugs: Promises and Challenges. *Trends Cancer* **2017,** *3* (6), 391-406.

[93] Raab-Westphal, S.; Marshall, J. F.; Goodman, S. L., Integrins as Therapeutic Targets: Successes and Cancers. *Cancers (Basel)* **2017,** *9* (9).

[94] Radisky, E. S.; Raeeszadeh-Sarmazdeh, M.; Radisky, D. C., Therapeutic Potential of Matrix Metalloproteinase Inhibition in Breast Cancer. *J. Cell Biochem.* **2017,** *118* (11), 3531-3548.

[95] Yamaguchi, H.; Condeelis, J., Regulation of the actin cytoskeleton in cancer cell migration and invasion. *BBA - Mol. Cell Res.* **2007,** *1773* (5), 642-652.

[96] Nummela, P.; Yin, M.; Kielosto, M.; Leaner, V.; Birrer, M. J.; Holtta, E., Thymosin beta4 is a determinant of the transformed phenotype and invasiveness of S-adenosylmethionine decarboxylase-transfected fibroblasts. *Cancer Res.* **2006,** *66* (2), 701-12.

[97] Menhofer, M. H.; Kubisch, R.; Schreiner, L.; Zorn, M.; Foerster, F.; Mueller, R.; Raedler, J. O.; Wagner, E.; Vollmar, A. M.; Zahler, S., The Actin Targeting Compound Chondramide Inhibits Breast Cancer Metastasis via Reduction of Cellular Contractility. *PLoS ONE* **2014,** *9* (11), e112542.

[98] Yoshioka, K.; Foletta, V.; Bernard, O.; Itoh, K., A role for LIM kinase in cancer invasion. *Proc. Natl. Acad. Sci. U.S.A.* **2003,** *100* (12), 7247-52.

[99] Zhao, X.; Mei, K.; Cai, X.; Chen, J.; Yu, J.; Zhou, C.; Li, Q., A randomized phase II study of recombinant human endostatin plus gemcitabine/cisplatin compared with gemcitabine/cisplatin alone as first-line therapy in advanced non-small-cell lung cancer. *Invest. New Drugs* **2012,** *30* (3), 1144-9.

[100] Carroll, R. E.; Benya, R. V.; Turgeon, D. K.; Vareed, S.; Neuman, M.; Rodriguez, L.; Kakarala, M.; Carpenter, P. M.; McLaren, C.; Meyskens, F. L., Jr.; Brenner, D. E., Phase IIa clinical trial of curcumin for the prevention of colorectal neoplasia. *Cancer Prev. Res. (Phila)* **2011,** *4* (3), 354-64.

[101] Lasinska, I.; Mackiewicz, J., Integrins as A New Target for Cancer Treatment. *Anticancer Agents Med. Chem.* **2018**.

[102] Palecek, S. P.; Loftus, J. C.; Ginsberg, M. H.; Lauffenburger, D. A.; Horwitz, A. F., Integrin-ligand binding properties govern cell migration speed through cell-substratum adhesiveness. *Nature* **1997,** *385* (6616), 537-40.

[103] Huttenlocher, A.; Ginsberg, M. H.; Horwitz, A. F., Modulation of cell migration by integrin-mediated cytoskeletal linkages and ligand-binding affinity. *J. Cell Biol.* **1996,** *134* (6), 1551-62.

[104] Steeg, P. S., Targeting metastasis. *Nat. Rev. Cancer* **2016,** *16*, 201.

[105] Sun, H. Q.; Yamamoto, M.; Mejillano, M.; Yin, H. L., Gelsolin, a multifunctional actin regulatory protein. *J. Biol. Chem* **1999,** *274* (47), 33179-82.

[106] Felding-Habermann, B.; Cheresh, D. A., Vitronectin and its receptors. *Curr. Opi. Cell Biol.* **1993,** *5* (5), 864-868.

[107] Pankov, R.; Yamada, K. M., Fibronectin at a glance. *J. Cell Sci.* **2002,** *115* (20), 3861-3863.

[108] Buckley, C. D.; Rainger, G. E.; Bradfield, P. F.; Nash, G. B.; Simmons, D. L., Cell adhesion: More than just glue (Review). *Mol. Membr. Biol.* **1998,** *15* (4), 167-176.

APPENDIX

6 Appendix

6.1 Supplementary Material

6.1.1 Supplementary Figures
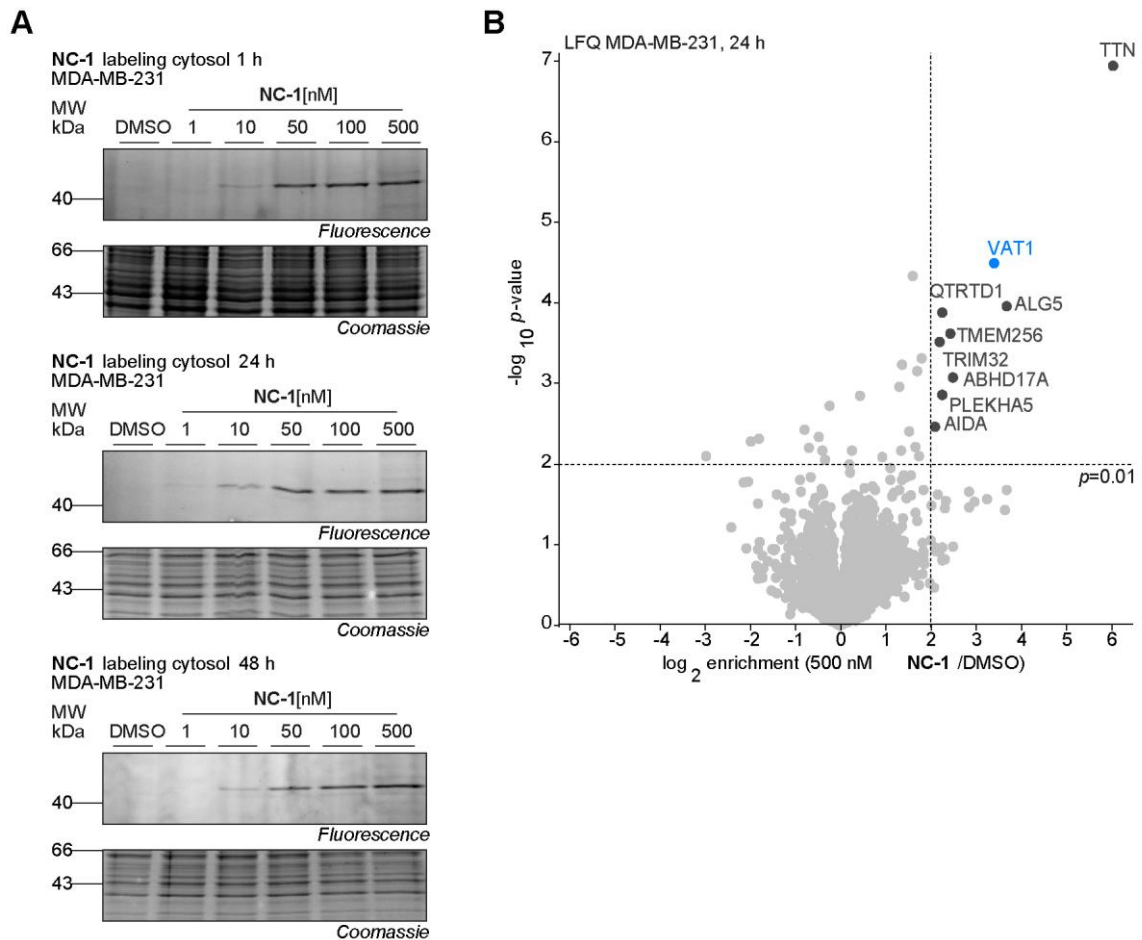
Supplementary Figure 1. Analytical probe labeling, target identification, and competitive labeling of VAT-1. **(A)** SDS-PAGE of time dependent analytical *in situ* labeling with NC-1 for 1 h, 24 h and 48 h in MDA-MB 231 cells. **(B)** Volcano plot of *in situ* label-free ABPP experiment in MDA-MB-231 cells which were incubated for 24 h with 500 nM NC-1 (n=4). Hits matching the criteria ((log$_2$(enrichment) > 2, p-value < 0.05) highlighted in dark grey are listed in Supplementary Table 3 in the Appendix. (performed by Carolin Gleißner, Technical University of Munich)
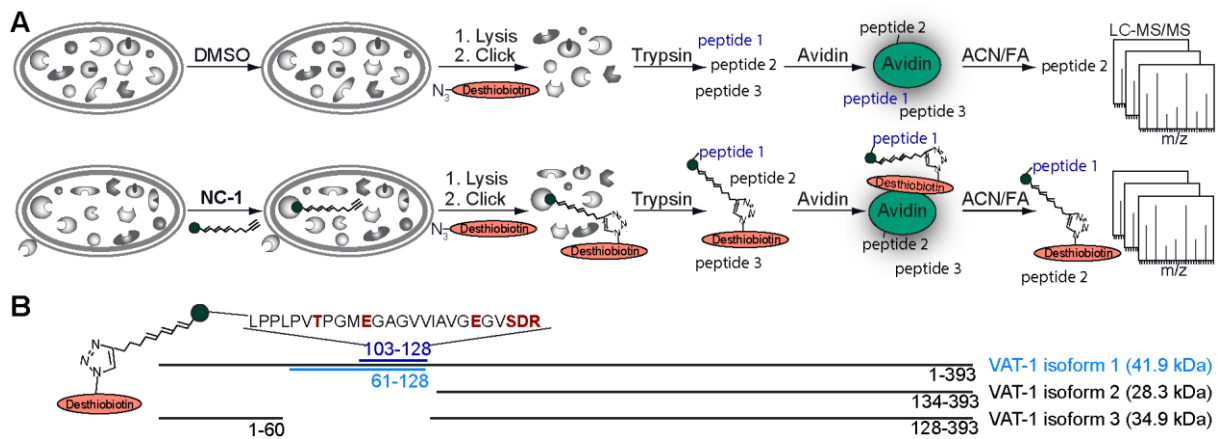
Supplementary Figure 2. Binding site peptide identification. (A) Schematic overview of ABPP based approach to identify binding site peptides. After protein digestion, only peptides bound to the probe are enriched on avidin beads and eluted with acetonitrile (MeCN) and formic acid (FA) for MS/MS detection. **(B)** Identified binding site peptide (aa 103-128) in NC-1 treated cells and location of the peptide in the part of VAT-1 which is unique to isoform 1. Mutated residues are shown in red. (performed by Carolin Gleißner, Technical University of Munich)

6.1.2   Supplementary Tables

Supplementary Table 1. Hits matching the criteria (($\log_2$(enrichment) > 2, p-value < 0.05) of SILAC targetID with 500 nM **NC-1** in MDA-MB-231

Protein name	Gene name	Enrichment	p-value	Sequence coverage [%]
Synaptic vesicle membrane protein VAT-1 homolog	VAT1	4.49	5.19	57
Reticulon	RTN3	4.23	3.16	22
Heme oxygenase 2	HMOX2	3.68	3.85	66.8
Redox-regulatory protein FAM213A	FAM213A	2.97	3.37	29.3
Transcriptional enhancer factor TEF-1	TEAD1	2.65	4.65	23
Glutathione S-transferase omega-1	GSTO1	2.55	4.36	49
Endonuclease domain-containing 1 protein	ENDOD1	2.55	4.76	16.2
Cytochrome b5 type B	CYB5B	2.29	4.13	50.7

Supplementary Table 2. Hits matching the criteria ((log$_2$(enrichment) > 2, p-value < 0.05) of LFQ targetID with 100 nM **NC-1** in MDA-MB-231

Protein name	Gene name	Enrichment	p-value	Sequence coverage [%]
Synaptic vesicle membrane protein VAT-1 homolog	VAT1	5.77	5.00	27
Heme oxygenase 2	HMOX2	5.07	4.67	34.5
Cytochrome b5 type B	CYB5B	2.58	3.00	18
Mitochondrial antiviral-signaling protein	MAVS	2.52	2.32	19.8

Supplementary Table 3. Hits matching the criteria ((log$_2$(enrichment) > 2, p-value < 0.01) of LFQ targetID with 500 nM **NC-1** for 24 h in MDA-MB-231

Protein name	Gene name	Enrichment	p-value	Sequence coverage [%]
Titin	TTN	6.05	6.95	0.2
Dolichyl-phosphate beta-glucosyltransferase	ALG5	3.69	3.96	18.3
Splicing factor U2AF 26 kDa subunit	U2AF1L4	3.68	1.68	44.4
Protein transport protein Sec61 subunit gamma	SEC61G	3.64	1.43	23.5
Synaptic vesicle membrane protein VAT-1 homolog	VAT1	3.41	4.49	45.5
Hyccin	FAM126A	3.26	1.57	6.5
Vesicular integral-membrane protein VIP36	LMAN2	2.97	1.53	11.2
Tubulin alpha-4A chain	TUBA4A	2.85	1.66	43.8
RAD50-interacting protein 1	RINT1	2.84	1.46	5.7
Alpha/beta hydrolase domain-containing protein 17A	ABHD17A	2.50	3.08	6.1
Transmembrane protein 256	TMEM256	2.43	3.62	22
Signal peptidase complex subunit 1	SPCS1	2.35	1.55	26.5
Metalloproteinase inhibitor 2	TIMP2	2.32	1.45	11.7
Pleckstrin homology domain-containing family A member 5	PLEKHA5	2.26	2.86	9.5
Queuine tRNA-ribosyltransferase subunit QTRTD1	QTRTD1	2.26	3.88	8.4
E3 ubiquitin-protein ligase TRIM32	TRIM32	2.20	3.51	5.1
Peptidyl-prolyl cis-trans isomerase	PPIF	2.16	1.62	32.4
Axin interactor, dorsalization-associated protein	AIDA	2.10	2.46	23
39S ribosomal protein L24, mitochondrial	MRPL24	2.02	1.48	28.7

Supplementary Table 4. Hits matching the criteria ((log$_2$(enrichment) > 1.5, p-value < 0.05) for competition with 500 nM **NCA** in MDA-MB-231

Protein name	Gene name	Enrichment	p-value	Sequence coverage [%]
Synaptic vesicle membrane protein VAT-1 homolog	VAT1	2.98	2.23	27
Heme oxygenase 2	HMOX2	1.82	2.16	34.5

Supplementary Table 5. Hits matching the criteria ((log$_2$(enrichment) > 1, p-value < 0.05) of VAT-1 co-IP with DSSO crosslinker in MDA-MB-231

Protein name	Gene name	Enrichment	p-value	Sequence coverage [%]
Synaptic vesicle membrane protein VAT-1 homolog	VAT1	10.03	3.33	70.5
Gelsolin	GSN	9.17	2.89	37.2
Talin-1	TLN1	7.19	3.32	44.6
Complement C5	C5	7.13	2.24	5.4
Alpha-2-macroglobulin	A2M	7.11	2.31	6
Aspartate--tRNA ligase, mitochondrial	DARS2	7.10	2.32	44.7
Complement C4-A	C4A	7.01	2.20	7.5
Thrombospondin-1	THBS1	6.67	2.01	15.9
Inter-alpha-trypsin inhibitor heavy chain H2	ITIH2	6.62	2.33	9.4
Serum paraoxonase/arylesterase 1	PON1	6.34	2.20	8.5
UTP--glucose-1-phosphate uridylyltransferase	UGP2	6.33	2.39	46.7
L-lactate dehydrogenase	LDHA	6.13	2.62	74.7
Peroxisomal multifunctional enzyme type 2	HSD17B4	6.02	2.08	53.4
Complement C3	C3	5.60	1.99	4.6
Heat shock protein 75 kDa, mitochondrial	TRAP1	5.52	3.16	27.5
Histidine-rich glycoprotein	HRG	5.52	1.83	1.9
Fibronectin	FN1	5.44	1.86	6.4
Succinate dehydrogenase [ubiquinone] flavoprotein subunit, mitochondrial	SDHA	5.33	3.11	47.9
L-lactate dehydrogenase	LDHB	5.32	3.34	46.4
Complement component 1 Q subcomponent-binding protein, mitochondrial	C1QBP	5.27	4.12	33.7
Inter-alpha-trypsin inhibitor heavy chain H1	ITIH1	5.25	1.81	3.6
Ceruloplasmin	CP	5.20	2.00	14.1
Glutathione peroxidase	GPX3	5.20	1.78	10.7
Cofilin-1	CFL1	5.20	2.29	61.4

Endoplasmin	TRA1	5.16	1.92	67
Inter-alpha-trypsin inhibitor heavy chain H3	ITIH3	4.93	1.62	13.4
Serpin H1	SERPINH1	4.78	1.62	40.2
Polyribonucleotide nucleotidyltransferase 1, mitochondrial	PNPT1	4.69	2.09	32.6
Monofunctional C1-tetrahydrofolate synthase, mitochondrial	MTHFD1L	4.63	2.44	23.7
Complement component C8 beta chain	C8B	4.44	2.09	14.4
Vinculin	VCL	4.22	2.95	17.8
Filamin-A	FLNA	4.21	1.99	39.6
Cytochrome b-c1 complex subunit 2, mitochondrial	UQCRC2	4.17	1.55	44.2
Pyruvate carboxylase	PC	4.12	1.91	40.7
Nucleoside diphosphate kinase	NME2	4.10	3.33	55.1
Malate dehydrogenase	MDH2	4.06	1.85	64.6
Alkyldihydroxyacetonephosphate synthase, peroxisomal	AGPS	4.03	3.10	34.5
	MYL6	4.01	2.19	65.1
Complement factor B	CFB	3.96	1.59	4.8
Procollagen galactosyltransferase 1	COLGALT1	3.88	2.03	17.7
Leucine-rich PPR motif-containing protein, mitochondrial	LRPPRC	3.87	1.39	49
Fructose-bisphosphate aldolase;Fructose-bisphosphate aldolase A	ALDOA	3.87	1.80	54.4
Glutaminase kidney isoform, mitochondrial	GLS	3.78	1.91	39.5
Ras-related protein Rab-1B	RAB1B	3.78	2.58	66.2
Procollagen-lysine,2-oxoglutarate 5-dioxygenase 3	PLOD3	3.65	1.57	33.9
Transmembrane protein 33	TMEM33	3.63	2.42	26.3
Plastin-2	LCP1	3.54	1.90	15.6
Tropomyosin alpha-4 chain	TPM4	3.46	2.46	52.4
Serum paraoxonase/lactonase 3	PON3	3.46	1.99	11
Succinate dehydrogenase [ubiquinone] iron-sulfur subunit, mitochondrial	SDHB	3.45	1.77	20
GDP-fucose protein O-fucosyltransferase 1	POFUT1	3.45	1.51	11.9
Acyl-coenzyme A thioesterase 8	ACOT8	3.42	1.84	25.7
Aconitate hydratase, mitochondrial	ACO2	3.41	2.51	18.8
Aldehyde dehydrogenase, mitochondrial	ALDH2	3.32	1.56	29.8
Medium-chain specific acyl-CoA dehydrogenase, mitochondrial	ACADM	3.31	3.21	30.9

Serotransferrin	TF	3.26	1.33	7.5
Proteasome subunit alpha type	PSMA5	3.15	2.61	17
Mitochondrial import receptor subunit TOM70	TOMM70A	3.02	1.84	20.7
Mitochondrial dicarboxylate carrier	SLC25A10	2.99	2.67	16.7
60S ribosomal protein L28	RPL28	2.87	1.31	32.9
Adipocyte plasma membrane-associated protein	APMAP	2.82	1.77	21.8
Proteasome subunit alpha type	PSMA7	2.78	1.80	28.2
Cell division control protein 42 homolog	CDC42	2.60	1.56	52.4
Sodium/potassium-transporting ATPase subunit alpha-1	ATP1A1	2.60	1.84	34.6
60S ribosomal protein L27	RPL27	2.59	1.69	22.2
CD44 antigen	CD44	2.57	1.74	29.1
Acetyl-CoA acetyltransferase, mitochondrial	ACAT1	2.56	2.26	25.1
Solute carrier family 2, facilitated glucose transporter member 1	SLC2A1	2.53	2.30	8.4
Tyrosine-protein phosphatase non-receptor type	PTPN1	2.49	1.47	16.8
ATP-dependent Clp protease ATP-binding subunit clpX-like, mitochondrial	CLPX	2.48	2.53	22.7
Ras-related C3 botulinum toxin substrate 2	RAC2	2.44	2.75	31.2
Procollagen-lysine,2-oxoglutarate 5-dioxygenase 1	PLOD1	2.38	1.53	18.2
Glutamate dehydrogenase	GLUD1	2.26	1.64	52.3
Elongation factor Tu, mitochondrial	TUFM	2.21	1.73	43.6
Integrin beta-1	ITGB1	2.20	2.95	8.3
Isoleucine--tRNA ligase, mitochondrial	IARS2	2.19	1.97	13.6
Ras-related protein Rab-11B	RAB11B	2.16	1.31	50
Voltage-dependent anion-selective channel protein 1	VDAC1	2.12	1.32	67.5
Hypoxia up-regulated protein 1	HYOU1	1.84	2.89	20.4
Neutral alpha-glucosidase AB	GANAB	1.83	1.97	32.8
Microtubule-associated protein RP/EB family member 1	MAPRE1	1.77	1.61	31.5
Transferrin receptor protein 1	TFRC	1.75	2.16	33.2
10 kDa heat shock protein, mitochondrial	HSPE1	1.74	1.54	55.9
Protein disulfide-isomerase A6	PDIA6	1.52	1.73	35.5
Endoplasmic reticulum resident protein 29	HEL-S-107	1.49	1.84	14.6
60 kDa heat shock protein, mitochondrial	HSPD1	1.43	2.90	79.8

Supplementary Table 6. Hits matching the criteria ((log$_2$(t-test difference) > 1, p-value < 0.05) of LFQ global proteome with 500 nM **NCA** in MDA-MB-231

Protein name	Gene name	Enrichment	p-value	Sequence coverage [%]
depleted				
Prostaglandin reductase 2	PTGR2	-6.01	3.02	26.5
Proteasome subunit beta type-10	PSMB10	-3.64	1.96	23.4
Tetratricopeptide repeat protein 17	TTC17	-5.41	2.78	3.8
Prenylated Rab acceptor protein 1	RABAC1	-8.35	3.80	19.2
Vacuolar protein sorting-associated protein 37C	VPS37C	-2.56	1.37	33.8
Tubulin beta-4A chain	TUBB4A	-2.62	1.40	57
[3-methyl-2-oxobutanoate dehydrogenase [lipoamide]] kinase, mitochondrial	BCKDK	-2.63	1.41	19.2
Guanine nucleotide exchange factor MSS4	RABIF	-3.80	2.05	29.3
Delta-like protein	JAG1	-2.79	1.50	4.5
WD repeat-containing protein 43	WDR43	-2.55	1.36	8.3
Bcl2-associated agonist of cell death	BAD	-4.47	2.37	69.1
28S ribosomal protein S18c, mitochondrial	MRPS18C	-2.68	1.44	16.8
Molybdenum cofactor sulfurase	MOCOS	-2.52	1.34	8.7
Mannose-P-dolichol utilization defect 1 protein	MPDU1	-3.78	2.04	20.6
enriched				
Rab GTPase-binding effector protein 1	RABEP1	1.64	1.32	10.7
cAMP-dependent protein kinase catalytic subunit beta	PRKACB	1.33	1.80	40.7
Ribonuclease T2	RNASET2	1.29	1.59	17.9
Cytosolic Fe-S cluster assembly factor NUBP1	NUBP1	1.21	2.08	11.2
Suppressor of tumorigenicity 7 protein-like	ST7	1.17	1.62	7.1
Protein Njmu-R1	C17orf75	1.17	2.52	12.6
Rho-related GTP-binding protein RhoF	RHOF	1.05	1.49	46

6.1.3 Supplementary Schemes

Neocarzilin A and C
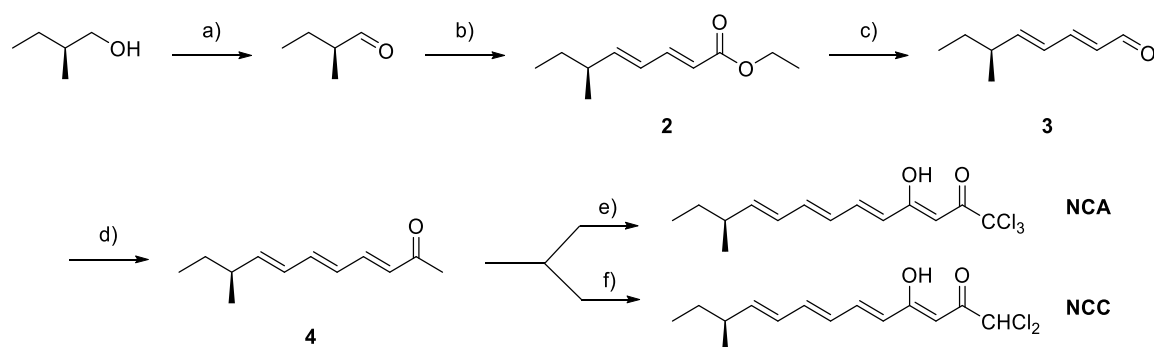
Supplementary Scheme 1. Synthesis of **Neocarzilins A** and **C**: a) TEMPO (1 mol-%), KBr (0.10 eq), NaOCl (2.00 eq), CH$_2$Cl$_2$/carbonate-buffer pH = 8.6, 0 °C, 45 min, 85%; b) 1. LiHMDS (1.00 eq), 2. ethyl (E)-4-(diethoxyphosphoryl)-but-2-enoate (1.00 eq), THF, -78 °C → -40 °C, 3 h, 76%; c) DIBAL-H (2.10 eq) MnO$_2$ (20.0 eq), THF, hexane, -78 °C → rt, 5 h, 72% over 2 steps; d) 1-(Triphenylphosphoranylidene)-2-propanone (2.00 eq), toluene, 100 °C, 16 h, 59%; e) 1. LiHMDS (1.05 eq); 2. Trichloroacetic anhydride (2.00 eq), THF, -78 °C, 3 h, 71%; f) 1. LiHMDS (1.05 eq), 2. Dichloroacetic anhydride (2.00 eq), THF, -78 °C, 3 h, 44%.

Neocarzilin A'
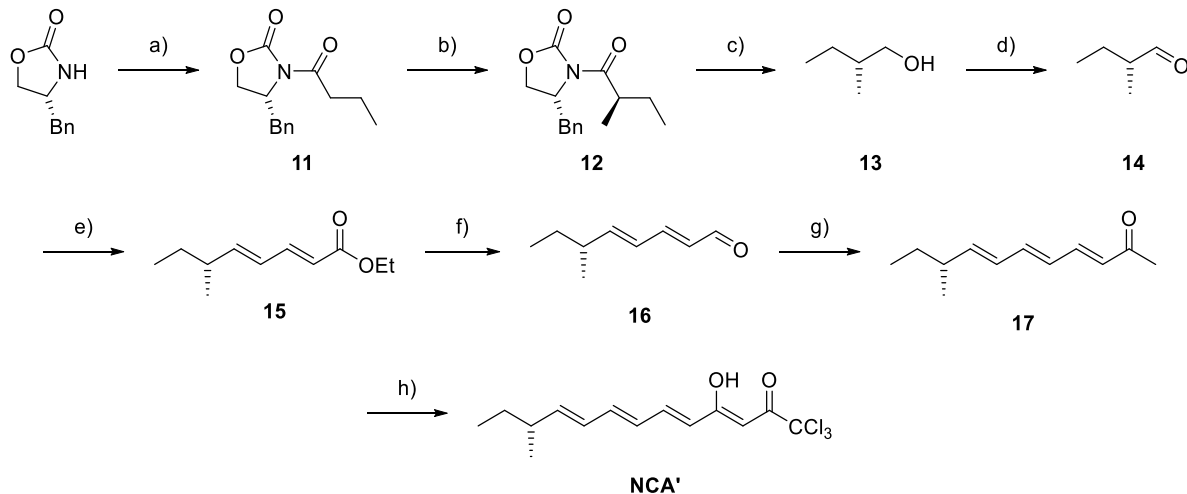
Supplementary Scheme 2. Synthesis of **Neocarzilin A'**: a) 1.) *n*-BuLi (1.10 eq), THF, -78 °C, 0.5 h, 2.) butyryl chloride, -78 °C, 0.5 h, -78 °C – rt, 0.5 h, 68%; b) 1.) NaHMDS (1.20 eq), THF, -78 °C, 1 h, 2.) MeI (2.50 eq), -78 °C, 2.5 h, 77%; c) LiBH$_4$ (0.70 eq), MeOH (1.48 eq), Et$_2$O, -20 °C → rt, 5 h, 66%; d) (COCl)$_2$ (1.50 eq), DMSO (2.50 eq), NEt$_3$ (5.00 eq), CH$_2$Cl$_2$, -78 °C, 0.5 h, rt, 2 h, 56%; e) 1. LiHMDS (1.50 eq), 2. ethyl (E)-4-(diethoxyphosphoryl)-but-2-enoate (1.50 eq), THF, -78 °C → -40 °C, 3 h, 30%; f) DIBAL-H (2.50 eq) MnO$_2$ (20.0 eq), THF, hexane, -78 °C → rt, 5 h, 78% over 2 steps; g) 1-(Triphenylphosphoranylidene)-2-propanone (2.00 eq), toluene, 100 °C, 16 h, 77%; h) 1. LiHMDS (1.10 eq); 2. Trichloroacetic anhydride (2.00 eq), THF, -78 °C, 3 h, 60%.

Neocarzilin B
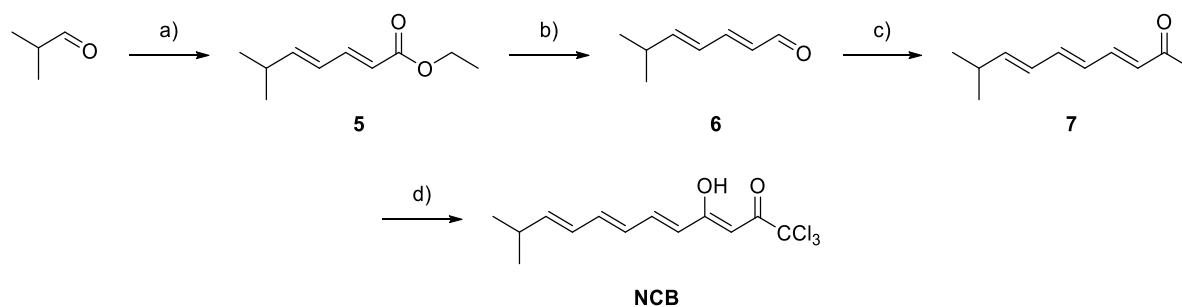
Supplementary Scheme 3. Synthesis of **Neocarzilin B**: a) LiHMDS (1.00 eq) ethyl (E)-4-(diethoxyphosphoryl)-but-2-enoate (1.00 eq), THF, -78 °C → rt, 4 h, 51%; b) DIBAL-H (2.10 eq), MnO$_2$ (20.0 eq), THF, hexane, -78 °C → rt, 5 h, 83% over 2 steps; c) 1-(Triphenylphosphoranylidene)-2-propanone (2.00 eq), toluene,100 °C, 16 h, 60%; d) 1. LiHMDS (1.00 eq), 2. trichloroacetic anhydride (2.00 eq), THF, -78 °C, 3 h, 83%.

Activity-based probe NC-1
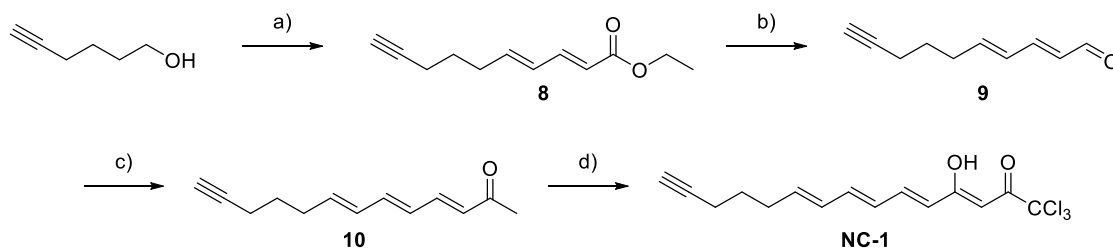
Supplementary Scheme 4. Synthesis of probe **NC-1**: a) 1. DMSO (2.22 eq), (COCl)$_2$ (1.11 eq), NEt$_3$ (4.50 eq); 2. LiHMDS (1.00 eq), ethyl (E)-4-(diethoxyphosphoryl)-but-2-enoate (4.15) (1.00 eq), CH$_2$Cl$_2$, THF, -78 °C → rt, 4 h, 38% over 2 steps; b) DIBAL-H (2.10 eq), MnO$_2$ (20.0 eq), THF, hexane, -78 °C → rt, 5 h, 54% over 2 steps; c) 1-(Triphenyl-phosphoranylidene)-2-propanone (2.00 eq), toluene, 100 °C, 16 h, 54%; d) 1. LiHMDS (2.00 eq); 2. trichloroacetic anhydride (1.00 eq), THF, -78 °C, 3 h, 45%.

6.2   Abbreviations

ABPP	Activity-based protein profiling
AM	Acetoxymethyl
APS	Ammonium persulfate
ATP	Adenosine triphosphate
BCA	Bicinchoninic acid
BPH	Benign prostatic hyperplasia
BRCA	Breast cancer susceptibility protein
BSA	Bovine serum albumin
Cdc42	Cell division control protein 42 homolog
Co-IP	Co-immunoprecipitation
CRISPR	Clustered regularly interspaced short palindromic repeats
CTB	CellTiter-Blue®
DCIS	Ductal carcinoma in situ
DMEM	Dulbecco´s modified eagle´s medium
DMSO	Dimethyl sulfoxide
DNA	Deoxyribonucleic acid
DSSO	Disuccinimidyl sulfoxide
DTT	Dithiothreitol
E.coli	Escherichia coli
ECL	Enhanced chemiluminescence
ECM	Extracellular matrix
EDTA	Ethylene diamine tetraacetic acid
EGF	Epidermal growth factor
EGTA	Ethylene glycol tetraacetic acid
Em	Emission
ER	Endoplasmatic reticulum
Ex	Excitation
FACS	Fluorescence-activated cell sorting
FAK	Focal adhesion kinase
FCS	Fetal calf serum
GFP	Green fluorescent protein
GO	Gene ontology
GTP	Guanosine-5'-triphosphate
HEPES	Hydroxyethyl-piperazineethane-sulfonic acid buffer
HER2	Human epidermal growth factor receptor 2
HMOX2	Heme oxygenase
HRP	Horseradish peroxidase
IC_{50}	Half maximal inhibitory concentration
ICAP-1	Integrin cytoplasmic domain-associated protein 1
k.o.	Knockout
LC	Liquid chromatography

LCIS	Lobular carcinoma in situ
LQF	Label-free quantification
MDR	Medium-chain dehydrogenases/reductases
Mfn1	Mitofusin 1
MIB	Mitofusin binding protein
MIDAS	Metal ion dependent adhesion site
MMP	Matrix metalloproteinase
MS	Mass spectrometry
MS-CETSA	Mass spectrometry-based cellular thermal shift assay
NCA/A'/B/C	Neocarzilin A/A'/B/C
NMR	Nuclear magnetic resonance
P/S	Penicillin/streptomycin
PBS	Phosphate buffered saline
PCR	Polymerase chain reaction
PE	Phosphatidylethanolamine
PFA	Paraformaldehyde
PI	Propidium iodide
PMSF	Phenylmethylsulfonyl fluoride
PS	Phosphatidylserine
Rac1/2	Ras-related C3 botulinum toxin substrate 1/2
RAP1A-GTP	Ras-related protein Rap-1A-Guanosin triphosphate
Rho	Ras homologous protein
RIAM	RAP1-GTP-interacting adapter molecule
RNA	Ribonucleic acid
ROCK	Rho-associated protein kinase
RPMI	Roswell park memorial institute medium
RT	Room temperature
SAR	Structure-activity relationship
SDS-PAGE	SDS-polyacrylamide gel electrophoresis
SEM	Standard error of the mean
SERM	Selective estrogen receptor modulator
sgRNA	Single guide RNA
SH3	Src-homology 3
SILAC	Stable isotope labeling of amino acids in cell culture
siRNA	Small interfering RNA
TBS-T	Tris-buffered saline - Tween20
TCE	Trichloroethylene
TEMED	Tetramethylethylendiamin
TEV	Tobacco etch virus
TNM	TNM Classification of Malignant Tumors
Tris	Tris(hydroxymethyl)aminomethane
VAT-1	Synaptic vesicle membrane protein 1
WT	Wild type

6.3   Symbols and Units

%	Percent
% (m/v)	Mass percent
% (v/v)	Volume percent
°C	Degree Celsius
µg	Microgram [10^{-6} g]
µL	Microliter [10^{-6} L]
µM	Micromolar [10^{-6} M]
cm^2	Square centimeter
g	Gram
h	Hour
kDa	Kilodalton
kg	Kilogram [10^3 g]
M	Molar concentration
mg	Milligram [10^{-3} g]
min	Minute
mL	Milliliter [10^{-3} L]
mM	Millimolar [10^{-3} M]
mm	Millimeter [10^{-3} m]
ng	Nanogram [10^{-9} g]
nM	Nanomolar [10^{-9} M]
nm	Nanometer [10^{-9} m]
rpm	Rounds per minute
s	Second
U	Enzyme unit
V	Volt
α	Alpha
β	Beta
ζ	Zeta

6.4 List of publications and conference contributions

6.4.1 Article

Neocarzilin A is a potent inhibitor of cancer cell motility targeting VAT-1 controlled pathways
Carolin M.-L. Gleissner*, <u>Carolin L. Pyka*,</u> Wolfgang Heydenreuter*, Thomas F. Gronauer, Carina Atzberger, Vadim S. Korotkov, Weiting Cheng, Stephan M. Hacker, Angelika M. Vollmar, Simone Braig and Stephan A. Sieber
ACS Central Science, 2019 June 18

*authors contributed equally

6.4.2 Presentation

Neocarzilin – a potential antitumor reagent in human breast adenocarcinoma
<u>Carolin L. Pyka</u>, Carolin M.-L, Gleissner, Carina Atzberger, Stephan A. Sieber, Simone Braig and Angelika M. Vollmar
Annual retreat of the Graduate School Life Science Munich (LSM)
2018, Spitzingsee, Germany

6.4.3 Posters

Neocarzilin – a potential antitumor agent in human breast adenocarcinoma
<u>Carolin L. Pyka</u>, Carina Atzberger, Weiting Cheng, Stephan A. Sieber, Simone Braig and Angelika M. Vollmar
Annual retreat of the Graduate School Life Science Munich (LSM)
2017, Wessobrunn, Germany

Neocarzilin A impairs breast adenocarcinoma cell motility by targeting VAT-1 protein
<u>Carolin L. Pyka</u>, Carolin M.-L. Gleissner, Wolfgang Heydenreuter, Thomas Gronauer, Carina Atzberger, Weiting Cheng, Stephan A. Sieber, Simone Braig and Angelika M. Vollmar
32nd Euro Congress on Cancer Science & Therapy
2019, Barcelona, Spain

6.5   Acknowledgements

An erster Stelle möchte ich mich ganz herzlich bei Ihnen, Frau Prof. Dr. Angelika Vollmar, bedanken, dass Sie mir die Möglichkeit gegeben haben, meine Dissertation am Lehrstuhl für Pharmazeutische Biologie anzufertigen. Ihre ansteckende Begeisterung für die Forschung habe ich als sehr motivierend empfunden und trotz Ihres oft strammen Terminplans haben Sie sich immer Zeit für Diskussionen und zur Beantwortung von Fragen genommen. Ich möchte außerdem besonders hervorheben, dass Ihr offener und fröhlicher Umgang mit dem gesamten Team entscheidend dazu beigetragen hat, dass ich in den letzten drei Jahren jeden Tag gerne zur Arbeit gekommen bin.

Mein zweiter Dank gilt meiner Betreuerin Dr. Simone Braig, die mir während meiner gesamten Promotion mit Rat und Tat beiseite stand. Danke Simone, dass Du, vor allem gegen Ende meiner Arbeit, das nötige Vertrauen in mich hattest unser gemeinsames Paper erfolgreich abzuschließen. In diesem Zusammenhang möchte ich mich ebenfalls ganz herzlich bei meinen Kooperationspartnern Prof. Dr. Stephan Sieber und Carolin Gleißner bedanken. Liebe Caro, ich hätte mir keine bessere Kooperationspartnerin wünschen können und danke Dir für die großartige Zusammenarbeit am Paper.

Meiner Prüfungskommission bestehend aus Frau Prof. Dr. Angelika Vollmar, Frau Prof. Dr. Johanna Pachmayr, Herrn Prof. Dr. Franz Bracher, Herrn PD Dr. Stylianos Michalakis, Frau Prof. Dr. Angelika Böttger und Herrn Prof. Dr. Johannes Stigler danke ich für die Bereitschaft zur Bewertung meiner Arbeit und dem damit verbundenen Zeitaufwand.

Ein herzliches Dankeschön geht auch an meine beiden Studentinnen Julie Petry (M. Sc.) und Vanessa Klapp (B. Sc.), die ich im Rahmen meiner Promotion betreuen durfte. Vielen Dank für Eure hervorragenden Leistungen und Eure tatkräftige Hilfe.

Des Weiteren möchte ich mich bei Julia Blenninger und Kerstin Loske für die technische Unterstützung des Neocarzilin-Projekts, sowie bei Frau Schnegg für die hilfreichen Tipps und Tricks zum Thema Western Blot und die erheiternden Konversationen am ChemiDoc bedanken. Ein

besonderes Dankeschön auch an Jana Peliskova, die gute Seele des Arbeitskreises, die uns alle täglich mit ihrem grenzenlosen Engagement unterstützt.

Selbstverständlich möchte ich mich auch beim gesamten Arbeitskreis Vollmar für die großartige fachliche, sowie mentale Unterstützung, vor allem gegen Ende meiner Promotion bedanken! Ein besonderer Dank geht an meine Team-Kolleginnen Chrissi und Olga für den sehr intensiven Austausch während der Teammeetings und auch abseits der Arbeit. Danke an die Herrenrunde Flo, Max, Martin und Daniel für Eure Hilfe bei jeglichen Belangen und die hilfreichen Beiträge in meinen Progress-Reports. Danke Conny, für die gute Zusammenarbeit im Stickstoff-Team, es war mir eine Ehre. Danke auch an meine ehemaligen Kolleginnen Meli und Chrissi für die große Unterstützung zu Beginn meiner Promotion und dafür, dass wir auch über das Labor hinaus unsere Freundschaft aufrechterhalten haben. Danke auch an alle Master- und Bachelorstudenten, vor allem an Vanessa, Antje, Franz, Hundi, Mo und Ehrenmann Flo, die frischen Wind in den Arbeitskreis gebracht haben und tatkräftig zum Gelingen des freitägliche Feierabendbieres (und das was sich manchmal daraus entwickelt hat) beigetragen haben. Danke Euch allen für die durchweg positive Stimmung, ich hätte mir keine besseren Kollegen wünschen können!

Mein letzter und wichtigster Dank gilt meinen Eltern und meinem Bruder Philipp. Vielen Dank für Eure überwältigende Unterstützung während meiner gesamten Ausbildung und dafür, dass Ihr all meine Ideen und Entscheidungen stets unterstützt habt und immer hinter mir steht. Ohne Euch wäre ich heute nicht da wo ich jetzt bin.